

AMINE-OXIDE ADSORBENTS FOR POST-COMBUSTION CO₂ CAPTURE

A Dissertation
Presented to
The Academic Faculty

By

Praveen Bollini

In Partial Fulfillment
Of the Requirements for the Degree
Doctor of Philosophy in the
School of Chemical & Biomolecular Engineering

Georgia Institute of Technology

December 2013

Copyright © 2013 by Praveen Bollini

AMINE-OXIDE ADSORBENTS FOR POST-COMBUSTION CO₂ CAPTURE

Approved by:

Dr. Christopher W. Jones, Advisor
School of Chemical & Biomolecular
Engineering
Georgia Institute of Technology

Dr. William J. Koros
School of Chemical & Biomolecular
Engineering
Georgia Institute of Technology

Dr. David Sholl
School of Chemical & Biomolecular
Engineering
Georgia Institute of Technology

Dr. Krista Walton
School of Chemical & Biomolecular
Engineering
Georgia Institute of Technology

Dr. Athanasios Nenes
School of Earth & Atmospheric Sciences
Georgia Institute of Technology

Date Approved: June 25, 2013

We shall not cease from exploration
And the end of all our exploring
Will be to arrive where we started
And know the place for the first time.

- Eliot, T. S. "Four Quartets 4: Little Gidding."

ACKNOWLEDGEMENTS

'Not everything that counts can be counted, and not everything that can be counted counts.' These are the only words I can think of (which have been stolen, of course) that come close to describing the deep sense of uneasiness I feel about acknowledgements sections. So, bearing the risk of coming across as eccentric and arrogant, I'm going to point out some attributes of individuals at Tech that have influenced me tremendously in the past four and a half years. These are lessons I will carry with me for the rest of my life.

Dr. Jones: It's not a matter of chance, it's a matter of choice.

Dr. Golden (Air Products): Work for a cause, not for applause.

Dr. Koros: No act of kindness is ever wasted.

Dr. Sholl: Humility, not arrogance is the true sign of wisdom.

Dr. Nenes: Spontaneity is a meticulously prepared art.

Dr. Walton: Professors can be human too.

Dun-Yen Kang: Underlying craziness, is the potential for genius.

Meha Rungta: Only in the calm waters can one see one's own reflection.

Dr. Brunelli: A Ph.D. is not enough.

Juanita Freeman: You don't need a Ph.D. to be a useful member of society.

ACKNOWLEDGEMENTS.....	iv
LIST OF TABLES	viii
LIST OF FIGURES.....	ix
SUMMARY.....	xiii
CHAPTER 1: CO₂ CAPTURE USING AMINE ADSORBENTS: INTRODUCTION & ASSESSMENT OF CRITICAL RESEARCH NEEDS	
1.1. Introduction & Motivation.....	1
1.2. Classes of Supported Amine Adsorbent Materials.....	2
1.3. CO ₂ –amine Adsorption.....	6
1.4. CO ₂ –amine Desorption.....	13
1.5. Material Stability.....	21
1.6. Critical Materials Research Needs.....	28
1.7. References.....	29
CHAPTER 2: : DYNAMICS OF AMINE ADSORBENTS: IMPACT OF HEAT EFFECTS	
2.1. Background.....	39
2.2. Experiments.....	42
2.3. Theory.....	46
2.4. Results & Discussion.....	51
2.5. Conclusions.....	65
2.6. Notation.....	66
2.7. References.....	68

**CHAPTER 3: DYNAMICS OF AMINE ADSORBENTS: INSIGHTS INTO
ADSORBENT DESIGN**

3.1. Background.....	77
3.2. Experiments	78
3.3. Theory.....	79
3.4. Results & Discussion.....	80
3.5. Conclusions.....	108
3.6. Notation.....	109
3.7. References.....	112

**CHAPTER 4: AN ADSORPTION CALORIMETRY APPARATUS TO STUDY
CO₂-SUPPORTED AMINE INTERACTIONS**

4.1. Background.....	118
4.2. Theory.....	123
4.3. Experiments.....	126
4.4. Results & Discussion.....	133
4.5. Conclusions.....	136
4.6. Notation.....	137
4.7. References.....	138

**CHAPTER 5: EFFICIENCY OF SUPPORTED AMINE ADSORBENTS FOR CO₂
CAPTURE: EFFECT OF AMINE STRUCTURE & DENSITY**

5.1. Background.....	146
5.2. Experiments.....	149
5.3. Results & Discussion.....	150
5.4. Conclusions.....	157

**CHAPTER 6: OXIDATIVE DEGRADATION OF SUPPORTED
AMINE ADSORBENTS**

6.1. Background	161
6.2. Experiments.....	162
6.3. Results & Discussion.....	166
6.4. Conclusions.....	185
6.5. References.....	186

**CHAPTER 7: OTHER CONSIDERATIONS IN ADSORBENT EVALUATION:
SORBENT DENSITY & WATER TOLERANCE**

7.1. Background.....	193
7.2. Experiments.....	196
7.3. Results & Discussion.....	199
7.4. Conclusions.....	206
7.5. References.....	207

CHAPTER 8: SUMMARY & RECOMMENDATIONS

LIST OF TABLES

Table 2.1. Parameters used in the simulations	51
Table 2.2. Amine loading and pore characteristics of the SBA-15 support and APS_SBA	53
Table 2.3. Optimal Toth isotherm parameters for APS_SBA.	54
Table 2.4: Optimal values of parameters used to fit models with the experimental data.	59
Table 3.1. Dual Site Langmuir parameters for zeolite 13X	84
Table 3.2. Toth isotherm parameters for the amine adsorbents used in this study	84
Table 3.3: Optimal values of parameters used to fit models with the experimental data	98
Table 3.4: Optimal values of fitting parameters obtained using the heterogeneous model	106
Table 4.1: Pressure range for measurement and number of low pressure data points for literature reports on CO ₂ -supported amine isosteric enthalpies of adsorption	124
Table 4.2: Isosteric heats at zero coverage for CO ₂ adsorption on Silicalite-1	137
Table 5.1: Surface areas and amine loadings of materials tested in this study	154
Table 6.1: Silane coupling agents used to prepare aminosilica materials for oxidative stability studies.	165
Table 6.2: Physical characteristics of the bare support and the various amine functionalized silica adsorbents	174
Table 6.3: Carbon and nitrogen XPS binding energies of the aminosilica adsorbents before and after oxidative treatments, along with possible functional group assignments	182

LIST OF FIGURES

Figure 1.1: Porous silica supports have been loaded with CO ₂ -adsorbing amine sites using three primary methods: physical impregnation, covalent tethering and in-situ polymerization within the pores.	3
Figure 1.2: Common silanes and polymeric, amine-containing materials used for hybrid material synthesis	5
Figure 1.3: Zwitterion mechanism for CO ₂ capture (valid for primary, secondary and sterically hindered amines) in solution	7
Figure 1.4: Mechanism for reaction of tertiary amines with CO ₂ based on solution studies	7
Figure 1.5: Schematic of chemical structure of the HAS adsorbent material	10
Figure 1.6: Idealized structure of the melamine dendrimer functionalized silica surface	11
Figure 1.7: DRIFTS spectra for Sayari's APS material, which displays formation of urea upon cyclic testing in dry conditions.	17
Figure 2.1: Schematic of the packed bed setup used in this study	46
Figure 2.2. XRD pattern of the SBA-15 silica support used in this study.	51
Figure 2.3: Experimentally measured CO ₂ adsorption isotherms (inset: low pressure data).	53
Figure 2.4. Breakthrough curve and temperature profile for the APS_SBA packed bed.	55
Figure 2.5: Fits obtained between predicted and experimental breakthrough curves, temperature profiles	57
Figure 2.6. Effect of wall heat transfer coefficient on simulated breakthrough curve and temperature profile	58
Figure 2.7. Effect of effective axial bed thermal conductivity on simulated breakthrough curve and temperature profile	59
Figure 2.8: Effect of linear driving force constant, k, on simulated breakthrough curve and temperature profile	59

Figure 2.9: Comparison of isothermal and non-isothermal model predictions at the optimal linear driving force constant value	61
Figure 2.10: Effect of feed relative humidity on CO ₂ breakthrough.	62
Figure 2.11: Comparison of isothermal and non-isothermal model predictions for feed gas velocities five times those in the packed bed experiments	64
Figure 3.1: Amine loading (normalized by the amine loading of APS_high), surface areas, and pore volumes, (normalized by the corresponding values of the SBA-15 support) of the amine adsorbents tested	81
Figure 3.2: Hypothetical representation of amine surfaces in the 3-aminopropylsilyl-grafted SBA-15 materials used here: APS_low with a low amine loading (top), APS_medium (middle), and APS_high, with the highest amine loading (bottom)	81
Figure 3.3: Isotherm fits obtained using models described and parameters reported in this work (inset: low partial pressures)	84
Figure 3.4: Fractional CO ₂ uptake for APS_medium (top) and APS_high materials (bottom) at different CO ₂ partial pressures	86
Figure 3.5: Fractional uptake of the APS_medium material (top) and APS_high material (bottom) plotted as a function of the square root of time	89
Figure 3.6: Total CO ₂ uptake as a function of time on the APS_medium and APS_high adsorbents at a CO ₂ partial pressure of 0.1 bar	90
Figure 3.7: Breakthrough curves for the four adsorbents (top) and temperature profiles in the packed bed (bottom)	92
Figure 3.8. Fits obtained between predicted and experimental breakthrough curves (top) temperature profiles (bottom)	96
Figure 3.9: Schematic representation of the four steps that transport CO ₂ to a surface adsorption site during a packed bed breakthrough experiment, (i) film diffusion, (ii) macropore diffusion, (iii) intraparticle diffusion and (iv) chemical reaction/adsorption	97
Figure 3.10: Best fit obtained for the breakthrough curve for the APS_high material using the linear driving force model	100
Figure 3.11: Effect of varying linear driving force constant, k, on simulated breakthrough curves for the homogeneous linear driving force model over the APS_high material	101

Figure 3.12: Effect of wall heat transfer coefficient on simulated breakthrough curves for the APS_high material	101
Figure 3.13: Schematic representation of the homogeneous and heterogeneous models used for modeling mass transfer in amine adsorbents	102
Figure 3.14: Comparison of the optimal predictions obtained using the homogeneous and heterogeneous linear driving force models for breakthrough over the APS_high adsorbent bed	105
Figure 3.15: Effect of temperature on uptake rates of APS_medium and APS_high adsorbents	107
Figure 3.16: Effect of temperature on linearity of the plot of fractional uptake plotted as function of the square root of time (top) and the total CO ₂ uptake plotted as function of time (bottom)	107
Figure 4.1: Schematic of the various phases according to the Gibbsian surface excess model	124
Figure 4.2: Schematic describing measurement of heat evolution in the calorimeter	130
Figure 4.3: Schematic of the experimental setup used to measure isosteric heats of adsorption	131
Figure 4.4: Adsorption isotherm (top) and isosteric heat of adsorption (bottom) for CO ₂ adsorption onto silicalite	135
Figure 5.1: Heat-coverage curves (top) and adsorption isotherms (bottom) for the aminopropylsilyl functionalized SBA-15 materials	151
Figure 5.2: Amine adsorbent structures used in this study and their nomenclature	153
Figure 5.3: Isosteric heats of adsorption and adsorption isotherms for amine materials with structures shown in Figure 5.2	155
Figure 5.4: Comparison of experimentally measured isosteric heats with those derived from the Toth model for the APS & MAPS materials	157
Figure 6.1: Hydrogen abstraction mechanism for MEA oxidation (a) and electron abstraction mechanism for MEA oxidation (b).	168
Figure 6.2: Minor products resulting from the oxidation of aqueous MEA solutions	170

Figure 6.3: TEM image of the mesocellular foam support MCF3	172
Figure 6.4: Nitrogen physisorption isotherm of the mesocellular foam support, MCF3	172
Figure 6.5: Organic to silica weight ratio of samples treated under oxidizing conditions at various temperatures normalized by the organic to silica weight ratio of the corresponding untreated adsorbents	174
Figure 6.6: CO ₂ adsorption capacities of oxygen-treated adsorbents normalized by the original CO ₂ adsorption capacities as a function of the temperature of oxidation	176
Figure 6.7: ¹³ C CP MAS NMR spectra of the untreated samples (blue, bottom) and samples treated at 135°C (red, top). a: MCF_APS, b: MCF_MAPS, c: MCF_DMAPS, d: MCF_DA	179
Figure 7.1: Bulk densities of tested materials using different packing techniques: Normal packing (black, solid) and under pressure (red, dashed)	200
Figure 7.2: Bulk density as a function of amine loading (numbers following MCF indicate percentage weight loading of PEI on a dry basis)	200
Figure 7.3: Bulk densities (under pressure) as a function of adsorbent pore volume	201
Figure 7.4: Comparison of bulk and framework densities for the crystalline materials used in this study.	202
Figure 7.5: Mass-based (black, solid) and volume-based capacities (red, dashed) for materials tested	204
Figure 7.6: CO ₂ adsorption capacities for materials measured in the presence of humidity	205

SUMMARY

Every day, millions of tons of carbon dioxide are emitted to the atmosphere from coal-fired power plants. Transition from a fossil fuel based economy to a renewable energy based economy can be made possible by retrofitting these power plants to capture and sequester the carbon dioxide, which would otherwise be emitted to the atmosphere. The technology of choice for this process is 'Amine Scrubbing', a mature technology that has been around for decades. Temperature swing adsorption, which is an alternative to the benchmark absorption process, is a more nascent technology. Temperature swing adsorption is an alternative that can potentially result in lower overall energy penalties on power plants, thus making it an interesting option to evaluate.

Amine functionalized silicas are promising chemisorbent materials for post-combustion CO₂ capture due to the high density of active sites per unit mass of adsorbent that can be obtained by tuning the synthesis protocol, thus resulting in high equilibrium CO₂ adsorption capacities. However, when compared to physisorbents, they have a few disadvantages. Firstly, oxidative degradation of the amine groups reduces the lifetime of these adsorbent materials. Furthermore, rapid heat release following the reaction between amines and CO₂ results in large local temperature spikes which may adversely affect adsorption equilibria and kinetics. Thirdly, there is a lack of fundamental understanding of CO₂-amine adsorption thermodynamics, which is key to scaling up these materials to an industrial-scale adsorption process. The primary goal of this dissertation is to further the qualitative and quantitative understanding of these three critical aspects of aminosilica adsorbents so these materials can be better evaluated and further tuned as adsorbents for post-combustion CO₂ capture applications.

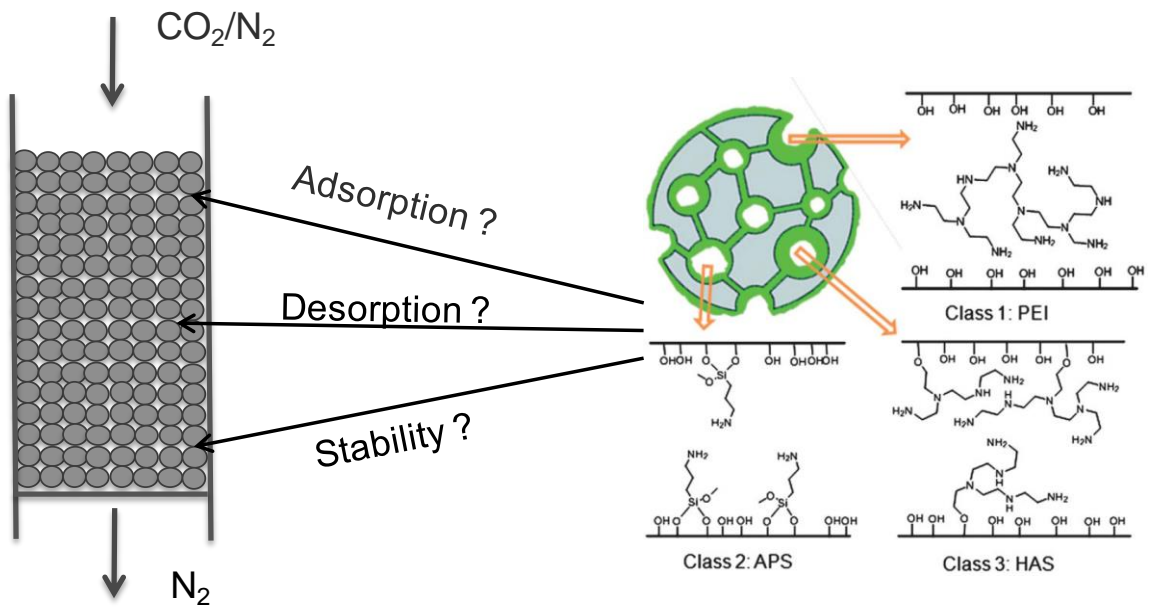
Packed bed adsorption typically occurs under non-isothermal conditions. In the case of CO₂ chemisorption onto supported amines, there is a rapid heat release that follows adsorption-reaction onto the surfaces of these adsorbents. This heat release can adversely affect performance of the aminosilica material and potentially complicate determination of fundamental kinetic parameters from experimental data. The results in this thesis demonstrate that experimental conditions exist, under which heat released on adsorption has an insignificant effect on adsorption kinetics, thus enabling accurate determination of kinetic parameters using simple isothermal models. Also, strong evidence is provided for the fact that unlike in the case of conventional physisorbents, diffusion limitations cause long tails in breakthrough curves, resulting in reduced breakthrough capacities. A new diffusion model that accounts for adsorbent heterogeneity was proposed, which provides good fits with experimental breakthrough data.

With the goal of overcoming the lack of low coverage-isosteric heat of adsorption data in the literature, an apparatus capable of measuring isosteric heats of CO₂ adsorption at ultra-low pressures/coverages was designed, tested, and validated against literature data. The instrument enabled the study of CO₂-amine interactions as a function of amine density and amine structure, both of which were found to have a significant impact on amine efficiency. For low amine density materials, physisorption onto the bare support was shown to be a major contributor to overall adsorption. In addition to enthalpic factors, entropic factors were also found to be of critical importance in designing more efficient supported amine adsorbents for post-combustion CO₂ capture.

With respect to the oxidative stability of these adsorbents, fundamental correlations were drawn between amine type, structure and oxidative stability. It was found that secondary monoamines are more prone to oxidative degradation compared to

primary and tertiary monoamines. The stability of primary amines, however, decreases when amines are present in close proximity to other amine groups as opposed to being isolated from them, indicating the presence of a co-operative oxidation mechanism. This co-operative mechanism is very important to understand since any CO₂ adsorbent that will be used in a full-scale adsorption process will likely have a large density of amine adsorption sites per unit mass.

Overall, the results presented in this dissertation serve to significantly enhance the fundamental understanding of those aspects of supported amine adsorbents that are of relevance to post-combustion CO₂ capture applications.



CHAPTER 1

CO₂ CAPTURE USING AMINE ADSORBENTS: INTRODUCTION & ASSESSMENT OF CRITICAL RESEARCH NEEDS

Parts of this chapter are reproduced from 'Bollini, P.; Didas, S. A.; Jones, C. W. Amine-oxide Hybrid Materials for Acid Gas Separations. *J. Mater. Chem.* **2011**, *21*, 15100.'

1.1. Introduction & Motivation

The ever-increasing concentration of CO₂ in the atmosphere associated with fossil fuel combustion has been linked to significant global climate change over the course of the last century. As a result, significant recent research has focused on development of materials and technologies that might be used to capture CO₂ from fossil emitting processes, especially from large point sources such as coal-fired power plants.^{1,2}

For post-combustion CO₂ capture from large point sources, well-established absorption processes based on solutions of aqueous amines are considered the benchmark technology that is most likely to be widely implemented in the near future. This technology, which has been practiced commercially on various scales for a number of years, is technologically feasible but carries with it high process costs, with the cost of regenerating the amine solution in the CO₂ stripping step being identified as a particularly expensive step. In the longer term, as a potentially lower cost option, many researchers have explored the use of solid adsorbents as potential alternatives to the use of amine solutions. An array of solid sorbents that selectively capture CO₂ from dilute gas streams are available, and have been recently reviewed.^{3,4} CO₂ adsorbents

are comprised of materials that capture CO₂ via strong chemisorptive interactions and materials that weakly bind CO₂ via physisorptive interactions. The chemisorbants offer a significant advantage over other adsorbent materials like zeolites in that they are more effective at adsorbing CO₂ selectively from wet gas streams like flue gas.

Among the array of available adsorbents, oxide-supported amine materials have recently emerged as a promising class of solids that can affectively adsorb CO₂ from humid gas streams at low temperature. These solids can then be regenerated using a variety of approaches, including use of a temperature swing (TSA), pressure or vacuum swing (PSA or VSA),⁵ or perhaps even electric-field swing adsorption (ESA) methodologies.⁶

Although oxide-supported amine materials have been used since 1992 to capture CO₂ from fluid streams, it was not until the last decade that significant activity on the design, synthesis and application of a variety of silica-supported amine materials significantly accelerated. In this chapter, a brief critical overview of the various aspects of mesoporous oxide-supported amine materials relevant to adsorption of CO₂ from dilute gas streams is presented. Detailed discussions of adsorption kinetics, adsorption thermodynamics, oxidative stability, and sorbent densities, which are topics that are dealt with in later chapters, have been avoided. In the concluding part of this chapter, critical materials research needs in the field are identified.

1.2. Classes of Supported Amine Adsorbent Materials

The array of silica-supported amine adsorbents has been categorized into three groups. While oxide-supported amine materials have been well-known for decades for use in chromatographic separations or for applications in catalysis, their

use for the selective adsorption of CO₂ in separation applications was first reported by Tsuda in 1992^{7,8}.

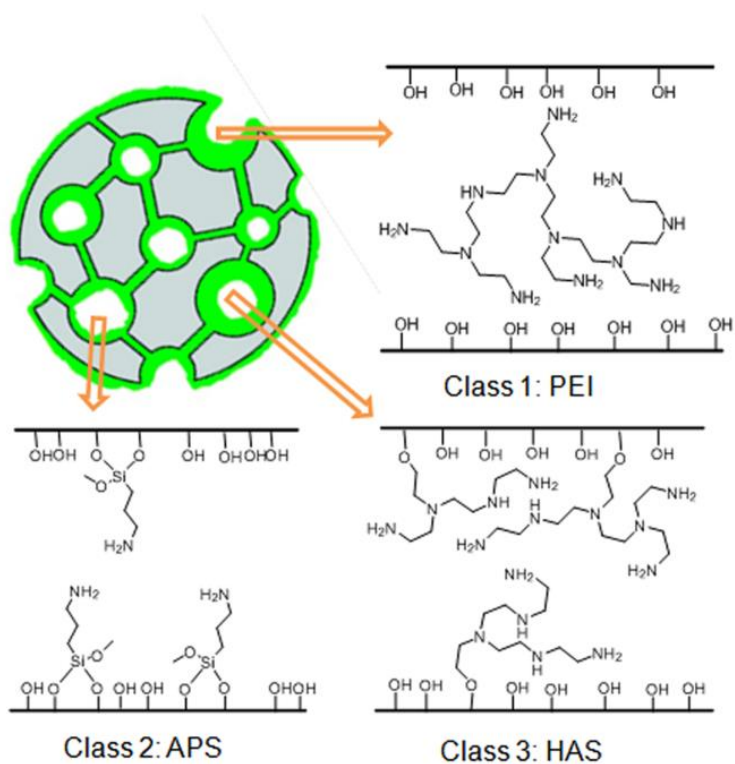


Figure 1.1: Porous silica supports have been loaded with CO₂-adsorbing amine sites using three primary methods: physical impregnation, covalent tethering and in-situ polymerization within the pores.

Class 1 adsorbents are conceptually the easiest to prepare and may be the most practical for use on large scales in gas separation applications.³ These materials are based on the physical combination of pre-synthesized amines and various silica supports. Typically, amine-containing polymers are used, as these have low volatility

and the silica-polymer composites are more robust to a variety of treatment conditions. However, amine-containing small molecules have also been used, including amine molecules that are well-studied in amine absorption applications. Typically, mesoporous supports are impregnated with the amines, to give composite materials with the amines physically adsorbed onto or into the support. The introduction of this class of materials for applications in CO₂ was by Song in 2002,⁹ and since then, several other groups have further explored this basic design.⁹⁻¹²

Class 2 adsorbents are based on the use of small amine-containing molecules, such as organosilanes, that can form covalent bonds to the oxide support. Examples of well-studied aminosilanes include 3-aminopropyltrimethoxysilane (APS), 3-(trimethoxysilyl)propylethylenediamine (diamine), and 3-[2-(2-aminoethylamino)ethylamino]propyltrimethoxy-silane (triamine), yielding one, two, or three amine sites per molecule grafted to the silica surface. These materials have been most often prepared by grafting of the amines onto pre-formed silica supports, but they can also be prepared by co-condensation with silica sources and included within the oxide framework during the silica synthesis.¹³ In the original application of this class of materials for CO₂ capture, Tsuda followed a co-condensation approach.^{7,8}

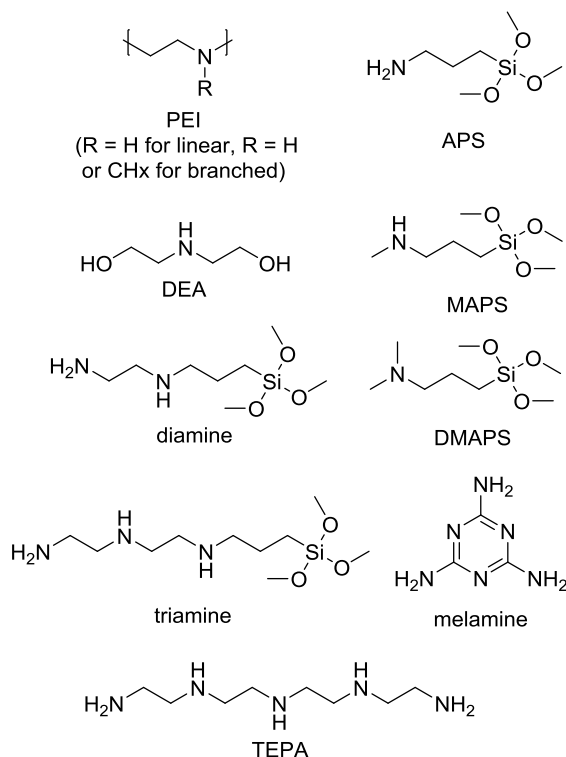


Figure 1.2: Common silanes and polymeric, amine-containing materials used for hybrid material synthesis.

The most recent class of supported amine adsorbents, referred to as Class 3 adsorbents, are prepared by the in-situ polymerization of reactive amine monomers on and in the silica support. While in-situ polymerization of amine-containing monomers on porous silica supports has been reported a number of times, for example in the work of Shantz¹⁴ and Rosenholm,^{15,16} their application for CO₂ capture was first reported by our group in 2008.¹⁷ Materials of this class can sometimes be considered a hybrid of class 1 and class 2 adsorbents, having the amine-silica covalent bonds of class 2 materials, and the large site density of polymer amines commonly found in polymer-containing class 1 materials.

1.3. CO₂ Adsorption

Amine-oxide hybrid materials adsorb CO₂ by exploiting acid-base interactions between CO₂ and amine groups immobilized onto the external surface or within the pores of a solid material. These amines are typically primary, secondary or tertiary amines. Primary and secondary amines (including sterically hindered amines) react with CO₂ via the zwitterion mechanism, proposed by Caplow in 1968,¹⁸ as shown in Figure 1.3. In this mechanism, an additional free base is needed, which is typically water, a hydroxyl ion or another amine. Thus, theoretically, in the absence of water, two moles of amine are required to capture one mole of CO₂ and in the presence of water only one mole of amine is required per mole of CO₂ captured. Water is thus regarded to improve the amine efficiency of carbon capture, i.e. the number of moles of CO₂ adsorbed per mole of primary/secondary/sterically hindered amine. Tertiary amines capture CO₂ via a different mechanism, as shown in Figure 1.3. This mechanism was first proposed by Donaldson and co-workers in 1980.¹⁹ This reaction mechanism is accessible to primary and secondary amines as well but the rate constants for this base catalyzed bicarbonate formation are typically smaller than those of the zwitterion mechanism described above. Note that CO₂ capture by tertiary amines requires water, and under dry conditions supported amine adsorbents based on tertiary amines are not highly effective. Also, the reaction mechanisms described above are based on mechanistic studies performed on CO₂ capture by aqueous amines.¹⁸⁻²⁰ Differences between the mechanism in solution versus on a solid surface, if any, are not very well understood.

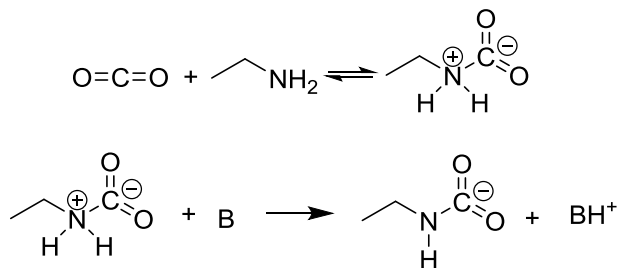


Figure 2.3: Zwitterion mechanism for CO₂ capture (valid for primary, secondary and sterically hindered amines) in solution.

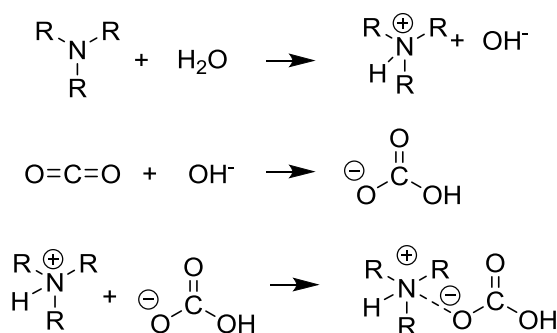


Figure 1.4: Mechanism for reaction of tertiary amines with CO₂ based on solution studies.

For an ultra-large-scale separation process like carbon capture from flue gas, adsorbents must be evaluated based on several criteria that include a high CO₂ working capacity, rapid adsorption and desorption kinetics, selective adsorption of CO₂ over other flue gas components, and stability under the range of practical operating conditions. Before being implemented in full-scale carbon capture applications, each adsorbent must be evaluated based on the aforementioned criteria. In this as well as the next few sections, these performance metrics will be discussed briefly in the context of amine-oxide hybrid materials for CO₂ capture.

1.3.1. CO₂ adsorption capacities

Since Tsuda's first report on the application of aminosilica materials as adsorbents for CO₂ separation in 1992,^{7,8} the general trend in the literature has been to seek amine-oxide hybrid materials that have increasingly large CO₂ adsorption capacities. Most published studies focus almost exclusively on measuring adsorption capacities and a quest for ever-higher capacities. Some of the highest CO₂ capacities reported in the literature have been summarized in a recent review.³ The highest CO₂ adsorption capacity reported for class 1 materials in the literature is that by Giannelis and co-workers.²¹ The tetraethylenepentamine (TEPA) impregnated mesoporous silica capsules in that study exhibited CO₂ adsorption capacities up to 7.9 mmol CO₂/g adsorbent. In that report, 10% CO₂ in argon was used as the test gas. The CO₂ containing gas stream was pre-humidified using a water saturator and the capacities were measured at 75°C using the fixed bed-mass spectrometry technique.

Apart from adsorption capacity, amine efficiency is another metric that can be used to assess CO₂ capture performance. The amine efficiency of an adsorbent is defined as the number of moles of carbon dioxide adsorbed per mole of amine functional groups and is expressed as a fraction. It is a measure of the fraction of amine groups present in an adsorbent that may actively participate in adsorbing CO₂. Note that the theoretical maximum value for amine efficiency under dry conditions is 50%, in the absence of significant physisorption at non-amine sites.

Adsorption isotherms of class 1 adsorbents show a plateau above a CO₂ partial pressure of 0.3 bar and a very high slope at low partial pressures, thus demonstrating significant promise as materials for CO₂ capture at low partial

pressures (both capture from flue gas as well as direct capture of CO₂ from ambient air).²² It is important to note that even though class 1 materials exhibit some of the highest CO₂ adsorption capacities reported in the literature, they sometimes have kinetic, stability and regenerability issues, as discussed in section 1.5.

Class 2 materials differ from class 1 materials in that there is an upper bound on the number of CO₂ capturing amine groups that can be present per unit mass of the adsorbent in the absence of silane polymerization (which better fills the support pores). This is because a monolayer or less of amine sites is prepared under most grafting and co-condensation syntheses. Therefore, the density of amine sites is directly related to the accessible surface area, unlike in the case of class 1 adsorbents, where support pore volumes dictate the maximum achievable amine loading for a given aminopolymer. On the other hand, because the formation of only a monolayer of sites on typical mesoporous silica supports occurs, class 2 materials tend to have more open porosity compared to class 1 and class 3 adsorbents. Sayari and co-workers demonstrated that the limitation on the amine loading can be overcome partly by prehydrating the silica surface by adding a small quantity of water to the reaction mixture prior to adding the silane coupling agent. The presence of water molecules in the pores results in surface polymerization of aminosilanes, thus yielding much higher amine loadings than on previously reported class 2 materials, the highest being 8 mmol N/g silica.²³ The optimally grafted material they developed showed a CO₂ capture capacity of 2.65 mmol/g at 25°C at a CO₂ partial pressure of 0.05 bar under dry adsorption conditions. Appropriate synthesis conditions can allow for significant amine loadings along with good residual sorbent porosity in class 2 materials.

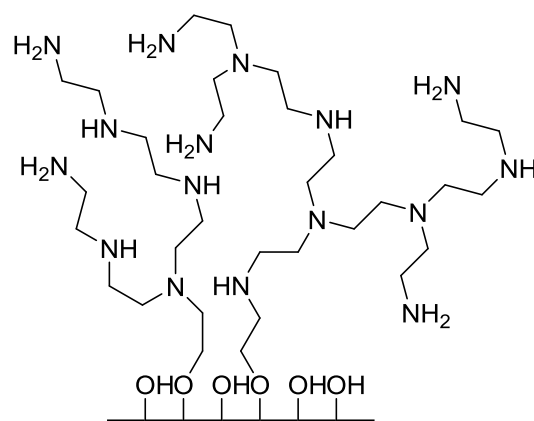


Figure 1.5: Schematic of chemical structure of the HAS adsorbent material.

Class 3 materials can combine the high CO₂ adsorption capacities of class 1 materials with the regenerative stability of class 2 materials. Hicks et al.¹⁷ synthesized hyperbranched aminosilica (HAS) adsorbents by in-situ polymerization of aziridine molecules on and in a mesoporous SBA-15 silica support. The structure of these adsorbents is shown in Figure 1.5. The original HAS material, with an adsorption capacity of 3.1 mmol CO₂/g adsorbent, exhibited almost ten times the adsorption capacity of a simple class 2 material synthesized on the same silica support. Further investigations into the structure and performance of these HAS materials revealed that during the functionalization of the SBA-15 silica support, polymerization of aziridine at the pore mouths occurred below a critical pore diameter of 5 nm, resulting in pore blockages.²⁴ Using supports with larger pore diameters was identified as a possible alternative to avoid these pore blocking effects. The HAS materials are promising candidates for CO₂ capture, based on CO₂ adsorption capacities, kinetics and selectivities. Nevertheless, more work is required to thoroughly understand the synthesis of these materials and to be able to exercise control over the location and size of the polymer chains.

Later, Chaffee's group reported the synthesis of another class 3 adsorbent.²⁵ Reaction of mesoporous foam silica materials with 2,4,6-trichloroazine and ethylenediamine in alternate steps yielded a melamine type dendrimer functionalized mesoporous silica material. This material, depicted in Figure 16, and originally developed by Shantz and coworkers,¹⁴ had an amine loading of 7.5 mmol N/g silica, although many amines were of the less useful tertiary variety. The material had a CO₂ adsorption capacity of about 3.5 mmol/g at a relatively high CO₂ partial pressure of 0.9 bar under dry conditions.

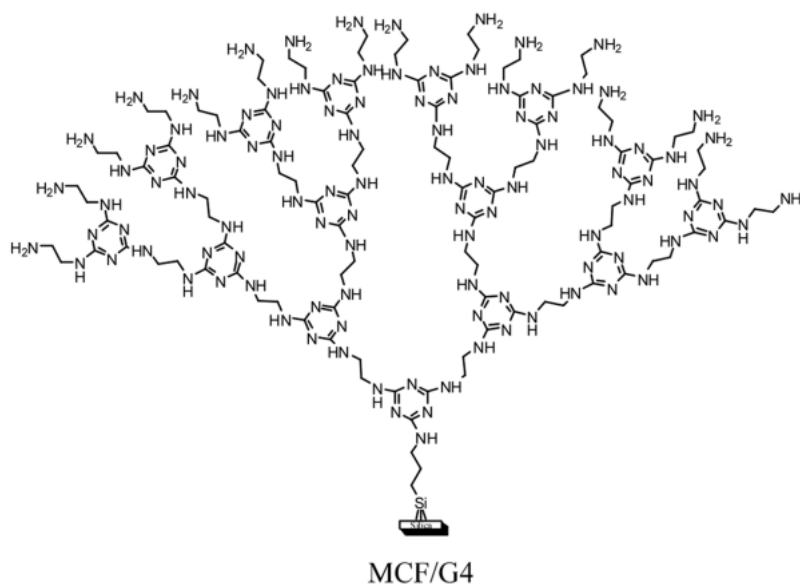


Figure 1.6: Idealized structure of the melamine dendrimer functionalized silica surface.

Reprinted from ref. ²⁵ with permission from Springer.

Overall, obtaining high CO₂ capacity with hybrid aminosilica materials is best achieved by developing material architectures that can allow for a large loading of

highly accessible amine groups. For class 1 materials based on amine polymers, this generally implies supports with large pore volumes. For class 2 materials, it appears that large surface areas are critical, in the absence of silane polymerization, as the grafting surface area dictates the overall amine loading. For class 3 materials, the critical role of porosity has not yet been fully elucidated.

All of the studies discussed in this section report adsorption capacities in terms of millimoles of CO₂ per unit mass of adsorbent. From an adsorption process standpoint, the adsorption capacity per unit volume is a much more appropriate metric in terms of comparing adsorbents for post-combustion CO₂ capture. The need for comparing adsorbents on a volumetric basis and the impact of sorbent densities on evaluation of adsorbents for CO₂ capture is discussed in chapter 7.

1.3.2. CO₂ adsorption selectivities

Any adsorbent, to be considered a candidate for CO₂ separation, needs to be capable of adsorbing CO₂ selectively over all the other major components of the gas being processed. In the case of flue gas, these components are nitrogen, water and oxygen, which are the major components of flue gas. Amine-functionalized oxide materials selectively adsorb CO₂ over both oxygen and nitrogen, as demonstrated in a number of publications.^{23,26–28} This is not surprising, as this is what nearly all nanoporous materials do,²⁹ but the CO₂-selective amines allow for exceptionally high selectivities. Also, as explained above, water improves the amine efficiency of CO₂ capture, i.e. the number of moles of CO₂ adsorbed per mole of nitrogen in the adsorbent. The high selectivity of CO₂ over all the major components of flue gas combined with the promotion of amine efficiency in the presence of water represents a

major advantage for supported amine adsorbents over physisorbents like zeolite 13X, that do not have high enough selectivities for CO₂ over the other gas components such as water.³⁰ Other components of flue gas present at much lower concentrations, such as SO_x and NO_x, can adsorb strongly on supported amine materials, as discussed below in section 1.5. Therefore, the flue gas stream will require significant scrubbing to lower the concentration of these contaminants to a level that makes the amine adsorbents stable for a sufficient number of cycles. Such gas clean-up is also required for the benchmark amine solution technology, which is already well established.

1.3.3. CO₂ adsorption kinetics

In an ultra-large scale operation like carbon capture from flue gas where adsorption cycles will likely be on the order of minutes, rates of adsorption are critical to process economics. These rates determine the amount of adsorbent to be used in a process and hence the size of the equipment and the CO₂ capture process. Although there have been a number of studies measuring the equilibrium CO₂ adsorption capacities of oxide-supported amine materials,³ providing valuable thermodynamic information about the synthesized material, there remains a lack of quantitative understanding of the kinetics of CO₂ adsorption and desorption using silica-supported amine materials. The shortcomings of the reports that do study CO₂ adsorption kinetics are discussed in chapter 2 and will not be repeated here.

1.4. CO₂-amine Desorption

Regeneration of supported amine CO₂ adsorbents can be achieved via a temperature or CO₂ partial pressure swing, either alone or in combination. To date,

regeneration of supported amine materials has, with few exceptions, been performed by temperature swing adsorption in a flow of inert purge gas (TSA/I).^{10,31–34} Using an inert gas such as nitrogen or argon to desorb CO₂ does not concentrate the CO₂, as required, before compression and sequestration. Thus, the majority of the papers in this field do not describe a technology that performs a useful separation. Other possible regeneration strategies include (i) temperature swing adsorption using a pure CO₂ stream as the sweep gas (TSA/CO₂), (ii) pressure swing adsorption (PSA), which includes the more often used vacuum swing adsorption (VSA), sometimes in combination with a temperature swing (T/VSA), and (iii) steam stripping. There are advantages and disadvantages to each of these methods, and each method presents challenges for the material designer as discussed below.

1.4.1. Temperature Swing Adsorption with Inert Gas Purge (TSA/I)

TSA/I is a common regeneration technique, as the elevated temperatures are useful in supplying the energy needed to reverse the highly exothermic adsorption of CO₂ on amine sites while the inert purge gas provides a concentration driving force. Thus, higher temperatures result in larger desorption rates and an increased likelihood that all of the CO₂ will desorb, thereby returning the adsorbent ideally to its full capacity for the next adsorption cycle.

Of the three classes of materials, class 1 materials have generally exhibited the least stability in long term testing.^{10,31–35} Specifically, the study by Tanthana et al. shows a significant loss of stability over 30 cycles at 115 °C for TEPA and TEPA modified with PEG on mesoporous silica. While the PEG modified material did exhibit a decreased degradation rate, both materials exhibited a loss of greater than 50%

capacity over the cycles.¹⁰ However, Liu et al. report a capacity loss of only 5% for TEPA impregnated into KIT-6 during 40 cycles of regeneration at 120 °C.³⁵ This is likely due to the fact that Tanthana tested regenerability in humid conditions while Liu performed adsorption in dry conditions and so the material may have leached amines due to water condensation and solubilization, thus resulting in a decreased capacity.^{10,35} In fact it has often been observed that class 1 materials lose significant capacity during cyclic testing under humid conditions due to the organic leaching out of the solids. Section 1.5 below provides a more detailed explanation of this phenomenon along with other modes of sorbent deactivation. However, Sayari et al. report the opposite trend in their humid adsorption/desorption study and observed that adsorption and desorption in humid gas streams improved stability for class 1 and 2 materials (PEI, APS and triamine on PE-MCM-41) as opposed to cyclic testing with dry gases.³⁶ It should be noted that the number of cycles tested for the class 1 material was about half that studied by Tanthana and so it is possible that with further cycling, leaching would be observed.^{10,36} Sayari's findings from this study are discussed in further detail below.

1.4.2. Temperature Swing Adsorption with CO₂ Purge (TSA/CO₂)

Three studies have been reported using TSA with dry CO₂ as a sweep gas for adsorbent regeneration.^{11,34,37} Although complete desorption is not possible with this method, as it lacks a significant partial pressure driving force for desorption, it does result in a high purity CO₂ product stream. The first study using this approach by Kim et al. considered both class 1 and 2 materials on MCM-48 (class 1: polyethyleneimine(PEI); class 2: aminopropyltriethoxysilane(APTES)), heating them to 120 °C in 1 atm of pure CO₂.³⁷ The thermal ramp decreased the amount of CO₂

adsorbed on all the materials starting at temperatures below 50 °C. However, a weight gain was observed for the two polymeric materials (PEI and polymerized APTES) once the temperature surpassed 62 °C. The authors attributed this behavior to an increased diffusivity at higher temperatures and thus greater accessibility to vacant sites in the polymer for these materials, leading to CO₂ adsorption in this temperature range. Both materials reverted to desorption upon a further increase of temperature between ca. 85 °C and 105 °C, depending on the material. Gray et al. used a temperature ramp with various concentrations of CO₂ gas (from 10-80% CO₂ in inert) as a desorption technique for class 1 materials.³⁴ However, none of the CO₂ purge mixtures met the stated requirement of having a working capacity of at least 3 mol/kg adsorbent and so the method was ruled out in favor of a TSA/I. Drage et al. also used pure CO₂ for desorption of a class 1 material (PEI on a mesoporous silica), but provided a larger thermal driving force by heating their materials to 180 °C.¹¹ The effect of this regeneration method on adsorbent stability was evaluated via cyclic adsorption/desorption measurements. At temperatures above 135 °C, a weight gain was observed, which was attributed to formation of urea species observed by NMR and DRIFTS. Attempts to regenerate the material by heating at elevated temperatures under inert conditions proved futile and it was concluded that regeneration in flowing CO₂ gas irreversibly degraded the material and thus was not a viable option for adsorbent regeneration.

In contrast, it has recently been shown by Sayari et al. that humid gases inhibit the formation of urea and can also regenerate spent materials that have already formed urea.³⁶ In that study, two class 2 materials (monoamine and triamine) as well as one class 1 material (PEI) based on a pore expanded MCM-41 support (PE-MCM-41) were used. At least 40 cycles of CO₂ adsorption/desorption were performed using both wet and dry nitrogen at various temperatures. All materials exhibited loss of capacity in the

dry cyclic study, the class 1 materials to a greater extent than the class 2 materials, while humid cyclic studies gave stability for all materials through 40 cycles. To further demonstrate the effectiveness of this method, 750 and 700 adsorption/desorption cycles at 70 °C were performed on TRI-PE-MCM-41 under dry and humid conditions, respectively. The dry case resulted in a 15% loss of capacity while the humid case showed continued sorbent stability. NMR and DRIFTS spectra, presented in Figure 1.7, confirmed the formation of urea in dry cyclic studies and also showed the removal of urea upon regenerating spent dry materials in humid nitrogen at 200 °C for 24 hours. As a result of these findings, further studies with humid CO₂ as sweep gas should be conducted to see if this strategy can be widely used to prevent sorbent degradation.

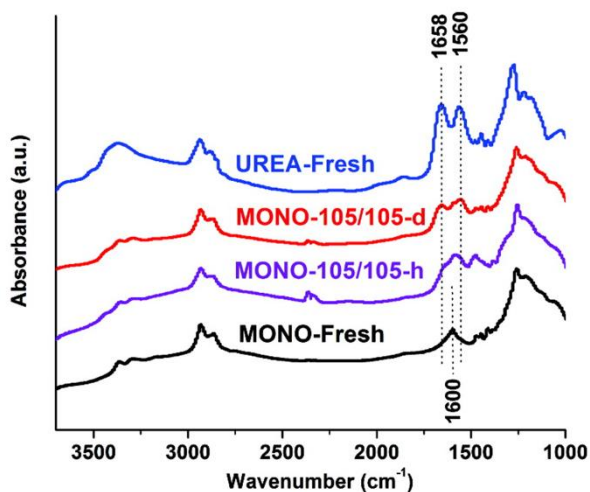


Figure 1.7: DRIFTS spectra for Sayari's APS material, which displays formation of urea upon cyclic testing in dry conditions. 'h' represents humid runs and 'd' represents dry runs. Reprinted with permission from ref. ³⁶ Copyright 2010, American Chemical Society.

1.4.3. Steam Stripping

Steam stripping, like TSA with a CO₂ purge, represents a potentially practical regeneration method for supported amine adsorbents as it can result in a concentrated CO₂ stream. Like TSA/I, the temperature and composition of a gas stream provide both a thermal and partial pressure driving force for desorption of CO₂ from the amine. The CO₂ rich steam can then be compressed to produce liquid water and a high purity CO₂ gas stream that may be ready for compression and sequestration. Additionally, low-grade steam (<110 °C) may generally be obtained at low cost from refineries and other facilities, as it is often unused and considered waste heat.

Thus far there is only one reported study on the regeneration of supported amines with saturated steam by Li et al.⁵ Saturated steam at 103 °C was used to regenerate class 1, 2 and 3 adsorbents (class 1: PEI on commercial silica; class 2: and monoamine on commercial silica; class 3: HAS on mesocellular foam silica) over 3 successive adsorption cycles. It was found that steam effectively regenerated all three classes of adsorbents. Furthermore, quick regeneration times were observed, with essentially all the CO₂ desorbing in the first ten minutes, and 66 % within the first three minutes of exposure to steam. From this study, it is far too early to make conclusions about the broader viability of steam-stripping for regeneration of supported amine CO₂ sorbents. For instance, although the initial report suggests that steam-stripping might be viable over all the materials tested, there was scatter in the regeneration data, making it hard to accurately assess the stability of the various adsorbents from the data presented. In addition, direct steam contact on the adsorbent material will likely lead to condensed water within the pores of the solid, and its removal will incur an energy penalty to the capture process. Follow-up work by Li et al. on the stability of a series of silica-supported amine adsorbents,

representing all three classes of materials (class 1: PEI; class 2: monoamine and diamine; class 3: HAS), supported on a large pore volume mesocellular silica foam material, showed that the stability of the silica support under prolonged steaming conditions may be problematic.³⁸ Under extensive, accelerated steaming conditions, it was shown that high pore volume, thin-walled supports such as mesocellular silica foams break down under conditions used in the study. Although the conditions tested were harsher than would be present in likely cyclic adsorption-desorption processes that employ steam-stripping, it can be generally regarded that the stability of many silica materials, such as the mesoporous foams used in that work, will be too limited for practical application in the presence of steam. In contrast, thicker-walled, lower pore volume supports may impart better stability to the composite adsorbent in the presence of steam, although one might expect all silica materials to degrade to some degree, especially in the presence of amine groups that can act as catalysts for hydrolysis of Si-O-Si bonds. Indeed, the stabilization of silica supported amine materials for use in a steaming environment is a critical research need if this oxide is to be used commercially in this manner.

It should also be noted that nearly entire field of oxide-supported amine sorbents is comprised of silica-supported amines, and other, more hydrolytically stable oxides should be evaluated in future studies that might use steam-regeneration methods. Chaikittisilp et al.³⁹ have reported relatively higher stability for PEI impregnated γ -Alumina adsorbents versus a PEI impregnated SBA-15 materials on contact with steam. This appears to be a promising approach to synthesize supported amine adsorbents that are more stable on exposure to steam.

1.4.4. Pressure Swing Adsorption (PSA) and derivatives

Pressure swing adsorption (PSA) is an alternative regeneration method that can provide a real separation of CO₂ from the adsorbent with no or minimal further purification downstream, unlike TSA/I. Pure PSA uses a partial pressure driving force to drive the CO₂ off the material as opposed to a thermal driving force discussed above. This can be achieved in several ways: pulling vacuum (VSA),^{40–42} operation at two different absolute pressures during adsorption and desorption (PSA), or sweeping with an inert purge gas in the absence of heating (PSA/I).^{25,36,43} PSA can also be used in conjunction with TSA to achieve desorption at lower temperatures with shorter regeneration times.^{27,36,40,44,45} For example, many authors have combined vacuum and temperature swing (T/VSA).^{27,40,44–47} It should be noted that on the large scales expected to be used for CO₂ capture from commercial coal plants, the cost and availability of vacuum equipment of appropriate size may be currently problematic.

Operation under VSA conditions results in a concentrated CO₂ purge stream that may require no additional downstream purification. However, longer desorption times are needed to recover capacity in comparison to TSA.⁴² Sayari has reported numerous studies on regeneration conditions using VSA, TSA/I and V/TSA with class 1 and 2 materials on PE-MCM-41 (class 1: PEI; class 2: monoamine and triamine).^{27,36,40,45} These studies have shown that at lower CO₂ concentration, such as 10% CO₂ in inert as opposed to pure CO₂, VSA can yield a capacity comparable to TSA when operating at 70 °C. Using V/TSA can also yield capacities comparable to TSA, with shorter times for desorption required. However, in a statistical study by Sayari on the effect of various parameters on regeneration, it was determined that there was no benefit in terms of faster desorption or increased recovery when using

vacuum at high desorption temperatures.⁴⁵ This does not take into account the added benefit of the more concentrated CO₂ stream that is recovered after desorption.

Overall, there are several regeneration methods that could be realistically used in an industrial application: (i) CO₂ purge, (ii) steam stripping and (iii) VSA or VTSA. VSA or V/TSA can give a concentrated product stream and can allow for shorter desorption times when vacuum is applied with slight heating, with essentially complete regeneration. Future regeneration studies should use methods such as these so that data relevant to practical desorption methods can be obtained.

1.5. Material Stability

As previously emphasized, capturing CO₂ effectively from power plant flue gas requires processing millions of cubic feet of flue gas every minute.⁴⁸ For an adsorption process with such high throughput, the quantity of adsorbent required will be very large. It is therefore imperative that the adsorbent be sufficiently stable under capture and regeneration conditions. The solid adsorbent must demonstrate adequate performance over at least thousands and ideally many millions of cycles. Power plant flue gas typically contains 10-15% CO₂, 5-10% O₂, 4-5% water vapor, thousands of ppm of SO_x (which must be reduced by scrubbing, in analogy to amine solution capture processes),^{49,50} NO_x (which can be removed by selective catalytic reduction),⁵¹ trace elements like Hg (each by definition less than 100 ppm in concentration) and the balance nitrogen. Apart from nitrogen, which is an inert gas, the effect of all the components in flue gas on adsorbent performance must be carefully evaluated. Any potential adsorbent degradation as a result of each of these components will depend on their partial pressure as well as the temperature at which

they come in contact with the material. The body of knowledge that currently exists with respect to the effects of each of these components on amine-oxide hybrid material stability is presented below, along with the shortcomings that exist in fully understanding the stability of these materials under realistic flue gas concentrations and practical operating conditions.

1.5.1. *Oxidative Degradation*

In the aqueous amine absorption process, which is the benchmark process for CO₂ capture from power plant flue gas, oxidative degradation reactions are responsible for approximately half the overall amine makeup rate, which is about 2.2 kg MEA per tonne of CO₂ captured.^{52–55} A number of reports discuss the oxidation of amines (especially monoethanolamine) in solution. In contrast, there is almost no literature on the oxidative stability of supported amine adsorbents, and thus there is little fundamental understanding of the oxidation of supported amines. The expected differences between supported amine oxidative stability and aqueous amine oxidative stability as well as the information pertaining to studies in the literature that include O₂ in the feed gas are discussed in detail in chapter 6.

1.5.2. *Effect of other acid gases: SO_x & NO_x*

It has been reported that in the aqueous amine absorption process, the presence of SO_x (primarily SO₂) and NO_x (primarily NO) can result in significant amine losses via the formation of heat stable corrosive salts.^{1,56} Flue gas desulfurization (FGD) scrubbers and selective catalytic NO_x reduction (SCR)

equipment can reduce the concentrations of these acid gases to near 10 ppm, so as to limit these degradation losses. The literature on the effect of SO_x and NO_x on supported amines, though limited, indicates that the degradation issues observed in solution processes will also be present in adsorption processes using supported amines, thus necessitating significant sulfur and nitrogen oxide scrubbing prior to CO_2 capture, as noted above. Khatri et al.⁵⁷ studied the adsorption of CO_2 and SO_2 onto aminopropyl functionalized SBA-15 (a class 2 material) and concluded that while adsorption of CO_2 was thermally reversible under the experimental conditions used, SO_2 adsorption was not, resulting in irreversible blocking of potential sites for CO_2 adsorption. In that study, regeneration was carried out by TSA/I, passing argon gas through the sample while simultaneously heating the sample from room temperature to 120°C at $10^\circ\text{C}/\text{min}$. Beckman and co-workers^{58,59} studied the adsorption of all three acid gases: CO_2 , SO_x and NO_x onto amine grafted polymeric adsorbents and reported that the thermal reversibility of the acid gas capture decreased in the order $\text{CO}_2 > \text{SO}_x > \text{NO}_x$. Xu et al.⁶⁰ performed desorption studies of NO_x and CO_2 on PEI impregnated MCM-41 (class 1) by TSA/I, passing inert gas at 90°C over the sample. While the sample exposed to CO_2 could be regenerated completely, the sample exposed to 60-70 ppm NO_x hardly desorbed any NO_x at all. More recently, Belmabkhout et al.³⁶ compared desorption of adsorbents exposed in separate experiments to 0.1 bar of CO_2 and 0.23 mbar of SO_2 . While the CO_2 on the triamine functionalized pore expanded MCM-41 (class 2) was completely desorbed under vacuum at 100°C for 2 hours, only 85% of the SO_2 was desorbed. Each of these studies show that SO_x and NO_x will likely have a detrimental effect on supported amine adsorbent stability, even if ppm levels of SO_x and NO_x are present in the flue gas stream. There is, however, neither a quantitative understanding of the

degradation process nor mechanistic insight into the irreversible adsorption mechanism that would help design amine-oxide hybrid adsorbents for CO₂ capture that are resistant to irreversible acid gas degradation. Studies to elucidate such information are clearly needed.

1.5.3. *Effect of water vapor*

As discussed briefly in section 1.4, in the case of class 1 materials, water vapor has an adverse effect on leaching of organics. Leaching has been discussed in greater detail in section 1.5.5. In the literature, apart from increasing the degree of amine leaching, there are no other reported adverse effects of the presence of water vapor on either the support structure or the chemical stability of amines during the adsorption stage. In fact, in one study on the effect of co-presence of water vapor and CO₂ in the feed on amine-oxide stability, Sayari and co-workers reported that in addition to enhancing the CO₂ adsorption capacity of the adsorbent, water vapor also had a stabilizing effect on the amine groups,³⁶ as discussed in section 1.4.2. Li et al.³⁸ evaluated the stability of sorbents to simulated steaming conditions and reported the appearance of carbonyl groups when all three classes (1,2 and 3) of aminosilica adsorbents were exposed to steam in the co-presence of air. The only exception was aminopropyl functionalized silica, in which case carbonyl groups were not detected. Whether or not these carbonyl groups corresponded to urea linkages was not verified in that particular study. Apart from the adverse effects on the chemical structure of the organic groups, structural collapse of the thin walled mesocellular foam silica support was also found to be partially responsible for the decrease in CO₂ adsorption performance in that work. Unlike oxidation effects, pore collapse was observed both

in the co-presence of steam and air as well as steam and nitrogen. As noted above, steam-stable hybrid amine adsorbents need to be developed.

1.5.4. Effect of mercury & other trace elements

Trace elements in flue gas include several heavy metals like mercury and some lighter elements like boron, beryllium and arsenic.^{61,62} Because of the harmful effects these trace elements have on human health, electrostatic precipitators and fabric filters are used to further reduce their concentrations in the flue gas exhaust.^{61,63} Parts per billion levels of mercury have been detected in absorption units when aqueous MEA was used as the sorbent, without any significant effects on the capture and regeneration performance.⁵³ It seems that the effect of oxidative degradation and degradation by acid gases apart from CO₂ may be more critical compared to irreversible damage caused by mercury and other trace elements. This is further supported by a recent report by Cui et al.,⁶⁴ in which a feasibility analysis was carried out for combined CO₂ and Hg capture using MEA. It was found that combined mercury and CO₂ capture using MEA was not feasible because of the low mercury absorption capacities. It is important to note that no degradation or adverse effect on the CO₂ capture performance of the MEA solution due to the co-presence of mercury was reported. Nonetheless, this topic requires significant further study from an environmental perspective, to assess the fate of these important trace elements in a process that includes post-combustion CO₂ capture using supported amine adsorbents.

1.5.5. Leaching of amines

An important potential degradation pathway for supported amine adsorbents is the leaching of organic groups from the solids, as noted in the above sections. Theoretically, this phenomenon should be more limited in class 2 and class 3 adsorbents due to the covalent bonding between the organic amines and the porous support, and in general, this is what is observed experimentally, although few authors have studied amine leaching with class 2 and class 3 solids, explicitly. In contrast, it might be expected that class 1 adsorbents may be susceptible to leaching of organics since in their case, the amine containing molecules are physically impregnated into the pores without strong chemical bonding between amines and the support. Jones and co-workers were the first to report leaching in class 1 materials for CO₂ capture applications.¹⁷ They observed that during fixed bed runs, the adsorption column became clogged by leached species when PEI-impregnated SBA-15 was tested under humid flue gas conditions at both 25 °C ($R_h = 99\%$) and 75 °C ($R_h = 8\%$). Also, adsorption capacities of TEPA impregnated SBA-15 fell sharply after the first cycle and continued to drop in subsequent cycles when tested using humidified gases. Leaching was identified as the most likely cause of reduction in adsorption capacities, owing to the visible characterization of organic leaching from the solids in the glass reactors.

Chen et al. also reported a drop in cyclic CO₂ adsorption capacities for TEPA impregnated silica monoliths, whereas the PEI impregnated monolith exhibited reversible CO₂ adsorption capacities at 65 and 75°C.⁶⁵ In this case, a thermogravimetric analyzer was used as the adsorption unit and all runs were carried out under dry conditions. Thus, the capacity loss reported may not necessarily be

associated with leaching, and may also be associated with other causes, such as urea formation.^{11,36 19, 89}

In the only report explicitly evaluating leaching of amines in class 2 CO₂ adsorbents, Langeroudi et al. reported that leaching did not occur during the actual adsorption-desorption cycles but did take place during an intermediate treatment step when the samples were immersed in water.⁶⁶ In that study, focused on assessing the stability of amine functionalized SBA-15 in water, the authors performed 24-hour immersion cycles in water at 40°C and found that after the first few immersion cycles about 40% of the amines had leached out of the adsorbent. When the adsorbent was not exposed to liquid water, however, it exhibited highly reproducible CO₂ adsorption capacities over a limited number of cycles. In conclusion, class 2 and class 3 adsorbents have a significant advantage over class 1 adsorbents in that they are more resistant to amine leaching under capture and typical regeneration conditions, although more systematic studies of amine leaching from all classes of materials are needed.

1.6. Critical Materials Research Needs

Based on a critical evaluation of studies reported in the literature, the aspects of amine adsorbents that must be further investigated to enable a more informed evaluation of this class of adsorbent materials as candidates for post-combustion CO₂ capture are as follows:

- 1) Synthesis/incorporation of amine adsorbents into more scalable platforms
- 2) Understanding CO₂ adsorption, desorption kinetics
- 3) Development of adsorbents stable to steam, oxygen, NO_x, and SO_x
- 4) Synthesis of more efficient amine adsorbents
- 5) More practical evaluation of adsorption capacities

The work reported in this dissertation contributes directly to enabling a more fundamental understanding with respect to aspects 2, 3, 4, and 5. CO₂ adsorption kinetics on supported amine adsorbents is discussed in chapters 2 and 3. Chapter 4 describes the setup and validation of an adsorption calorimeter capable of studying surface heterogeneity of supported amine adsorbents. The correlation between adsorption enthalpies and amine efficiencies is explored in chapter 5. Amine structure-oxidative stability relationships are drawn in chapter 6 and the effect of sorbent densities on assessment of adsorbents for post-combustion CO₂ capture is assessed in chapter 7.

1.7. References

- (1) Aaron, D.; Tsouris, C. Separation of CO₂ from flue gas: A review. *Sep. Sci. Technol.* **2005**, *40*, 321-348.
- (2) Ebner, A. D.; Ritter, J. A. State-of-the-art adsorption and membrane separation processes for carbon dioxide production from carbon dioxide emitting industries. *Sep. Sci. Technol.* **2008**, *44*, 37-41.
- (3) Choi, S.; Drese, J. H.; Jones, C. W. Adsorbent Materials for Carbon Dioxide Capture from Large Anthropogenic Point Sources. *ChemSusChem* **2009**, *2*, 796.
- (4) Hedin, N.; Chen, L.; Laaksonen, A. Sorbents for CO₂ capture from flue gas- aspects from materials and theoretical chemistry. *Nanoscale* **2010**, *2*, 1819-41.
- (5) Li, W.; Choi, S.; Drese, J. H.; Hornbostel, M.; Krishnan, G.; Eisenberger, P. M.; Jones, C. W. Steam-stripping for regeneration of supported amine-based CO₂ adsorbents. *ChemSusChem* **2010**, *3*, 899-903.
- (6) Grande, C. a; Ribeiro, R. P. P. L.; Rodrigues, A. E. Challenges of electric swing adsorption for CO₂ capture. *ChemSusChem* **2010**, *3*, 892-8.
- (7) Tsuda, T.; Fujiwara, T. Polyethyleneimine and macrocyclic polyamine silica gels acting as carbon dioxide adsorbents. *J. Chem. Soc., Chem. Commun.* **1992**, *1*, 1659-1661.
- (8) Tsuda, T.; Fujiwara, Y.; Saegusa, T. Amino silica gels acting as carbon dioxide absorbent. *Chem. Lett.* **1992**, *11*, 2161-2164.

- (9) Xu, X.; Song, C.; Andresen, J. M.; Miller, B. G.; Scaroni, A. W. Novel polyethylenimine-modified mesoporous molecular sieve of MCM-41 type as high-capacity adsorbent for CO₂ capture. *Energy Fuels* **2002**, *16*, 1463-1469.
- (10) Tanthana, J.; Chuang, S. S. C. In situ infrared study of the role of PEG in stabilizing silica-supported amines for CO₂ capture. *ChemSusChem* **2010**, *3*, 957-64.
- (11) Drage, T. C.; Arenillas, A.; Smith, K. M.; Snape, C. E. Thermal stability of polyethylenimine based carbon dioxide adsorbents and its influence on selection of regeneration strategies. *Microporous Mesoporous Mater.* **2008**, *116*, 504-512.
- (12) Franchi, R. S.; Harlick, P. J. E.; Sayari, A. Applications of pore-expanded mesoporous silica . 2 . Development of a high-capacity, water-tolerant adsorbent for CO₂. *Ind. Eng. Chem. Res* **2005**, *44*, 8007-8013.
- (13) Kumar, P.; Gulians, V. V. Periodic mesoporous organic–inorganic hybrid materials: Applications in membrane separations and adsorption. *Microporous Mesoporous Mater.* **2010**, *132*, 1-14.
- (14) Acosta, E. J.; Carr, C. S.; Simanek, E. E.; Shantz, D. F. Engineering nanospaces: Iterative synthesis of melamine-based dendrimers on amine-functionalized SBA-15 leading to complex hybrids with controllable chemistry and porosity. *Adv. Mater.* **2004**, *16*, 985-989.
- (15) Rosenholm, J. M.; Linde, M. Wet-Chemical analysis of surface concentration of accessible groups on different amino-functionalized mesoporous SBA-15 silicas. *Chem. Mater.* **2007**, *19*, 5023-5034.

- (16) Rosenholm, J. M.; Penninkangas, A.; Lindén, M. Amino-functionalization of large-pore mesoscopically ordered silica by a one-step hyperbranching polymerization of a surface-grown polyethyleneimine. *Chem. Commun.* **2006**, 3909-11.
- (17) Hicks, J. C.; Drese, J. H.; Fauth, D. J.; Gray, M. L.; Qi, G.; Jones, C. W. Designing Adsorbents for CO₂ Capture from Flue Gas-Hyperbranched Aminosilicas Capable of Capturing CO₂ Reversibly. *J. Am. Chem. Soc.* **2008**, *130*, 2902.
- (18) Caplow, M. Kinetics of carbamate formation and breakdown. *J. Am. Chem. Soc.* **1968**, *90*, 6795-6803.
- (19) Donaldson, T. L.; Nguyen, Y. N. Carbon dioxide reaction kinetics and transport in aqueous amine membranes. *Ind. Eng. Chem. Fundam.* **1980**, *19*, 260-266.
- (20) Vaidya, P. D.; Kenig, E. Y. CO₂-Alkanolamine reaction kinetics: A review of recent studies. *Chem. Eng. Technol.* **2007**, *30*, 1467-1474.
- (21) Qi, G.; Wang, Y.; Estevez, L.; Duan, X.; Anako, N.; Park, A. H. A.; Li, W.; Jones, C. W.; Giannelis, E. P. High Efficiency Nanocomposite Sorbents for CO₂ Capture Based on Amine-functionalized Mesoporous Capsules. *Energy Environ. Sci.* **2011**, *4*, 444.
- (22) Jones, C. W. CO₂ Capture from Dilute Gases as a Component of Modern Global Carbon Management. *Annu. Rev. Chem. Biomol. Eng.* **2011**, *2*, 31.
- (23) Harlick, P. J. E.; Sayari, A. Applications of Pore-Expanded Mesoporous Silica . 5 . Triamine Grafted Material with Exceptional CO₂ Dynamic and Equilibrium Adsorption Performance. *Ind. Eng. Chem. Res.* **2007**, *46*, 446.

- (24) Drese, J. H.; Choi, S.; Lively, R. P.; Koros, W. J.; Fauth, D. J.; Gray, M. L.; Jones, C. W. Synthesis-Structure-Property Relationships for Hyperbranched Aminosilica CO₂ Adsorbents. *Adv. Funct. Mater.* **2009**, *19*, 3821.
- (25) Liang, Z.; Fadhel, B.; Schneider, C. J.; Chaffee, A. L. Stepwise growth of melamine-based dendrimers into mesopores and their CO₂ adsorption properties. *Microporous Mesoporous Mater.* **2008**, *111*, 536-543.
- (26) Belmabkhout, Y.; Sayari, A. Effect of pore expansion and amine functionalization of mesoporous silica on CO₂ adsorption over a wide range of conditions. *Adsorption* **2009**, *15*, 318-328.
- (27) Belmabkhout, Y.; Serna-Guerrero, R.; Sayari, A. Amine-bearing Mesoporous Silica for CO₂ Removal from Dry and Humid Air. *Chem. Eng. Sci* **2010**, *65*, 3695.
- (28) Belmabkhout, Y.; Serna-guerrero, R.; Sayari, A. MCM-41 silica : Application for gas purification. *Ind. Eng. Chem. Res.* **2010**, *49*, 359-365.
- (29) Keskin, S.; van Heest, T. M.; Sholl, D. S. Can metal-organic framework materials play a useful role in large-scale carbon dioxide separations? *ChemSusChem* **2010**, *3*, 879-91.
- (30) Lively, R. P.; Chance, R. R.; Kelley, B. T.; Deckman, H. W.; Drese, J. H.; Jones, C. W.; Koros, W. J. Hollow fiber adsorbents for CO₂ removal from flue gas. *Ind. Eng. Chem. Res.* **2009**, *48*, 7314.
- (31) Ma, X.; Wang, X.; Song, C. "Molecular basket" sorbents for separation of CO₂ and H₂S from various gas streams. *J. Am. Chem. Soc.* **2009**, *131*, 5777-83.

- (32) Lu, C.; Bai, H.; Su, F.; Chen, W.; Hwang, J. F.; Lee, H.-H. Adsorption of carbon dioxide from gas streams via mesoporous spherical-silica particles. *J. Air & Waste Manage. Assoc.* **2010**, *60*, 489-496.
- (33) Zheng, F.; Tran, D. N.; Busche, B. J.; Fryxell, G. E.; Addleman, R. S.; Zemanian, T. S.; Aardahl, C. L. Ethylenediamine-Modified SBA-15 as Regenerable CO₂ Sorbent. *Ind. Eng. Chem. Res.* **2005**, *44*, 3099.
- (34) Gray, M. L.; Hoffman, J. S.; Hreha, D. C.; Fauth, D. J.; Hedges, S. W.; Champagne, K. J.; Pennline, H. W. Parametric study of solid amine sorbents for the capture of carbon dioxide. *Energy Fuels* **2009**, *23*, 4840-4844.
- (35) Liu, Y.; Shi, J.; Chen, J.; Ye, Q.; Pan, H.; Shao, Z.; Shi, Y. Dynamic performance of CO₂ adsorption with tetraethylenepentamine-loaded KIT-6. *Microporous Mesoporous Mater.* **2010**, *134*, 16-21.
- (36) Sayari, A.; Belmabkhout, Y. Stabilization of amine-containing CO₂ adsorbents: dramatic effect of water vapor. *J. Am. Chem. Soc.* **2010**, *132*, 6312-4.
- (37) Kim, S.; Ida, J.; Gulians, V. V.; Lin, J. Y. S. Tailoring pore properties of MCM-48 silica for selective adsorption of CO₂. *J. Phys. Chem. B* **2005**, *109*, 6287-93.
- (38) Li, W.; Bollini, P.; Didas, S. A.; Choi, S.; Drese, J. H.; Jones, C. W. Structural changes of silica mesocellular foam supported amine-functionalized CO₂ adsorbents upon exposure to steam. *ACS Appl. Mater. Interfaces* **2010**, *2*, 3363-72.

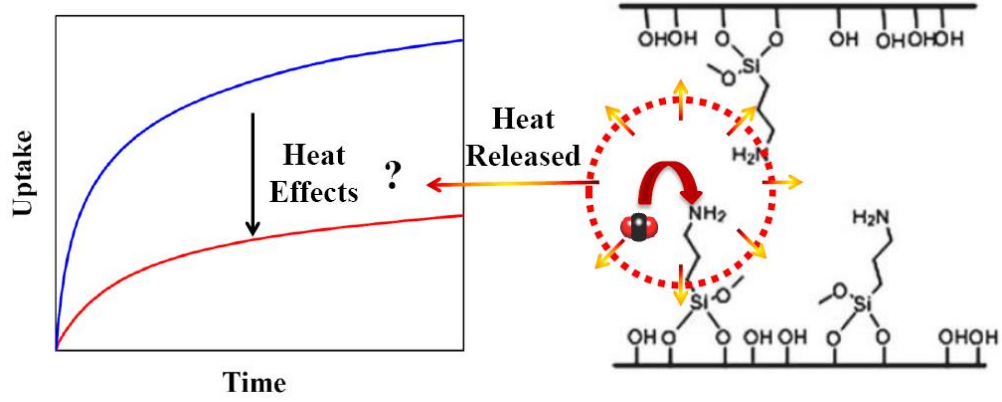
- (39) Chaikittisilp, W.; Kim, H. J.; Jones, C. W. Mesoporous Alumina-Supported Amines as Potential Steam-Stable Adsorbents for Capturing CO₂ from Simulated Flue Gas and Ambient Air. *Energy Fuels* **2011**, *25*, 5528.
- (40) Belmabkhout, Y.; Sayari, A. Isothermal versus Non-isothermal Adsorption–Desorption Cycling of Triamine-Grafted Pore-Expanded MCM-41 Mesoporous Silica for CO₂ Capture from Flue Gas. *Energy Fuels* **2010**, *24*, 5273.
- (41) Chaffee, A. L.; Knowles, G. P.; Liang, Z.; Zhang, J.; Xiao, P.; Webley, P. A. CO₂ capture by adsorption: Materials and process development. *Int. J. Greenhouse Gas Control* **2007**, *1*, 11-18.
- (42) Lu, C.; Su, F.; Hsu, S.-C.; Chen, W.; Bai, H.; Hwang, J. F.; Lee, H.-H. Thermodynamics and regeneration of CO₂ adsorption on mesoporous spherical-silica particles. *Fuel Process. Technol.* **2009**, *90*, 1543-1549.
- (43) Zelenak, V.; Halamova, D.; Gaberova, L.; Bloch, E.; Llewellyn, P. Amine-modified SBA-12 mesoporous silica for carbon dioxide capture: Effect of amine basicity on sorption properties. *Microporous Mesoporous Mater.* **2008**, *116*, 358-364.
- (44) Belmabkhout, Y.; De Weireld, G.; Sayari, A. Amine-Bearing Mesoporous Silica for CO₂ and H₂S Removal from Natural Gas and Biogas. *Langmuir* **2009**, *25*, 13275.
- (45) Serna-Guerrero, R.; Belmabkhout, Y.; Sayari, A. Influence of regeneration conditions on the cyclic performance of amine-grafted mesoporous silica for CO₂ capture: An experimental and statistical study. *Chem. Eng. Sci* **2010**, *65*, 4166-4172.

- (46) Bacsik, Z.; Atluri, R.; Garcia-Bennett, A. E.; Hedin, N. Temperature-induced uptake of CO₂ and formation of carbamates in mesocaged silica modified with n-propylamines. *Langmuir* **2010**, *26*, 10013-24.
- (47) Sanz, R.; Calleja, G.; Arencibia, A.; Sanz-Pérez, E. S. CO₂ Adsorption on Branched Polyethyleneimine-impregnated Mesoporous Silica SBA-15. *Appl. Surf. Sci.* **2010**, *256*, 5323.
- (48) Lively, R. P.; Chance, R. R.; Koros, W. J. Enabling Low-Cost CO₂ Capture via Heat Integration. *Ind. Eng. Chem. Res.* **2010**, *49*, 7550.
- (49) Srivastava, R. K.; Jozewicz, W.; Singer, C. SO₂ scrubbing technologies: A review. *Environ. Prog.* **2001**, *20*, 219-228.
- (50) Rochelle, G. T.; King, C. J. The Effect of Additives on Mass Transfer in CaCO₃ or CaO Slurry Scrubbing of SO₂ from Waste Gases. *Ind. Eng. Chem. Fundam.* **1977**, *16*.
- (51) Valdessolis, T.; Marban, G.; Fuertes, A. B. Low-temperature SCR of NO_x with NH₃ over carbon-ceramic supported catalysts. *Applied Catalysis B* **2003**, *46*, 261-271.
- (52) Chi, S.; Rochelle, G. T. Oxidative degradation of monoethanolamine. *Ind. Eng. Chem. Res.* **2002**, *41*, 4178-4186.
- (53) Strazisar, B. R.; Anderson, R. R.; White, C. M. Degradation pathways for monoethanolamine in a CO₂ capture facility. *Energy Fuels* **2003**, *17*, 1034-1039.
- (54) Sexton, A. J. *Amine oxidation in CO₂ capture processes. Dissertation, University of Texas at Austin*; 2008.

- (55) Goff, G. S.; Rochelle, G. T. Oxidation inhibitors for copper and iron catalyzed degradation of monoethanolamine in CO₂ capture processes. *Ind. Eng. Chem. Res.* **2006**, *45*, 2513-2521.
- (56) Yagi, T.; Shibuya, H.; Sasaki, T. Application of chemical absorption process to CO₂ recovery from flue gas generated in power plants. *Energy Convers. Mgmt.* **1992**, *33*, 349-355.
- (57) Khatri, R. A.; Chuang, S. S. C.; Soong, Y.; Gray, M. Thermal and Chemical Stability of Regenerable Solid Amine Sorbent for CO₂ Capture. *Energy Fuels* **2006**, *196*, 1514.
- (58) Diaf, A.; Garcia, J. L.; Beckman, E. J. Thermally Reversible Polymeric Sorbents for Acid Gases: *J. Appl. Polym. Sci.* **1994**, *53*, 857.
- (59) Diaf, A.; Beckman, E. J. Thermally Reversible Polymeric Sorbents for Acid Gases, IV. Affinity Tuning for the Selective Dry Sorption of NO_x. *React. Polym.* **1995**, *25*, 89.
- (60) Xu, X.; Song, C.; Miller, B. G.; Scaroni, A. W. Adsorption Separation of Carbon Dioxide from Flue Gas of Natural Gas-fired Boiler by a Novel Nanoporous "Molecular Basket" Adsorbent. *Fuel Process. Technol.* **2005**, *86*, 1457.
- (61) Xu, M.; Yan, R.; Zheng, C.; Qiao, Y.; Han, J.; Sheng, C. Status of trace element emission in a coal combustion process: a review. *Fuel Process. Technol.* **2004**, *85*, 215-237.
- (62) Hatanpw, E.; Kajander, K.; Laitinen, T. G.; Piepponen, S.; Revitzer, H. A study of trace element behavior in two modern coal-fired power plants I . Development and

optimization of trace element analysis using reference materials. *Fuel Process. Technol.* **1997**, *51*, 205-217.

- (63) Pavlish, J. H.; Sondreal, E. a; Mann, M. D.; Olson, E. S.; Galbreath, K. C.; Laudal, D. L.; Benson, S. a Status review of mercury control options for coal-fired power plants. *Fuel Process. Technol.* **2003**, *82*, 89-165.
- (64) Cui, Z.; Aroonwilas, A.; Veawab, A. Simultaneous capture of mercury and CO₂ in amine-based CO₂ absorption process. *Ind. Eng. Chem. Res.* **2010**, *49*, 12576-12586.
- (65) Chen, C.; Yang, S.-T.; Ahn, W.-S.; Ryoo, R. Amine-impregnated silica monolith with a hierarchical pore structure: Enhancement of CO₂ capture capacity. *Chem. Commun.* **2009**, 3627-9.
- (66) Langeroudi, E. G.; Kleitz, F.; Iliuta, M. C. Grafted amine/CO₂ interactions in (gas-) liquid-solid adsorption/absorption equilibria. *J. Phys. Chem. C* **2009**, *113*, 21866-21876.



CHAPTER 2

DYNAMICS OF AMINE ADSORBENTS: IMPACT OF HEAT EFFECTS

Parts of this chapter are reproduced from 'Bollini, P.; Brunelli, N. A.; Didas, S. A.; Jones, C. W. Dynamics of CO₂ Adsorption on Amine Adsorbents. 1. Impact of Heat Effects. *Ind. Eng. Chem. Res.* **2012**, *51*, 15145.'

2.1. Background

As explained in chapter 1, amine-oxide hybrid adsorbents have attracted significant attention in recent years as candidates for post-combustion CO₂ capture, owing to their high CO₂ adsorption capacities, exceptional selectivities, and the favorable effect of water on equilibrium adsorption capacities.^{1,2} Other important aspects of adsorbent performance, like adsorbent stability in the presence of flue gas impurities¹⁻⁷ and dynamic adsorption performance^{8,9} have only recently started attracting attention.

Sayari and co-workers⁸ were the first authors to quantitatively investigate rates of CO₂ adsorption on amine functionalized silica materials. CO₂ uptake rates were measured on a gravimetric apparatus and three different models were used to interpret the kinetic data: (i) a pseudo first-order model, (ii) a pseudo second-order model, and (iii) the Avrami kinetic model, which has a variable order that can include non-integer values. Avrami's model, which was found to give the best fit with experimental uptake rates, was then used to model fixed bed column breakthrough measurements. Because the Avrami

model gave a better fit with experimental data, Sayari and co-workers concluded it is a better model to study dynamics of amine adsorbents compared to the other models tested in their study. The authors hypothesized that this may be due to the fact that the Avrami model is capable of taking into account complex reaction mechanisms, unlike pseudo first and pseudo second-order reaction mechanisms. In hypothesizing that it is this complex reaction mechanism that necessitates the use of the Avrami model, the authors assume that the improved fit obtained using the Avrami model was a direct consequence of a physical/chemical phenomenon occurring in the packed bed, not simply the result of using more fitting parameters in the case of the Avrami model. Note that the good correlation between model predictions and experimental data was interpreted as being a result of the complexity of the amine-CO₂ reaction mechanism and not that of CO₂ diffusion through the amine adsorbent. In chapter 3 of this dissertation, for a different set of materials, strong evidence is presented which suggests that diffusion limitations in amine adsorbents with moderate to high amine loadings can adversely affect breakthrough kinetics. Also, in the Sayari study, as a simplifying assumption, both gravimetric uptake measurements and column breakthrough measurements were assumed to occur under isothermal conditions. Given the high heats of CO₂ adsorption onto most amine adsorbents,¹⁰ it is desirable for future studies to quantitatively assess this assumption. The equilibrium model used in the Sayari report corresponds to a heat of adsorption of 67 kJ/mol, which is more than twice the heat of adsorption onto a physisorbant like 13X, for which the assumption of isothermal operation may yield accurate kinetic parameters.^{11,12} Furthermore, in this work, significant bed temperature rises are observed when amine adsorbents are exposed to a gas stream containing CO₂ at partial pressures relevant to flue gas capture (0.1 bar, *vide infra*).

More recently, Yang and co-workers⁹ fit breakthrough curves of Li-LSX, K-LSX, NaX and amine grafted SBA-15 measured at 400 ppm feed CO₂ concentration using isothermal models. While the rate of adsorption and hence heat released might be expected to be smaller in magnitude for a 400 ppm feed concentration versus the 5% CO₂ feed concentration used in Sayari's report, the diffusion coefficients reported were still pseudo diffusion coefficients, because the authors chose to neglect heat effects. Amine grafted SBA-15 exhibited the poorest mass transfer characteristics of all the adsorbents tested in that study. However, because a different bed packing procedure was employed and different flow rates were used for amine grafted SBA-15 and the zeolite adsorbents in that study, direct rate based comparisons cannot be easily drawn from the Yang study. Furthermore, because there is not a good understanding of the importance of heat effects, in general, in supported amine systems, it is possible that the larger degree of spreading of the mass transfer zone in the case of amine-grafted SBA-15 was a result of a combination of heat and mass transfer effects and not just purely mass diffusion effects. In that work, Yang and co-workers suggested that it is the CO₂-amine reaction rate that controls CO₂ breakthrough kinetics and not diffusion to the adsorption site.

In this chapter, we report simultaneous measurements of thermal and concentration breakthroughs in an amine adsorbent packed bed, which made it the first study of its kind in the supported amine adsorbent literature. In addition, detailed heat and mass transfer modeling is carried out to better understand the impact of heat effects on packed bed adsorption kinetics. In the final part of this chapter, the impact of humid feed streams on CO₂ adsorption dynamics is investigated, with the goal of better understanding the performance of these adsorbents under more practically relevant operating conditions.

2.2. Experiments

2.2.1. Materials

The following chemicals were commercially available and used as received: Pluronic 123 (Aldrich), 37% hydrochloric acid (Aldrich), tetraethylorthosilicate (Aldrich), 3-aminopropyltrimethoxysilane (Aldrich), Toluene (Aldrich).

2.2.2. Synthesis

SBA-15 was chosen as the support for this study because of its simple one dimensional, hexagonally arranged pore structure and its widespread use in the amine adsorbent literature.¹³⁻¹⁸ The SBA-15 was synthesized by modifying procedures previously reported in the literature.¹⁹⁻²¹ In a 2 L Erlenmeyer flask, 24 g of the copolymer template, Pluronic 123, was dissolved in 120 ml hydrochloric acid and 636 g distilled water. The solution was stirred for three hours to dissolve the polymer. Then, 46.26 g tetraethylorthosilicate (TEOS) was added to the solution and stirred for 20 hours. During this time, a white precipitate was formed. The solution was then heated to 100°C and maintained at that temperature for 24 hours. The reaction mixture was quenched with distilled water, filtered, and washed with copious amounts of distilled water. The powder was dried overnight in a convection oven at 75°C and then calcined in flowing air at 550°C for 6 hours. The temperature in the calcination oven was first ramped to (1 °C/min) and held at 200°C for 2 hours before being ramped to (1 °C/min) and held at 550°C for 6 hours.

To synthesize amine-functionalized SBA-15 (APS_SBA), the calcined SBA-15 was first dried overnight on a Schlenk line at 120°C. Then, 2 g of SBA-15 was dispersed in 200 ml of toluene with stirring for 3 hours. After this, 2 g 3-aminopropyltrimethoxysilane (APTMS) was added to the solution. The solution was allowed to stir for 24 hours. The resulting solid was then filtered with copious amounts of toluene, dried in a vacuum oven at 50°C overnight and stored in a vial. For packed bed experiments, pellets were pressed under a pressure of 4000 psi and sieved between 150 and 500 microns.

2.2.3. *Material characterization*

The amine loading of the adsorbent was calculated from thermogravimetric analysis experiments. A Netzsch STA409PG TGA was used for this purpose, whereby 10-20 mg of the sample was loaded into the sample pan. The temperature of the furnace was increased from room temperature to 900°C at a rate of 10°C/min under a mixed gas stream of air, flowing at 90 ml/min and nitrogen, flowing at 30 ml/min. The mass loss below 150°C was interpreted as the loss of water and that between 150 and 900°C was interpreted as mass loss resulting from the combustion of organic portion of the adsorbent.²²⁻²⁴ The mass remaining at 900°C is associated with the silica support itself (this assumption is validated by the fact that the silica support itself shows minimal weight loss up to 900°C). A Micromeritics Tristar II was used to carry out nitrogen physisorption measurements. Isotherm data was collected at 77K for porosity characterization. The isotherm data was then fit with appropriate models to calculate the surface areas, pore volumes and average pore diameters. The BET model was used to

calculate surface areas. Powder X-ray diffraction patterns were obtained on a PANalytical X-ray diffractometer using Cu K α radiation.

2.2.4. *Equilibrium CO₂ isotherms*

Equilibrium CO₂ adsorption capacities were measured on a TA Instruments Q500 thermogravimetric analyzer (TGA). In such an experiment, 20-30 mg of the powder sample was loaded onto the sample pan. The adsorbent was heated to 120°C in flowing helium and held at that temperature for 3 hours to desorb any pre-adsorbed CO₂ and water adsorbed from ambient air. The temperature was then ramped down to the desired temperature (25°C/45°C) and allowed to equilibrate in helium for 30 minutes, after which the gas flow was switched to the desired concentration of CO₂. For example, if the capacity was to be measured at 0.1 bar, a 10% CO₂, 90% helium gas was used. Both the helium and CO₂-helium gas flow rates were set to 90 ml/min. The times required to equilibrate were dependent on the adsorbent used and the partial pressure of CO₂ in the furnace. For all runs, the rate of weight change was less than 0.001% wt. per hour when the run was terminated to calculate the adsorption capacity.

2.2.5. *Packed bed CO₂ breakthrough experiments*

Figure 2.1 shows a schematic of the packed bed setup used to study adsorption dynamics. Measurements were carried out in a 1 cm diameter Pyrex tube equipped with a frit to hold the adsorbent particles. Two ports were created in the tube: one immediately downstream of the frit, to enable measurement of outlet gas concentrations using a mass spectrometer (Pfeiffer Vacuum Omnistar) and the other, two thirds of the

way into the bed (i.e. 0.5 cm above the frit), used to insert the hypodermic probe of a type T (Copper-Constantan) thermocouple. This setup allowed for the simultaneous measurement of amine adsorbent bed temperatures and outlet gas concentrations. The volume of the packed bed was kept constant for all breakthrough experiments reported in this study (1.2 cm³). The adsorbent was poured into the Pyrex tube, which was wrapped with heating tape to heat the bed during the desorption step and keep the bed insulated from the surroundings during the adsorption step. Mass flow controllers were used to control both the helium gas (inert purge) as well as the test gas (10% CO₂, balance helium) and 3-way switching valves were used to switch from the purge gas to the test gas. First, helium was flowed through the bed at 20 ml/min while the bed temperature was raised to 120°C. The temperature was held at 120°C for 3 hours, after which it was lowered back to room temperature and allowed to equilibrate at that temperature for 30 minutes. The flow was then switched from helium to the CO₂ containing gas stream while continuously monitoring the outlet gas concentration and bed temperature. For runs with humid feeds, the CO₂ containing gas stream was passed through a Wetsys controlled humidity generator (Setaram Inc.), thus enabling measurements as a function of feed relative humidity. Before the start of the experiment, the mass spectrometer was calibrated with a gas stream containing known concentrations of H₂O and CO₂.

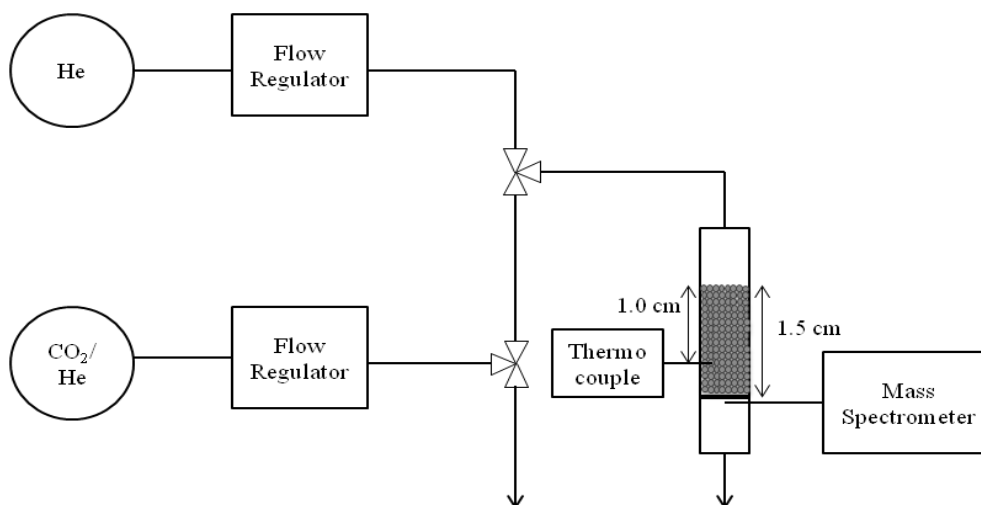


Figure 2.1: Schematic of the packed bed setup used in this study

2.3. Theory

In this section, the underlying assumptions and details of the models used to describe the equilibrium and dynamic behavior of the adsorbents tested in this study are described.

2.3.1. Isotherm models

Sayari and co-workers²⁴ used the two-site Toth isotherm model to describe the equilibrium behavior of amine adsorbents. The Toth isotherm (equations 1 and 2) is a modification of the Langmuir equation. The Langmuir model invokes the assumption of an energetically homogeneous surface, whereas by modifying the Langmuir equation slightly by introducing the parameter t' , surfaces that are non-homogeneous can be modeled. When t' is equal to one, the model reduces to the Langmuir model. The further the parameter t' deviates from unity, the more heterogeneous the adsorbent surface. Sayari et al. used a two-site Toth model, one each for chemisorption and physisorption

of CO₂ molecules, and the saturation capacity n_s and the Toth parameter t' were treated as temperature dependent parameters.

$$q_e = \frac{n_s bP}{(1+(bP)^t)^{1/t'}} \quad (2.1)$$

$$b = b_0 \exp\left(\frac{Q_{ads}}{RT_0} \left(\frac{T_0}{T} - 1\right)\right) \quad (2.2)$$

In this work, we chose to employ a simpler model that assumes only one type of site, but accounts for energetic heterogeneity through the value of the parameter t' . Whereas Sayari and co-workers took into account the temperature dependence of the saturation capacity and the Toth parameter in an empirical manner,²⁵ we have simply added one additional temperature independent parameter, t' , to the Langmuir model to describe the equilibrium isotherm behavior of the amine adsorbents used in this study. The use of this simple model is made possible, in part, by the fact that the isotherms we have used were fit over a much smaller CO₂ partial pressure range (0-0.1 bar) compared to Sayari's study (0-20 bar).

2.3.2. Heat and mass transfer models

Several assumptions were made in deriving column mass and energy balances, as listed below:

- 1) One-dimensional models were used for the mass balance, i.e. concentration gradients in only the axial direction were considered.
- 2) Wall effects were neglected.
- 3) Pressure drop in the bed was neglected.

- 4) Linear velocity of the gas through the bed remains constant.
- 5) The fluid flows through the bed in the form of an axially dispersed plug.
- 6) Only CO₂ adsorption was considered, i.e. the helium diluent was treated as non-adsorbing.
- 7) A linear driving force rate expression was used to describe adsorption kinetics.
- 8) Temperature gradients in only the axial direction were considered. A lumped resistance model was used, wherein all thermal resistances in the radial direction were lumped into the wall heat transfer coefficient.
- 9) Local thermal equilibrium was assumed between the gas and solid phases.
- 10) The temperature dependence of adsorbent mass transfer coefficients and thermal properties were assumed to be negligible.

Wall effects were neglected because the bed to particle diameter ratios were much larger than 10.²⁶ The short length of the adsorbent bed and the low flow rate implies the pressure drop in the bed can be neglected (the pressure drop across the bed corresponding to a 20 ml/min flow rate calculated using the Ergun equation is approximately 1 Pa or 10⁻⁵ bar). Since the maximum mole fraction of adsorbable species in the gas was only 0.1, the gas phase linear velocity can be justifiably assumed to be approximately constant.

The linear driving force model has been widely used to model adsorption processes.²⁷⁻²⁹ The linear driving force constant, k , in equation 2.5, is a lumped parameter that takes into account various resistances to mass transfer. As for the assumptions made with respect to the heat transfer process, Ruthven and co-workers have shown that a simple one dimensional heat transfer model with all the heat transfer resistance lumped together at the wall is sufficient to describe dynamic column behavior

in most systems.^{30,31} Equations 2.3 – 2.8 are the resulting governing equations. The parameter values used in the computations are listed in Table 2.1.

Column Mass Balance:

$$\epsilon D_L \frac{\partial^2 C_A}{\partial Z^2} - U \frac{\partial C_A}{\partial Z} - \rho_B \frac{\partial q}{\partial t} = \epsilon \frac{\partial C_A}{\partial t} \quad (2.3)$$

Column Energy Balance:

$$\begin{aligned} -K_Z \frac{\partial^2 T}{\partial Z^2} + U \rho_g C_g \frac{\partial T}{\partial Z} + (\epsilon \rho_g C_g + (1 - \epsilon) \rho_s C_s) \frac{\partial T}{\partial t} - Q_{ads} \rho_B (1 - \epsilon) \frac{\partial q}{\partial t} + \\ \frac{2h}{R} (T - T_0) = 0 \end{aligned} \quad (2.4)$$

$$\frac{\partial q}{\partial t} = k (q_e - q) \quad (2.5)$$

Initial conditions:

$$@ t=0; \quad q=0, \quad C_A=0, \quad T=T_0 \quad (2.6)$$

Boundary Conditions:

$$C_A(0)=0.1 \quad T(0)=T_0 \quad (2.7)$$

$$\frac{\partial T}{\partial Z} \Big|_{Z=L} = 0 \quad \frac{\partial C_A}{\partial Z} \Big|_{Z=L} = 0 \quad (2.8)$$

Table 2.1. Parameters used in the simulations.

Parameter	Value
D_L	$10^{-5} \text{ m}^2/\text{s}$
ρ_B	$600 \text{ kg}/\text{m}^3$
ρ_g	$0.334 \text{ kg}/\text{m}^3$
ϵ	0.5
C_s	$5100 \text{ J}/\text{kg}\cdot^\circ\text{C}$
C_g	$920 \text{ J}/\text{kg}\cdot^\circ\text{C}$

2.3.3. Simulation of column dynamics

gPROMS (Process Systems Enterprise) was used to simulate the column dynamics. A second order central finite difference scheme was used to discretize the partial differential equations. Two hundred nodes were found to be sufficient to simulate the dynamics. The dynamic simulations took between 5 and 10 seconds to be completed on an Intel Pentium 4 processor. Parameter estimation runs took approximately 4-5 minutes to be completed.

2.4. Results & Discussion

2.4.1. Material characterization

The X-ray diffraction pattern of the bare SBA-15 silica support (Figure 2.2) agrees well with those reported in the literature for SBA-15.³²⁻³⁴ The amine loading (estimated from TGA measurements) and pore characteristics (obtained from nitrogen physisorption measurements) of the SBA-15 support and the aminopropyl functionalized SBA-15 (APS_SBA) are listed in Table 2.2. Incorporation of amine groups resulted in approximately a 60% reduction in surface area, 43% reduction in total pore volume, and 1 nanometer reduction in average pore diameter. The reduction in total surface area, pore volume and average pore diameter suggests that the pore surface of the SBA-15 support is functionalized in addition to the external surface on the outside of each particle.

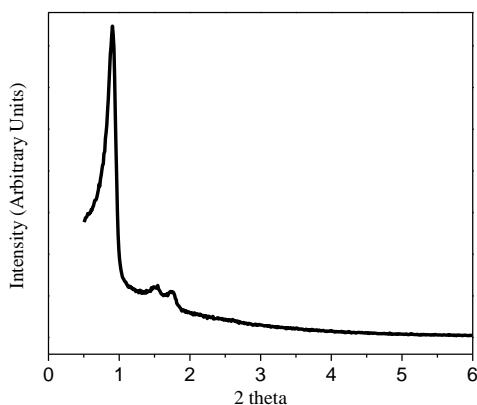


Figure 2.2: XRD pattern of the SBA-15 silica support used in this study.

Table 2.2. Amine loading and pore characteristics of the SBA-15 support and APS_SBA.

	Amine Loading ^a (mmol N/g)	BET Surface Area (m ² /g)	Pore Volume ^b (ml/g)	Pore Diameter ^b (nm)
Support	0	860	1.04	6.5
APS_SBA	2.1	347.2	0.59	5.5

(a) Amine loading estimated using TGA data. (b) Pore volumes and pore diameters for the mesoporous materials obtained using the Broekhoff-de Boer Frenkel Halsey Hill (BdB-FHH) analysis. Amine loading, surface area, and pore volumes are reported per gram dry silica.

2.4.2. Equilibrium Isotherms

Experimentally measured CO₂ adsorption isotherms at 25°C and 45°C are shown in Figure 2.3. As a result of the high heats of adsorption of CO₂ onto primary amines, at low partial pressures, the adsorption capacities rise rapidly as a function of CO₂ partial pressure: an attribute that makes them promising candidates for CO₂ removal from ambient air.^{9,35-45} Figure 2.3 also shows the fits obtained between experimental isotherm data and model predictions obtained using the Toth isotherm parameters listed in Table 2.3. Good agreement between model predictions and experimental data was achieved, both at low (inset) and high partial pressures, and at both 25°C and 45°C.

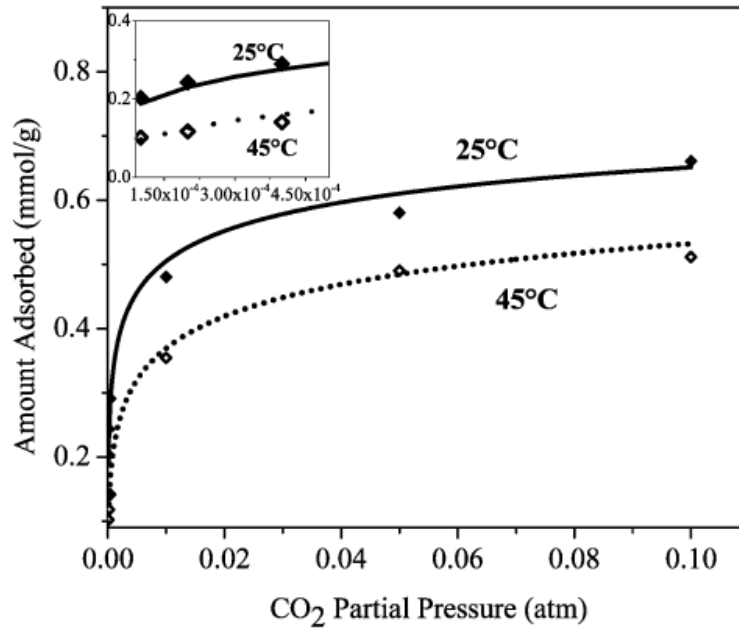


Figure 2.3: Experimentally measured CO₂ adsorption isotherms (inset: low pressure data). Isotherm data reported in mmol CO₂ per g adsorbent (and not per g silica). Solid and dotted curves represent isotherm fits obtained using the Toth isotherm model.

Table 2.3. Optimal Toth isotherm parameters for APS_SBA.

n_s (mol/kg)	b_0 (10^{-10} Pa)	Q_{ads} (kJ/mol)	t
1	300	75	0.22

2.4.3. Packed bed column dynamics

Amine adsorbent breakthrough studies reported in the literature typically only report the outlet concentration of CO₂ as function of time.^{8,9,46,47} However, in this study, temperature measurements inside the amine adsorbent beds are reported for the first

time alongside concentration breakthrough measurements at the outlet to yield additional insights into the interaction between heat and mass transfer effects in the packed bed. The measured concentrations and temperatures during CO₂ breakthrough experiments are shown in Figure 2.4. The concentration is normalized by the feed concentration and the absolute temperature normalized by the ambient temperature. Breakthrough occurred at approximately 220 seconds and saturation of the adsorbent bed was complete at approximately 900 seconds. The temperature profile measured at a distance of 1 cm into the bed (two thirds of the way into the adsorbent bed) starts rising almost immediately after the feed gas is switched to 10% CO₂ in helium. This immediate rise in temperature suggests that the thermal front reaches 1 cm into the bed before the concentration front does, indicating that under the experimental conditions of this study, the thermal front precedes the mass transfer front. Note that even though the thermal front moves at a faster velocity compared to the mass transfer front, they are not necessarily independent of each other since there is an overlap between the two as a result of the disperse nature of both fronts. The amplitude of the thermal wave is 0.25. This corresponds to a temperature rise of 5.6°C. Despite using gas velocities of only a few mm/sec, a significant rise in bed temperature was detected. Tests were only conducted at low flow rates (particle Reynolds number of 0.05) due to the small size of the adsorbent bed. To understand how the rise in bed temperature affects breakthrough, adsorption breakthrough behavior was modeled as described below.

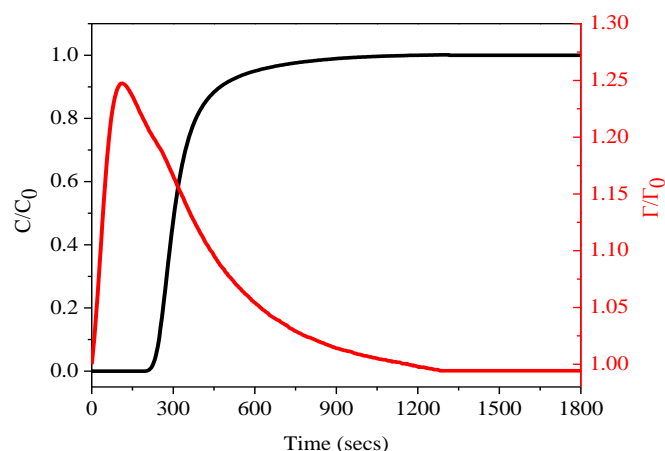


Figure 2.4. Breakthrough curve and temperature profile for the APS_SBA packed bed.

2.4.4. Computational Analysis of Adsorption Breakthrough

To better understand the interactions between heat and mass transfer effects and to assess accurately the kinetic performance of the amine functionalized SBA-15 material, the models outlined above were used to computationally model the adsorption process. Figure 2.5 shows the fits obtained between predicted and experimentally measured concentration breakthrough and temperature profiles. Good agreement was achieved between model predictions and experiments for the breakthrough curve. Both the breakthrough time and the shape of the breakthrough were modeled accurately. The agreement between model predictions and experiments for the temperature profile were also reasonably good, but not as accurate as the breakthrough. One possible reason why only moderately good fits for the temperature profile were achieved versus excellent fits for the concentration breakthrough curve may be that the solid and gas phases were assumed to be at equilibrium at all times. In reality, there is a finite rate of heat transfer from the adsorbent particle, where heat is generated as a result of adsorption, and the

gas phase, which helps carry away that heat. At low Reynolds numbers, as is the case with our experiments, it is possible that the assumption of equilibrium between the two phases is not entirely valid. Naturally, the higher the heat transfer rate between the solid and gas phases, the closer the two phases are to equilibrium, and the less spread out the temperature profiles in the packed bed. This explains why the models described in this study predict temperature profiles that are less dispersed compared to those measured experimentally (Figure 2.5). In theory, this hypothesis can be tested by implementing energy balances separately on the solid and gas phases and coupling them through a heat transfer rate term. However, to obtain the most accurate heat transfer model to describe CO₂ adsorption dynamics was not the aim of this study. Rather, our goal was to use simple mass and heat transfer models that could allow us to study the interaction between heat and mass transfer effects with sufficient accuracy, thereby enabling us to gain insights into the possible impact of heat effects on laboratory-scale packed bed CO₂-amine adsorption kinetics. Therefore, a parametric study was carried out to investigate the effect of heat released on packed bed breakthrough.

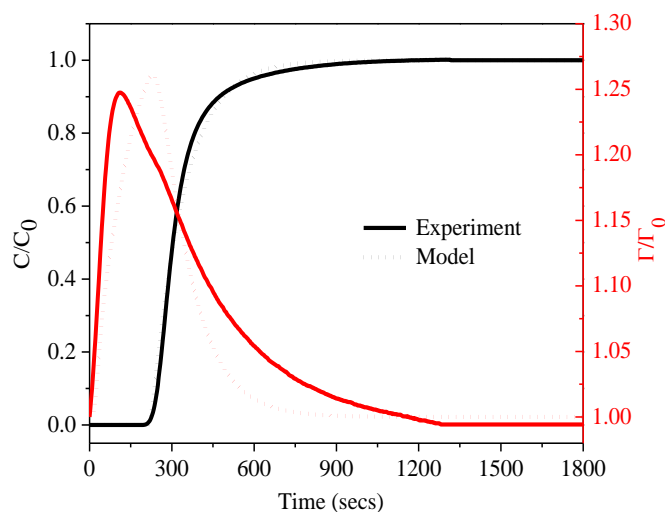


Figure 2.5: Fits obtained between predicted and experimental breakthrough curves, temperature profiles

2.4.5. Parametric study

Table 2.4 shows the optimal values of the fitting parameters used to generate the simulated temperature and concentration profiles. The wall heat transfer coefficient does not have any detectable effect on the simulated concentration breakthrough and temperature profile curves (Figure 2.6). This result implies that under the experimental conditions relevant to this study, axial conduction is the major pathway for heat loss from the bed and not heat loss to the adsorber walls. This is likely due to the heavy layer of heating tape surrounding the Pyrex tube that prevents rapid heat loss through the walls. This is further evident upon studying the effect of axial bed thermal conductivity on model predictions (Figure 2.7). Although the axial bed thermal conductivity has a significant effect on the temperature profile, it does not affect the breakthrough curve. As the thermal conductivity of the bed decreases, more heat is accumulated in the bed,

resulting in a larger temperature rise. This is the first indication that CO₂ breakthrough under these conditions is relatively insensitive to bed temperature profiles. The only parameter that has any observable impact on the breakthrough curve is the linear driving force constant k . As shown in Figure 2.8, a 50% reduction in the linear driving force constant resulted in an under-prediction of the sharpness of the breakthrough front, i.e. the adsorption kinetics.

Table 2.4: Optimal values of parameters used to fit models with the experimental data.

k (sec ⁻¹)	Kz (W/m.K)	h (W/m ² .K)
0.012	1.76	0.88

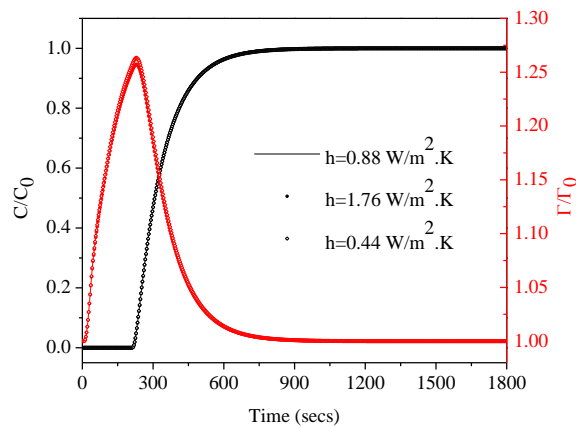


Figure 2.6. Effect of wall heat transfer coefficient on simulated breakthrough curve and temperature profile.

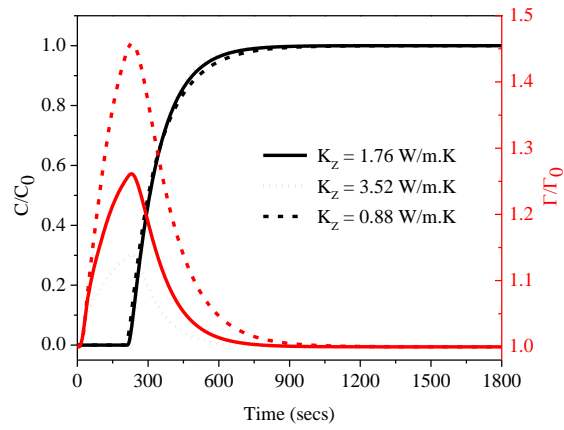


Figure 2.7. Effect of effective axial bed thermal conductivity on simulated breakthrough curve and temperature profile.

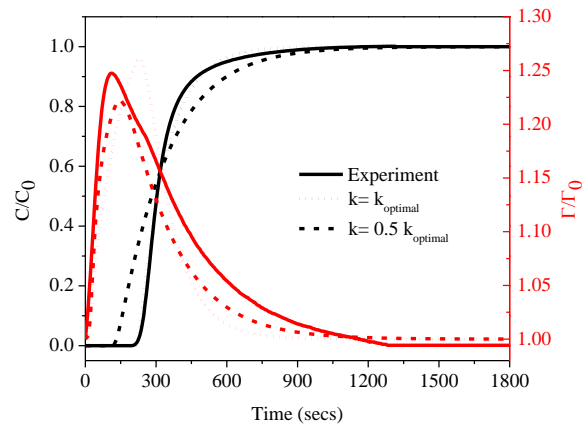


Figure 2.8: Effect of linear driving force constant, k , on simulated breakthrough curve and temperature profile

2.4.6. *Effect of heat removal*

One of the motivations behind this modeling study of the heat and mass transfer dynamics was to investigate how heat effects alter the dynamic adsorption performance of amine adsorbents. Figure 2.9 shows the effect of heat removal on the simulated breakthrough curve by comparing the optimal non-isothermal model prediction with the isothermal model prediction, obtained by assuming all parameters except for the wall heat transfer coefficient to be the same. For the isothermal case, the wall heat transfer coefficient was increased until the temperature rise in the bed was less than 0.001°C . The results show that heat removal has minimal effect on the breakthrough curve. These results lead to two important conclusions. First, despite the fact that the amine adsorbent tested in this study results in a significant temperature spike in the adsorbent bed due to the high enthalpy of CO_2 adsorption on amine sites, the large local rise in temperature does not necessarily have an adverse effect on CO_2 breakthrough. Secondly, the results suggest that isothermal models are sufficient to predict breakthrough behavior under the conditions used here. As discussed previously, when the value of k was lowered to 50% of its optimal value and its effect on the breakthrough evaluated, it was found that this reduction in the linear driving force constant resulted in a much more dispersed breakthrough compared to the experimentally measured ones. Thus, under the experimental conditions relevant to this study, use of the right linear driving force constant, which represents the rate of mass transfer corresponding to the adsorbent and hence the shape of the breakthrough, is much more critical for accurate modeling results compared to explicit modeling of heat transfer effects, despite the fact that the amine adsorbent systems are highly non-isothermal during the breakthrough experiments.

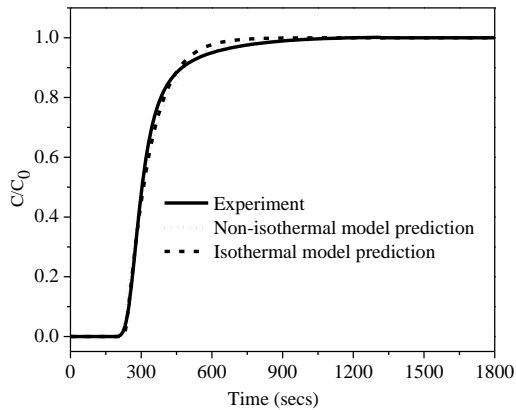


Figure 2.9: Comparison of isothermal and non-isothermal model predictions at the optimal linear driving force constant value

2.4.7. Dynamics under wet feed conditions

The breakthrough data discussed so far in this chapter was measured under dry conditions. As emphasized in chapter 1, performance under humid conditions is extremely important to evaluate from a practical perspective, since flue gas is saturated with water vapor. Figure 2.10 shows the breakthrough data obtained as a function of relative humidity of the feed gas. As the relative humidity of the feed gas increases, the water vapor breakthrough time decreases, while the CO₂ breakthrough curve remains unchanged. Furthermore, the CO₂ breakthrough measured using humid feeds was indistinguishable from that measured using a dry feed. This is an unexpected result, since relative humidity is expected to have a favorable effect on breakthrough, due to the higher amine efficiencies generally observed under humid conditions versus dry conditions (chapter 1, section 1.3). What was observed, however, is that under dynamic conditions, the breakthrough time for water even at relative humidities as high as 70%

are more than an order of magnitude higher than those for CO₂. This large difference in breakthrough times is a result of two factors. Firstly, amine functionalized silicas have been shown to have exceptionally high water adsorption capacities, sometimes as high as 23 mmol H₂O/g.⁴⁵ Secondly, in these experiments, the concentration of water vapor in the feed is much lower than that of CO₂. For example, at 25°C and 70% relative humidity, the water vapor concentration in the feed is approximately 2%, whereas that for CO₂ is slightly lower than 10%. This combination of high water adsorption capacities and low feed concentrations results in extremely slow movement of the water vapor front relative to the CO₂ front, thereby causing delayed water breakthrough. This set of data, which is consistent with another literature report,⁴⁸ shows that for amine adsorbents that are highly hydrophilic, co-presence of humidity in the feed may not necessarily impact the dynamic performance of the bed due to the lack of bed penetration by the water vapor front.

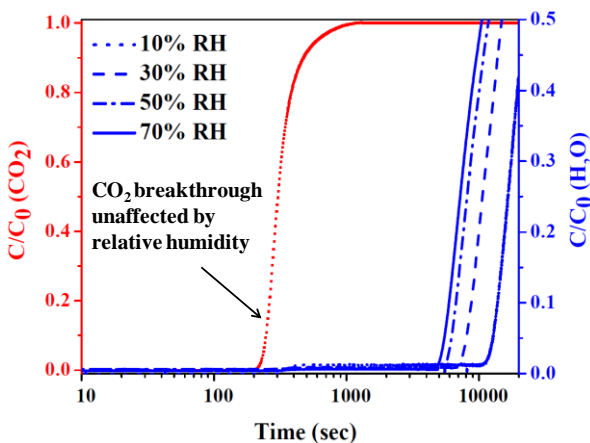


Figure 2.10: Effect of feed relative humidity on CO₂ breakthrough. The CO₂ breakthrough data for the dry case and the four different relative humidities are represented as one curve, since they all overlap.

2.4.8. *Relevance to realistic operating conditions*

Several authors have studied heat effects in packed beds.^{30,31,47,49–52} In general, these reports agree that finite rates of heat transfer to adsorber walls result in long tails in breakthrough curves. Because of the high heat of CO₂ adsorption onto primary amines, the observation that heat effects have only a minimal effect on breakthrough is a surprising and even a somewhat counterintuitive result. It must be noted though, that we do not suggest that heat effects in amine adsorbent packed beds can be neglected at *all* times in *all* laboratory scale experiments. Rather, we suggest that the experimental conditions in this study are such that heat effects are not as important as mass diffusion effects to the overall adsorption kinetics. A careful assessment of experimental conditions in any specific study is needed before making any assumptions regarding the importance of heat effects.

The models implemented in this study allow the simulation of different experimental conditions to test the effect of heat released on breakthrough for a number of different experimental conditions. For example, isothermal and non-isothermal model predictions for a feed gas velocity five times those in our experiments have been compared. Column dynamics were simulated with exactly the same parameters as those used for the run in Figure 2.9 (the optimal set of parameters), except for the use of higher flow rates and a deeper adsorbent bed. The adsorbent bed length was increased by the same factor as the feed gas velocity so breakthrough curves could be compared on the same time scale as the original experimental run. This test was designed to assess if the increased adsorption rate in the bed as a result of higher flow rates and the consequent larger temperature rise would have an adverse effect on CO₂ breakthrough. The non-isothermal and isothermal model predictions are shown in Figure 2.11. In this case, model predictions yielded a temperature rise of 32.5°C, which is significantly

higher than the 5.6°C rise measured and simulated for the lower flow rate (*vide supra*). As a result of the higher temperature rise, the non-isothermal model predicts premature breakthrough followed by a long tail, whereas if enough heat is removed from the system such that an isothermal process is realized, a sharp breakthrough with no observable tail is predicted. Note that since the same linear driving force constant that corresponded to experiments at a flow rate of 20 ml/min was used to simulate the run at 100 ml/min. This means that the temperature rise estimated from simulation for that run is likely on the lower side since we expect that the linear driving force constant value would increase with flow rate.

These results further emphasize the fact heat effects for CO₂-amine adsorption are important to investigate and understand from a practical standpoint, despite the fact that in our lab scale experiments they have an insignificant effect on adsorption kinetics. Heat effects would also likely scale very differently in beds with larger diameters where the wall heat transfer area per unit volume adsorbent would be significantly lower.

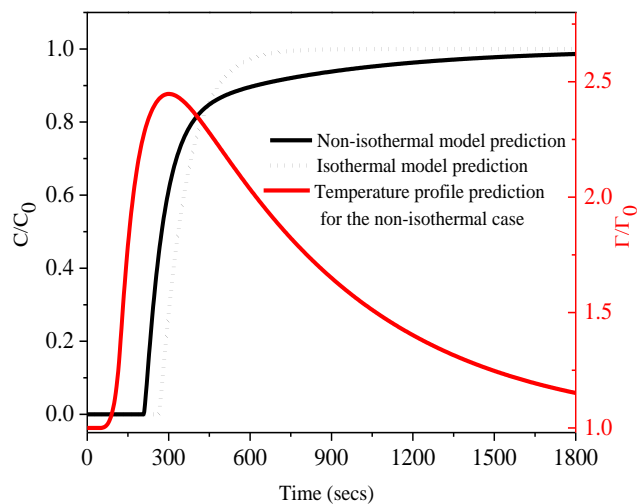


Figure 2.11: Comparison of isothermal and non-isothermal model predictions for feed gas velocities five times those in the packed bed experiments

It should be further noted that the packed bed configuration may not be ideally suited for CO₂ capture from coal-fired power plant exhaust and that other more thermally manageable configurations like monoliths⁵³ and hollow fiber sorbents⁵⁴ have been evaluated in the literature. In this study, packed beds were used to study dynamics because CO₂ breakthrough measurements on amine adsorbent packed beds are abundant in the literature. With the exception of Sayari and Yang's groups,^{8,9} none have used these breakthrough measurements to obtain kinetic parameters. One factor that may be hypothesized to prevent researchers from obtaining accurate kinetic parameters from breakthrough experiments is heat effects associated with adsorption exotherms. The results in this study show that under certain experimental conditions, breakthrough kinetics for amine adsorbents can be accurately analyzed by simply ignoring heat effects. In the next chapter, we show that this conclusion is also valid for amine adsorbents with higher amine loadings and higher CO₂ adsorption capacities. The models described here are also used to gain insights into the design of faster cycling amine adsorbents and not just materials with large CO₂ adsorption capacities, on which the academic community has almost singularly focused to date.

2.5. Conclusions

Packed bed mass and heat transfer using a typical amine functionalized silica material were investigated both experimentally and theoretically. Both heat and mass transfer processes in amine packed beds were modeled successfully. CO₂ breakthrough was found to be insensitive to the thermal behavior of the adsorbent bed under the conditions used. Model predictions indicate that under the experimental conditions relevant to this study, heat effects did not have a significant effect on adsorption kinetics.

However, if higher flow rates are used, larger temperature spikes could result in adverse effects on CO₂ breakthrough and in these cases, heat effects would have to be taken into account when obtaining kinetic parameters from fixed bed breakthrough experiments. While heat effects still remain an important factor to consider for CO₂-amine adsorption, our results indicate that experimental conditions exist under which kinetic parameters may be obtained using relatively simple isothermal models.

2.6. Notation

n_s : Saturation capacity

b : Affinity parameter

b_0 : Affinity parameter at reference temperature

t' : Toth heterogeneity parameter

z : Distance in the axial direction (m)

t : Time (s)

ε : Bed void fraction

R : Radius of the packed bed (m)

L : Length of the packed bed (m)

ρ_B : Adsorbent bulk density (kg/m³)

ρ_S : Solid density (kg/m³)

ρ_g : Gas density (kg/m³)

C_g : Gas phase specific heat capacity (J/kg.°C)

C_s : Solid phase specific heat capacity (J/kg. °C)

C_A : Adsorbate gas phase concentration (mol/m³)

C : Adsorbate concentration at the outlet of the bed (mol/m³)

C_0 : Adsorbate concentration in the feed (mol/m³)

q : Adsorbed phase concentration (mol/kg)

q_e : Equilibrium adsorbed phase concentration (mol/kg)

Γ : Gas temperature (°C)

Γ_0 : Ambient temperature (°C)

T : Gas temperature (K) ($\Gamma+273.15$)

T_0 : Ambient temperature (K) ($\Gamma_0+273.15$)

P : Gas pressure (N/m²)

U : Gas superficial velocity (m/s)

D_L : Axial dispersion coefficient (m²/s)

K_z : Effective bed thermal conductivity in the axial direction (W/m.°C)

k : Linear driving force constant (s⁻¹)

Q_{ads} : Heat of adsorption at zero surface coverage (J/mol)

h : Wall heat transfer coefficient (W/m². °C)

2.7. References

- (1) Choi, S.; Drese, J. H.; Jones, C. W. Adsorbent Materials for Carbon Dioxide Capture from Large Anthropogenic Point Sources. *ChemSusChem* **2009**, *2*, 796.
- (2) Bollini, P.; Didas, S. A.; Jones, C. W. Amine-oxide Hybrid Materials for Acid Gas Separations. *J. Mater. Chem.* **2011**, *21*, 15100.
- (3) Diaf, A.; Garcia, J. L.; Beckman, E. J. Thermally Reversible Polymeric Sorbents for Acid Gases: *J. Appl. Polym. Sci.* **1994**, *53*, 857.
- (4) Diaf, A.; Beckman, E. J. Thermally Reversible Polymeric Sorbents for Acid Gases, IV. Affinity Tuning for the Selective Dry Sorption of NO_x. *React. Polym.* **1995**, *25*, 89.
- (5) Khatri, R. A.; Chuang, S. S. C.; Soong, Y.; Gray, M. Thermal and Chemical Stability of Regenerable Solid Amine Sorbent for CO₂ Capture. *Energy Fuels* **2006**, *196*, 1514.
- (6) Xu, X.; Song, C.; Miller, B. G.; Scaroni, A. W. Adsorption Separation of Carbon Dioxide from Flue Gas of Natural Gas-fired Boiler by a Novel Nanoporous "Molecular Basket" Adsorbent. *Fuel Process. Technol.* **2005**, *86*, 1457.
- (7) Belmabkhout, Y.; Sayari, A. Isothermal versus Non-isothermal Adsorption–Desorption Cycling of Triamine-Grafted Pore-Expanded MCM-41 Mesoporous Silica for CO₂ Capture from Flue Gas. *Energy Fuels* **2010**, *24*, 5273.

- (8) Serna-Guerrero, R.; Sayari, A. Modeling Adsorption of CO₂ on Amine-functionalized Mesoporous Silica. 2: Kinetics and Breakthrough Curves. *Chem. Eng. J.* **2010**, *161*, 182.
- (9) Stuckert, N. R.; Yang, R. T. CO₂ Capture from the Atmosphere and Simultaneous Concentration Using Zeolites and Amine-grafted SBA-15. *Environ. Sci. Technol.* **2011**, *45*, 10257.
- (10) Knofel, C.; Martin, C.; Hornebecq, V.; Llewellyn, P. L. Study of Carbon Dioxide Adsorption on Mesoporous Aminopropylsilane-Functionalized Silica and Titania Combining Microcalorimetry and in Situ Infrared Spectroscopy. *J. Phys. Chem. C* **2009**, *113*, 21726.
- (11) Yoo, J.; Cho, S. H.; Yang, T. Comparison of Activated Carbon and Zeolite 13X for CO₂ Recovery from Flue Gas by Pressure Swing Adsorption. *Langmuir* **1995**, *34*, 591.
- (12) Rezaei, F.; Mosca, A.; Webley, P.; Hedlund, J.; Xiao, P. Comparison of Traditional and Structured Adsorbents for CO₂ Separation by Vacuum-Swing Adsorption. *Ind. Eng. Chem. Res.* **2010**, *49*, 4832.
- (13) Drese, J. H.; Choi, S.; Lively, R. P.; Koros, W. J.; Fauth, D. J.; Gray, M. L.; Jones, C. W. Synthesis-Structure-Property Relationships for Hyperbranched Aminosilica CO₂ Adsorbents. *Adv. Funct. Mater.* **2009**, *19*, 3821.
- (14) Sanz, R.; Calleja, G.; Arencibia, A.; Sanz-Pérez, E. S. CO₂ Adsorption on Branched Polyethyleneimine-impregnated Mesoporous Silica SBA-15. *Appl. Surf. Sci.* **2010**, *256*, 5323.

- (15) Zheng, F.; Tran, D. N.; Busche, B. J.; Fryxell, G. E.; Addleman, R. S.; Zemanian, T. S.; Aardahl, C. L. Ethylenediamine-Modified SBA-15 as Regenerable CO₂ Sorbent. *Ind. Eng. Chem. Res.* **2005**, *44*, 3099.
- (16) Yan, X.; Zhang, L.; Zhang, Y.; Yang, G.; Yan, Z. Amine-Modified SBA-15 : Effect of Pore Structure on the Performance for CO₂ Capture. *Ind. Eng. Chem. Res.* **2011**, *50*, 3220.
- (17) Khatri, R. A.; Chuang, S. S. C.; Soong, Y.; Gray, M. Carbon Dioxide Capture by Diamine-Grafted SBA-15: A Combined Fourier Transform Infrared and Mass Spectrometry Study. *Ind. Eng. Chem. Res.* **2005**, *44*, 3702.
- (18) Shiels, R. A.; Jones, C. W. Homogeneous and heterogeneous 4-(N,N-dialkylamino)pyridines as effective single component catalysts in the synthesis of propylene carbonate. *J. Mol. Catal. A: Chem.* **2007**, *261*, 160.
- (19) Hicks, J. C.; Drese, J. H.; Fauth, D. J.; Gray, M. L.; Qi, G.; Jones, C. W. Designing Adsorbents for CO₂ Capture from Flue Gas-Hyperbranched Aminosilicas Capable of Capturing CO₂ Reversibly. *J. Am. Chem. Soc.* **2008**, *130*, 2902.
- (20) Bu, X.; Feng, P.; Gier, T. E.; Zhao, D.; Stucky, G. D. Hydrothermal Synthesis and Structural Characterization of Zeolite-like Structures Based on Gallium and Aluminum Germanates. *J. Am. Chem. Soc.* **1998**, *120*, 13389.
- (21) Hicks, J. C.; Jones, C. W. Controlling the Density of Amine Sites on Silica Surfaces Using Benzyl Spacers. *Langmuir* **2006**, *22*, 2676.
- (22) Bass, J. D.; Katz, A. Thermolytic Synthesis of Imprinted Amines in Bulk Silica. *Chem. Mater.* **2003**, *15*, 2757.

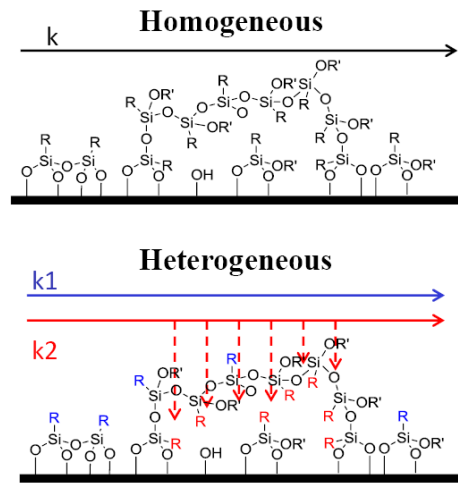
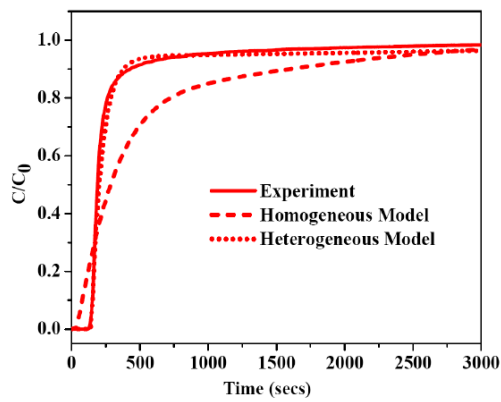
- (23) Brunelli, N. A.; Venkatasubbaiah, K.; Jones, C. W. Cooperative Catalysis with Acid – Base Bifunctional Mesoporous Silica : Impact of Grafting and Co-condensation Synthesis Methods on Material Structure and Catalytic Properties. *Chem. Mater.* **2012**, *24*, 2433.
- (24) Serna-Guerrero, R.; Belmabkhout, Y.; Sayari, A. Modeling CO₂ Adsorption on Amine-functionalized Mesoporous Silica: 1. A Semi-empirical Equilibrium Model. *Chem. Eng. J.* **2010**, *161*, 173.
- (25) Do, D. D. Adsorption Analysis: Equilibria and Kinetics. In *Adsorption Analysis: Equilibria and Kinetics*; p. Imperial College Press: London, 1998.
- (26) Ruthven, D. M. *Principles of Adsorption & Adsorption Processes*; pp. John Wiley & Sons: New York, 1984.
- (27) Sircar, S.; Hufton, J. R.; Products, A. Why Does the Linear Driving Force Model for Adsorption Kinetics Work? *Adsorption* **2000**, *6*, 137.
- (28) Sircar, S. Linear-driving-force Model for Non-isothermal Gas Adsorption Kinetics. *J. Chem. Soc., Faraday Trans.* **1983**, *79*, 785.
- (29) Li, Z.; Yang, R. T. Concentration Profile for Linear Driving Force Model for Diffusion in a Particle. *AIChE J.* **1999**, *45*, 196.
- (30) Farooq, S.; Ruthven, D. M. Heat effects in adsorption column dynamics. 1. Comparison of one- and two-dimensional models. *Ind. Eng. Chem. Res.* **1990**, *29*, 1076.

- (31) Farooq, S.; Ruthven, D. M. Heat Effects in Adsorption Column Dynamics. 2. Experimental Validation of the One-Dimensional Model. *Ind. Eng. Chem. Res.* **1990**, *29*, 1084.
- (32) Zhao, D.; Sun, J.; Li, Q.; Stucky, G. D.; Barbara, S. Morphological Control of Highly Ordered Mesoporous Silica SBA-15. *Chem. Mater.* **2000**, *22*, 275.
- (33) Kruk, M.; Jaroniec, M.; Ko, C. H.; Ryoo, R. Characterization of the Porous Structure of SBA-15. *Chem. Mater.* **2000**, *12*, 1961.
- (34) Han, Y.-J.; Kim, J. M.; Stucky, G. D. Preparation of Noble Metal Nanowires Using Hexagonal Mesoporous Silica SBA-15. *Chem. Mater.* **2000**, *12*, 2068.
- (35) Jones, C. W. CO₂ Capture from Dilute Gases as a Component of Modern Global Carbon Management. *Annu. Rev. Chem. Biomol. Eng.* **2011**, *2*, 31.
- (36) Choi, S.; Drese, J. H.; Eisenberger, P. M.; Jones, C. W. Application of Amine-tethered Solid Sorbents for Direct CO₂ Capture from the Ambient Air. *Environ. Sci. Technol.* **2011**, *45*, 2420.
- (37) Choi, S.; Gray, M. L.; Jones, C. W. Amine-tethered Solid Adsorbents Coupling High Adsorption Capacity and Regenerability for CO₂ Capture from Ambient Air. *ChemSusChem* **2011**, *4*, 628.
- (38) Gebald, C.; Wurzbacher, J. A.; Tingaut, P.; Zimmermann, T.; Steinfeld, A. Amine-based Nanofibrillated Cellulose as Adsorbent for CO₂ Capture From Air. *Environ. Sci. Technol.* **2011**, *45*, 9101.

- (39) Wurzbacher, J. A.; Gebald, C.; Steinfeld, A. Separation of CO₂ from Air by Temperature-vacuum Swing Adsorption Using Diamine-functionalized Silica Gel. *Energy Environ. Sci.* **2011**, *4*, 3584.
- (40) Belmabkhout, Y.; Serna-Guerrero, R.; Sayari, A. Amine-bearing Mesoporous Silica for CO₂ Removal from Dry and Humid Air. *Chem. Eng. Sci.* **2010**, *65*, 3695.
- (41) Wang, X.; Ma, X.; Schwartz, V.; Clark, J. C.; Overbury, S. H.; Zhao, S.; Xu, X.; Song, C. A Solid Molecular Basket Sorbent for CO₂ Capture From Gas Streams With Low CO₂ Concentration Under Ambient Conditions. *Phys. Chem. Chem. Phys.* **2012**, *14*, 1485.
- (42) Chaikittisilp, W.; Khunsupat, R.; Chen, T. T.; Jones, C. W. Poly(allylamine) - Mesoporous Silica Composite Materials for CO₂ Capture from Simulated Flue Gas or Ambient Air. *Ind. Eng. Chem. Res.* **2011**, *50*, 14203.
- (43) Chaikittisilp, W.; Kim, H. J.; Jones, C. W. Mesoporous Alumina-Supported Amines as Potential Steam-Stable Adsorbents for Capturing CO₂ from Simulated Flue Gas and Ambient Air. *Energy Fuels* **2011**, *25*, 5528.
- (44) Chaikittisilp, W.; Lunn, J. D.; Shantz, D. F.; Jones, C. W. Poly(L-lysine) Brush-Mesoporous Silica Hybrid Material as a Biomolecule-Based Adsorbent for CO₂ Capture from Simulated Flue Gas and Air. *Chem. Eur. J.* **2011**, *17*, 10556.
- (45) S.A. Didas, A.R. Kulkarni, D.S. Sholl, C. W. J. Role of Amine Structure on CO₂ Adsorption from Ultra-dilute Gas Streams such as Ambient Air. *ChemSusChem* **2012**, *5*, 2058.

- (46) Belmabkhout, Y.; De Weireld, G.; Sayari, A. Amine-Bearing Mesoporous Silica for CO₂ and H₂S Removal from Natural Gas and Biogas. *Langmuir* **2009**, *25*, 13275.
- (47) Kim, J.; Chue, K.; Kim, K.; Choi, S. Non-isothermal Adsorption of Nitrogen-Carbon Dioxide Mixture in a Fixed Bed of Zeolite-X. *J. Chem. Eng. Jpn.* **1994**, *27*, 45.
- (48) Rezaei, F.; Lively, R. P.; Labreche, Y.; Chen, G.; Fan, Y.; Koros, W. J.; Jones, C. W. Aminosilane-grafted polymer/silica hollow fiber adsorbents for CO₂ capture from flue gas. *ACS Appl. Mater. Interfaces* **2013**, *5*, 3921-31.
- (49) Sircar, S.; Kumar, R. Adsorption of a Dilute Adsorbate: Effects of Small Changes in Column Temperature. *Ind. Eng. Chem. Process Des. Dev.* **1983**, *22*, 280.
- (50) Sircar, S.; Kumar, R.; Anselmo, K. Effects of Column Nonisothermality or Nonadiabaticity on the Adsorption Breakthrough Curves. *Ind. Eng. Chem. Process Des. Dev.* **1983**, *22*, 10.
- (51) Hwang, K.; Jun, J.; Lee, W. Fixed-Bed Adsorption for Bulk Component System. Non-equilibrium, Non-isothermal and Non-adiabatic Model. *Chem. Eng. Sci.* **1995**, *50*, 813.
- (52) Farooq, S.; Ruthven, D. M. Heat Effects in Pressure Swing Adsorption Systems. *Chem. Eng. Sci.* **1988**, *43*, 1017-1031.
- (53) Rezaei, F.; Grahn, M. Thermal Management of Structured Adsorbents in CO₂ Capture Processes. *Ind. Eng. Chem. Res.* **2012**, *51*, 4025.

- (54) Lively, R. P.; Chance, R. R.; Kelley, B. T.; Deckman, H. W.; Drese, J. H.; Jones, C. W.; Koros, W. J. Hollow fiber adsorbents for CO₂ removal from flue gas. *Ind. Eng. Chem. Res.* **2009**, *48*, 7314.



CHAPTER 3

DYNAMICS OF AMINE ADSORBENTS: INSIGHTS INTO ADSORBENT DESIGN

Parts of this chapter are reproduced from 'Bollini, P.; Brunelli, N. A.; Didas, S. A.; Jones, C. W. Dynamics of CO₂ Adsorption on Amine Adsorbents. 2. Insights into Adsorbent Design. *Ind. Eng. Chem. Res.* **2012**, *51*, 15153.'

3.1. Background

Silica-supported amine materials are widely evaluated as components of potential adsorption processes for separation of CO₂ from power plant flue gases.¹ However, while supported amine materials offer the advantage of working efficiently in humid gas streams and many materials have been reported that offer large adsorption capacities,² relatively little is known about adsorption and desorption dynamics over these materials.

In the preceding chapter, heat and mass transfer models were described that are capable of capturing amine packed bed heat and mass transfer effects with moderate (heat transfer) and excellent (mass transfer) accuracy. It was demonstrated that under the experimental conditions of that study, heat effects do not have a significant effect on CO₂ breakthrough. In fact, it was shown that the breakthrough shape was governed purely by the linear driving force constant, k , which is dependent on the rates of mass diffusion and chemical reaction. In this chapter, the models are applied to packed bed

breakthrough runs on a series of different supported amine materials based on 3-aminopropylsilyl-functionalized SBA-15 silica to gain insights into the impact of amine loading and adsorbent structure on adsorption dynamics.

3.2. Experiments

3.2.1. Synthesis

The SBA-15 silica synthesis is described in the preceding chapter. To synthesize amine functionalized SBA-15, the calcined SBA-15 was first dried overnight on a high vacuum line at 120°C. Then, 2 grams of SBA-15 was dispersed in 200 ml of toluene with stirring for 3 hours. After this, 3-aminopropyltrimethoxysilane (APTMS) was added to the solution. Three different aminosilica materials were synthesized. In the first case (APS_low), 0.4 grams 3-aminopropyltrimethoxysilane was added. In the second (APS_medium), 2 grams 3-aminopropyltrimethoxysilane were added to the solution. This material is the same material that was discussed in detail in the preceding chapter (chapter 2). Once APTMS was added, the solution was allowed to stir for 24 hours. The resulting solids were then filtered with copious amounts of toluene, dried in a vacuum oven at 50°C overnight and stored in a vial. To synthesize the adsorbent material with a high amine loading, after dispersing the pre-dried SBA-15 support in toluene, 0.6 ml water was added to the solution and stirred for 3 hours. Then, 4 grams of APTMS was added to the solution and the temperature was raised quickly to 85°C. A condenser was attached to the reaction flask prior to heating the reaction. After stirring for 24 hours, the resulting solids were filtered with toluene and stored in a vial after being dried overnight at 50°C. Zeolite 13X powder was purchased from Sigma Aldrich. For batch uptake and packed bed experiments, pellets were pressed under a pressure of 275 bar, crushed

and then sieved between 150 and 500 microns. No binder was used in preparing the pellets.

3.2.2. *Material characterization*

Thermogravimetric analysis, X-ray diffraction, and nitrogen physisorption experiments were carried out in a manner as described in the preceding chapter.

3.2.3. *Batch uptake measurements*

Batch uptake measurements were carried out similar to the equilibrium adsorption capacity measurements described before (see chapter 2), but with pellets instead of powders to enable comparison of gas uptake across different adsorbents.

3.3. **Theory**

Different isotherm models were used to describe the isotherms of zeolite 13X and the amine adsorbents. For the amine adsorbents, the single-site Toth model was used, which has been described in chapter 2. The dual site Langmuir (DSL) model is the simplest, physically reasonable isotherm model used in the literature to describe zeolite 13X behavior.³⁻⁸ The model assumes the adsorbent surface to have two distinct adsorption sites, each having their own distinct saturation capacity and adsorption affinity. Equation 3.1 shows the DSL isotherm equation. The temperature dependence of the affinity parameters is captured using equation 3.2.

The mass and heat transfer models described in chapter 2 along with the parameters used are implemented here as well.

$$q_e = \left(\frac{n_s bP}{1+bP} + \frac{m_s dP}{1+dP} \right) \quad (3.1)$$

$$b = b_0 \exp\left(\frac{H_{ads}}{RT_0} \left(\frac{T_0}{T} - 1\right)\right) \quad d = d_0 \exp\left(\frac{H'_{ads}}{RT_0} \left(\frac{T_0}{T} - 1\right)\right) \quad (3.2)$$

3.4. Results & Discussion

3.4.1. Material characterization

The X-ray diffraction patterns of the zeolite 13X powder and the SBA-15 support agree with those reported in the literature. The amine loading increases in the order APS_low, APS_medium, APS_high (Figure 3.1). A progressive decrease in surface areas and pore volumes was observed as more amines were incorporated onto/into the SBA-15 support. The material with the highest amine loading (APS_high) had only 27% of the surface area and 38% residual pore volume compared to the parent SBA-15 material. Sayari and co-workers have demonstrated that the presence of water in the reaction mixture facilitates coupling of aminosilane molecules, leading to a coverage of amines higher than that corresponding to a perfect monolayer (as depicted in Figure 3.2).⁹ This coupling of aminosilane molecules leads to only a small fraction (38%) of the

total pore volume of the bare support being accessible post-functionalization in the case of the APS_high material.

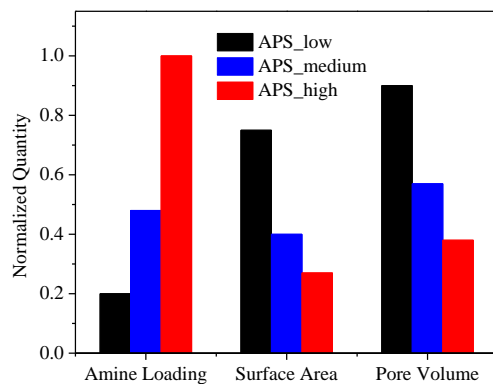


Figure 3.1: Amine loading (normalized by the amine loading of APS_high), surface areas, and pore volumes, (normalized by the corresponding values of the SBA-15 support) of the amine adsorbents tested.

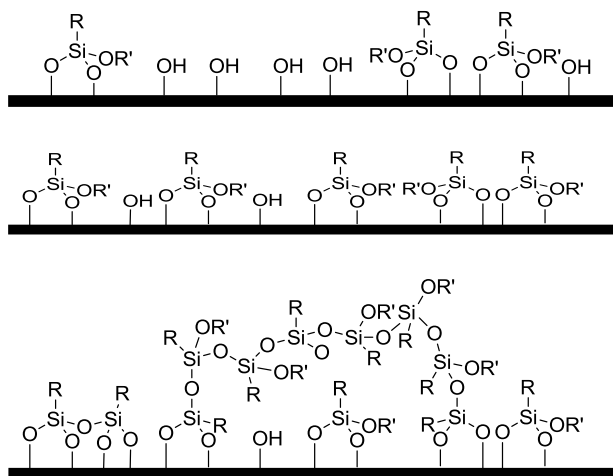


Figure 3.2: Hypothetical representation of amine surfaces in the 3-aminopropylsilyl-grafted SBA-15 materials used here: APS_low with a low amine loading (top), APS_medium (middle), and APS_high, with the highest amine loading (bottom)

Figure 3.3 shows the experimentally measured dry CO₂ adsorption isotherms as well as the model predicted isotherms. At CO₂ partial pressures greater than 0.05 bar (bottom), the zeolite 13X material exhibits higher CO₂ adsorption capacity compared to the amine adsorbents reported in this study. However, at or below partial pressures of 0.0004 bar (inset), the medium and high loading amine adsorbents have significantly higher CO₂ adsorption capacities compared to zeolite 13X. This is because of the high chemical affinity of the amine adsorption sites for CO₂ molecules compared to the physisorption sites in the 13X aluminosilicate framework or on the bare silica support, which makes amine adsorbents extremely promising materials for CO₂ capture from ultra-dilute sources like ambient air.¹⁰⁻²⁰ At higher partial pressures, however, the amine adsorption sites begin to saturate and the larger number of available adsorption sites present in the 13X material lead to higher equilibrium capacities versus the amine adsorbents reported in this study. While the low heat of adsorption of CO₂ on zeolite 13X is responsible for the flat shape of the isotherm at low partial pressures, in the case of the APS_low material, the isotherm data suggest that the amine loading is low enough that most of the amine adsorption sites are saturated below a partial pressure of 0.0004 bar.

Isotherm models (Dual-site Langmuir for zeolite 13X and single-site Toth for the aminosilica adsorbents) were used to model the equilibrium behavior of the adsorbent materials. Isotherm parameters used to fit the data for the zeolite 13X and the three amine adsorbents are reported in Tables 3.1 and 3.2 respectively. Good agreement between model predictions and experiments were obtained both at low partial pressures (Figure 3.3, inset) and high partial pressures (Figure 3.3). Normalized standard deviations were calculated for all isotherm curves using a method similar to that used in

the literature²¹ and were found to be less than 11% for all the isotherms reported in this study.

Table 3.1. Dual Site Langmuir parameters for zeolite 13X

n_s (mol/kg)	m_s (mol/kg)	b_0 (10^{-10} Pa ⁻¹)	d_0 (10^{-10} Pa ⁻¹)	H_{ads} (KJ/mol)	H'_{ads} (KJ/mol)
2.55	2.41	7.4	0.40	32.90	33.0

Table 3.2. Toth isotherm parameters for the amine adsorbents used in this study.

Material	n_s (mol/kg)	b_0 (10^{-10} Pa)	Q_{ads} (KJ/mol)	t'
APS_low	0.37	1	75	0.22
APS_medium	1	300	75	0.22
APS_high	1.5	300	75	0.25

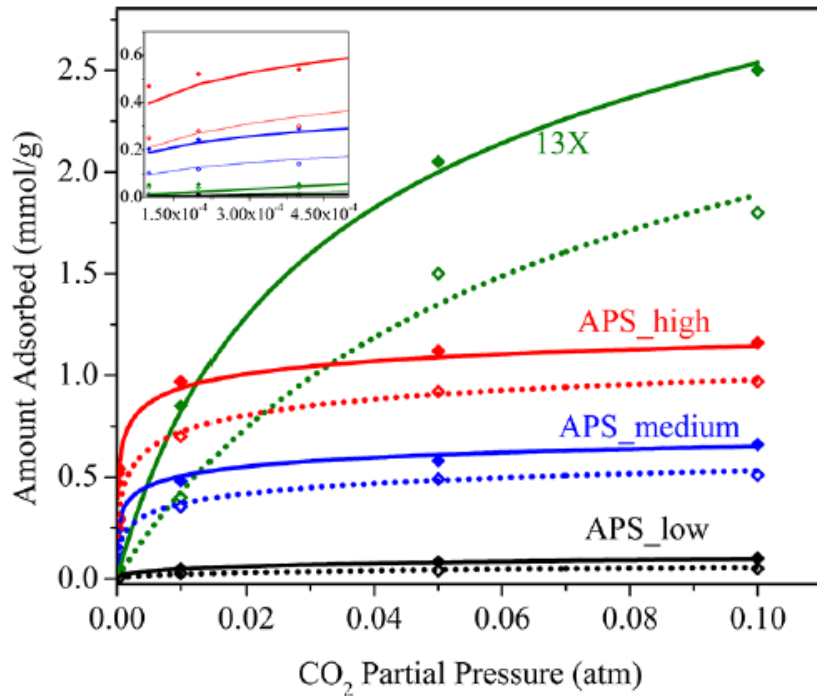


Figure 3.3: Isotherm fits obtained using models described and parameters reported in this work (inset: low partial pressures). Points: experimental data, Lines: model predictions. Solid diamonds: 25°C, Open diamonds: 45°C

3.4.2. Batch CO₂ uptake measurements

Figure 3.4 shows the fractional uptake as a function of time measured on a thermogravimetric analyzer at 6 different partial pressures of CO₂. The APS_{medium} material (top) showed the same fractional uptake curve at three of the lowest partial pressures 0.0001, 0.0002, and 0.0004 bar. This indicates that the CO₂ diffusion coefficients at these low partial pressure values are not dependent on the CO₂ partial pressure. On the other hand, for the APS_{high} material (bottom), the fractional uptake increased as the CO₂ partial pressure was increased from 0.0001 to 0.0002 to 0.0004 bar, indicating that in this case, the CO₂ diffusivity is more partial pressure dependent

compared to the APS_medium material. A possible explanation of this phenomenon is that in the adsorbent with the high amine loading and significantly reduced porosity, surface diffusion of CO₂ contributes significantly to the overall diffusion rate. Surface diffusion is highly dependent on the ability of adsorbed CO₂ molecules to jump from one adsorption site to the next and the feasibility of jumping from site to site should increase with increasing amine loading as the amines are closer to each other at high loadings. At partial pressures greater than 0.01 bar, for both the APS_medium and APS_high materials, the data are significantly different from those at lower pressures. The APS_medium material showed a rapid initial uptake followed by a small tail, whereas the APS_high material exhibited a less rapid initial uptake followed by a long tail. The major difference between the two materials is that the APS_high material adsorbed a significant fraction of its overall CO₂ capacity after the onset of the tail, unlike the APS_medium material.

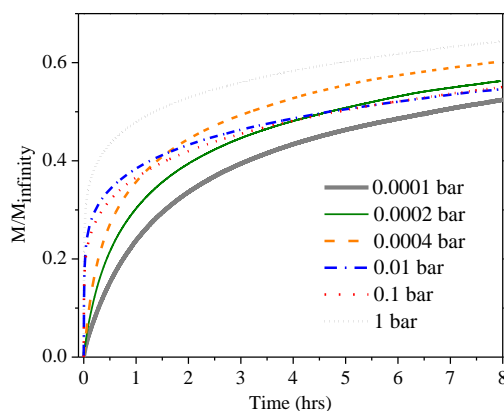
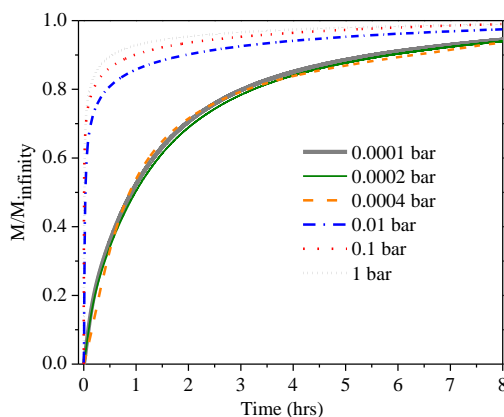


Figure 3.4: Fractional CO₂ uptake for APS_{medium} (top) and APS_{high} materials (bottom) at different CO₂ partial pressures

The different behaviors observed for the APS_{medium} and APS_{high} materials may be associated with differences in mass diffusion or heat transfer. Other factors should be relatively equal, since the porous supports are identical, meaning that external transport effects around similarly-sized particles should be similar, and the adsorption sites are chemically similar (primary 3-aminopropyl groups). To probe the influence of heat vs. mass transport effects on the uptake curves, an isothermal model is applied to

analyze the data. Equation 3.3 is a simple shell mass balance inside a spherical adsorbent particle.

Diffusion Equation:

$$\frac{\partial q}{\partial t} = \frac{1}{r^2} \frac{\partial}{\partial r} \left(r^2 D \frac{\partial q}{\partial r} \right) \quad (3.3)$$

Initial condition:

$$q(r, 0) = 0 \quad (3.4)$$

Boundary conditions:

$$q(R, t) = q_{eq} \quad (3.5)$$

$$\left(\frac{\partial q}{\partial r} \right)_{r=0} = 0 \quad (3.6)$$

Assuming constant diffusivity and applying the relevant initial and boundary conditions (eqns 3.3-3.6) yields equation 3.7. For fractional uptakes less than 0.3, equation 3.7 reduces to equation 3.8, which predicts a linear correlation between fractional uptake and the square root of time.²² Plotting fractional uptake as a function of the square root of time should yield straight lines provided the diffusion-adsorption process is relatively isothermal.

$$\frac{M_t}{M_\infty} = 1 - \frac{6}{\pi^2} \sum_{n=1}^{\infty} \frac{1}{n^2} \exp\left(-\frac{n^2\pi^2 D t}{R^2}\right) \quad (3.7)$$

$$\frac{M_t}{M_\infty} = \frac{6}{\sqrt{\pi}} \left(\frac{D t}{R^2}\right)^{1/2} \quad (3.8)$$

Figure 3.5 shows the fractional CO₂ uptakes plotted versus the square root of time. For the medium loading material, at all 6 partial pressures, the plots are approximately linear, except for the induction period associated with diffusion of CO₂ into the initially CO₂-free system. On the other hand, for the high loading material, the plots at partial pressures less than 0.0004 are approximately linear, whereas those at higher partial pressures are highly non-linear above a fractional uptake of 0.15. If heat effects cause this non-linearity, the data suggest that for the APS_{medium} material, heat effects do not adversely affect the uptake rates, whereas they have a significant effect on the uptake for the APS_{high} material. However, if the total uptake in mmol CO₂/g adsorbent at 0.01 bar is considered (Figure 3.6), the material with the lower of the two amine loadings (APS_{medium}) had a more rapid initial uptake rate. Given the fact that both materials have primary amine groups and hence, similar heats of adsorption (Table 3.2), the heat is released more rapidly in case of the APS_{medium} material in comparison to the APS_{high} material, suggesting that heat effects are not the cause of the observed non-linearity in Figure 3.5. This anomalous behavior of the APS_{high} adsorbent suggests that the non-linearity is not likely related to heat effects and may in fact be a result of another property of the APS_{high} material. This question is addressed more thoroughly below.

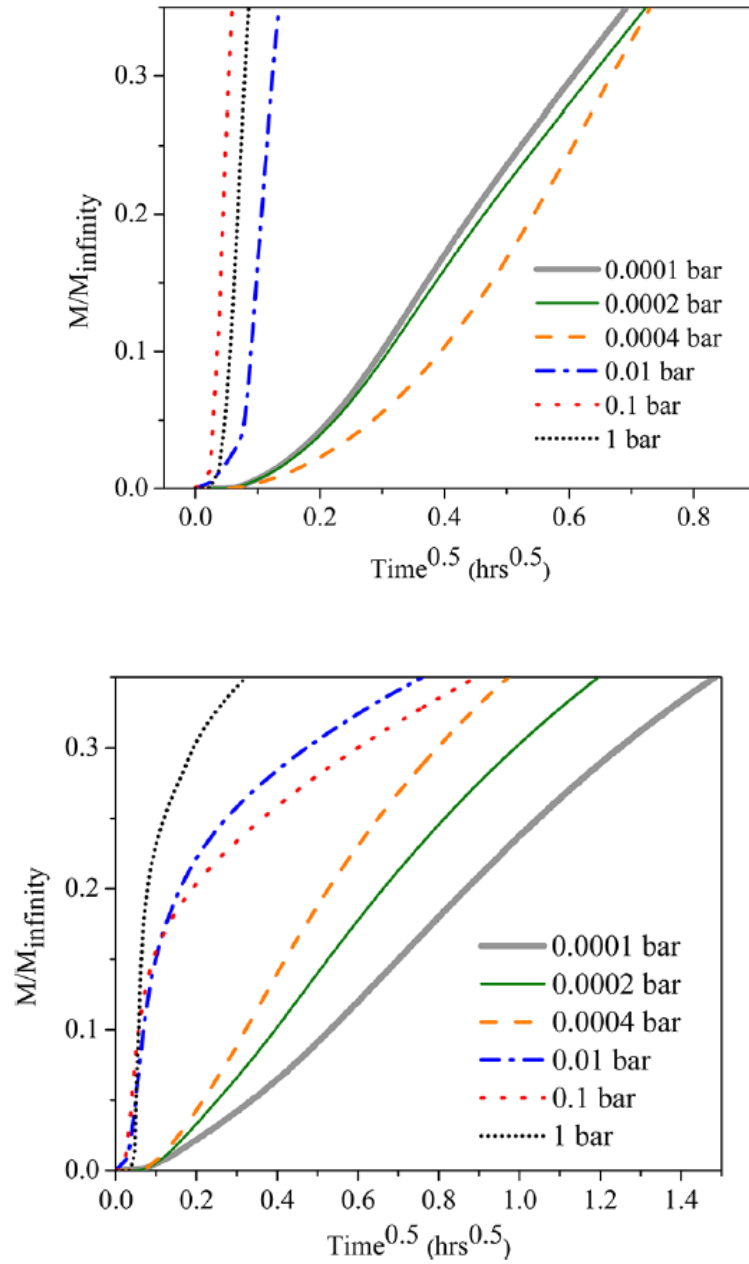


Figure 3.5: Fractional uptake of the APS_medium material (top) and APS_high material (bottom) plotted as a function of the square root of time.

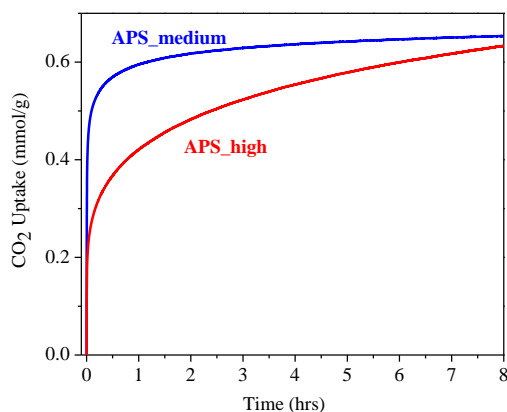


Figure 3.6: Total CO₂ uptake as a function of time on the APS_{medium} and APS_{high} adsorbents at a CO₂ partial pressure of 0.1 bar.

3.4.3. Packed bed breakthrough experiments

Amine adsorbent breakthrough studies reported in the literature typically only report the outlet concentration of CO₂ as function of time.^{17,18,23} However, as described in the preceding chapter, in this study, temperature measurements inside the amine adsorbent beds are also reported alongside the concentration breakthrough measurements at the outlet to yield additional insights into the interaction between heat and mass transfer effects in the packed bed.

Figure 3.7 shows the measured concentrations and temperatures during CO₂ breakthrough experiments using the three amine adsorbents and zeolite 13X. The concentration is normalized by the feed concentration and the temperature is normalized by the ambient temperature. Breakthrough occurred at the shortest time with the APS_{low} material, as expected, since it had the lowest equilibrium adsorption capacity (Figure 3.3) of the materials tested in this study. A bed made from this material also

gave a sharp breakthrough front, suggesting that the bed was utilized very efficiently. The APS_medium material had a breakthrough time larger than that of the APS_low material as a result of its higher adsorption capacity, but the breakthrough curve was slightly more spread compared to the APS_low material. Surprisingly, the APS_high material exhibited a shorter breakthrough time compared to the APS_medium material. This result may be initially counterintuitive because materials with higher equilibrium adsorption capacities generally also show longer breakthrough times. However, the breakthrough curve is consistent with the equilibrium data presented in Figure 3.3 and with the kinetic data shown in Figure 3.4, which demonstrate that a significant fraction of the CO₂ adsorption for the APS_high material occurs at very long times, as can be observed in the long tail in the breakthrough for this material, as shown in Figure 3.7.

The breakthrough time is a critical parameter representing adsorption column dynamics because typically, switching from adsorption to desorption is carried out when the outlet concentration rises to a certain fraction of the feed concentration and thus, a higher breakthrough time implies a smaller number of cycles for the same gas throughput. These data illustrate an important point that has been somewhat overlooked in the amine adsorption literature, where work has focused too much on achieving ever higher equilibrium adsorption capacities with no regard for adsorption kinetics. Specifically, it clearly shows that a higher equilibrium capacity does not necessarily translate to better cyclic adsorption performance. While the breakthrough itself is relatively sharp, a significant fraction of the uptake occurs after breakthrough, associated with the long tail that starts at a mole fraction of around 0.8. As discussed below, long tails in breakthrough curves are often related with heat effects associated with finite heat transfer rates through the column walls. However, as alluded to above, this observation

could also be associated with hindered diffusion in the constricted pores of high-loading materials.

As expected, the zeolite 13X material had the largest breakthrough time of all the materials tested in this study, owing to its high equilibrium capacity and the dry conditions used (zeolite 13X is significantly less selective using humid feeds), but on the other hand, it also has a breakthrough that is significantly more disperse compared to the rest of the materials tested in this study.

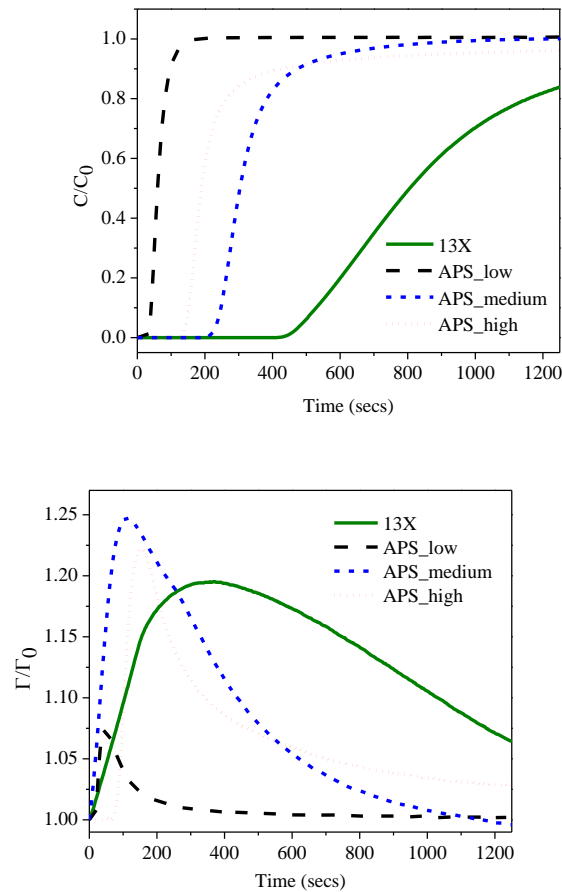


Figure 3.7: Breakthrough curves for the four adsorbents (top) and temperature profiles in the packed bed (bottom)

Figure 3.7 also depicts the evolution of the bed temperature during breakthrough for each adsorbent. The bed made from the APS_low material exhibited the smallest temperature rise of the materials reported here, owing to its smaller adsorption capacity. The APS_medium material exhibited a larger temperature rise compared to the APS_low material, as expected, due to the higher adsorption capacity combined with the fact that it had a similar heat of adsorption. The APS_high material showed a smaller temperature rise compared to the APS_medium material, and it also exhibited a longer tail in the temperature profile, consistent with the tail in the breakthrough curve, as they both run to approximately the same time. The zeolite 13X material, despite its higher CO₂ adsorption capacity, generated a thermal wave that was smaller than the wave from the APS_medium and the APS_high materials. This observation for zeolite 13X is a combination of both the lower heat of adsorption (less than half that of the amine adsorbents reported in this study) and the more dispersed breakthrough front exhibited by the zeolite 13X material, as shown in Figure 3.7, which indicates slow adsorption kinetics.

The behavior of the APS_high material is the most anomalous and interesting, and with the data discussed thus far, it is not clear whether the lower thermal wave and pronounced tail in the breakthrough is associated with (i) slow heat loss through the column walls or (ii) slow rates of adsorption in the amine adsorbent due to diffusional resistances, or some combination of these two effects. To address this more fully, the adsorption breakthrough behavior was studied in detail using the models described in chapter 2 of this thesis.

3.4.4. Computational Analysis of Adsorption Breakthrough

The models outlined in the preceding chapter were used to computationally model the adsorption process. Good agreement was achieved between the model predictions and experiments, as shown in Figure 3.8.

Table 3.3 shows the optimal values of the fitting parameters obtained for zeolite 13X, APS_low and APS_medium. The linear driving force constant is a lumped constant that accounts for four distinct resistances, (i) film resistance on the outside surface of the pellet, (ii) macropore diffusion resistance inside the pellet, (iii) intraparticle diffusion resistance inside each individual adsorbent particle, and (iv) the resistance associated with chemical reaction of CO₂ molecules with the amine groups (Figure 3.9).²⁴ As the same pellet size and the same gas flow rate were used for all packed bed breakthrough experiments, the film mass transfer coefficients should be approximately the same for all four adsorbent materials. Likewise, because pellets of the same size that were pressed under the same pressure were used, the macropore diffusion resistances associated with all four of the materials can be expected to be approximately the same. Hence, the differences in linear driving force constant values are most likely the result of differences in the total rate associated with diffusion and physisorption combined in the case of 13X, and diffusion and reaction combined, in the case of the three amine materials.

From the data in Table 3.3, it is clear that both the amine adsorbents had significantly higher linear driving force constants compared to zeolite 13X. These results imply that mesoporous amine adsorbents with open pores (such as APS_low and APS_medium) can provide more rapid access of the CO₂ molecules to the adsorption sites compared to the microporous zeolite 13X. More specifically, the optimal linear driving force constant for the medium loading material was more than twice that of

zeolite 13X and for the low loading material, it was more than 10 times greater than that of zeolite 13X.

Clearly, the amine loading has a significant impact on the transport properties of the amine adsorbent, as quantified by the linear driving force parameter. There are reports in the literature that suggest that as the amount of aminosilane used in the silica grafting solution is increased, the greater the chances of amine clustering in the hydrophobic solutions during the surface grafting process.²⁵⁻²⁷ To this end, it is possible that the grafted amine groups in case of the APS_medium material are significantly more clustered compared to the APS_low material, since the grafting solution had five times the amount of aminosilane. The linear driving force constants obtained here suggest that the higher loading of amines on APS_medium as well as possibly an increased extent of amine-clustering impacts the transport of CO₂ molecules to the amine adsorption sites.

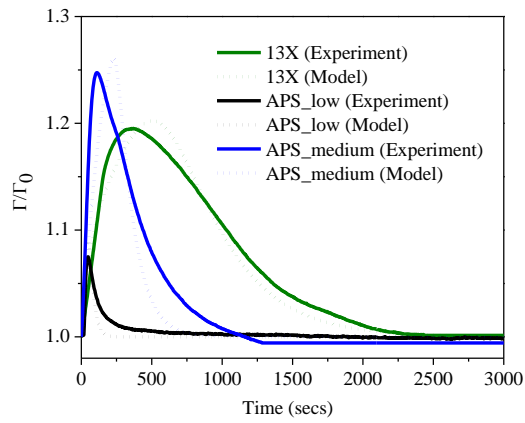
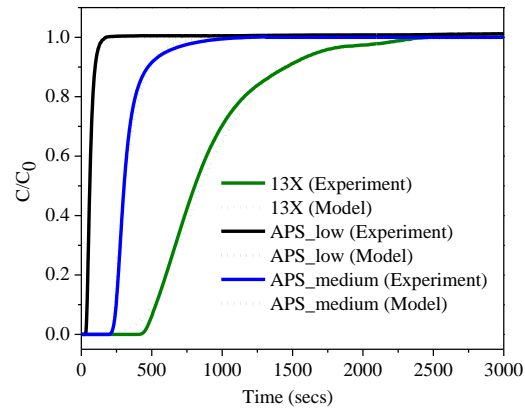


Figure 3.8. Fits obtained between predicted and experimental breakthrough curves (top) temperature profiles (bottom).

Table 3.3: Optimal values of parameters used to fit models with the experimental data

Material	k (sec ⁻¹)	K _z (W/m.K)	h (W/m ² .K)
13X	0.0051	0.85	0.48
APS_low	0.061	3.72	1.84
APS_medium	0.012	1.76	0.88

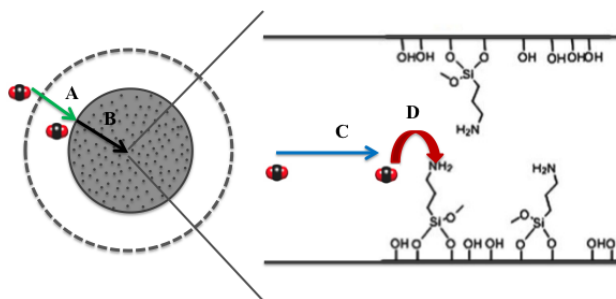


Figure 3.9: Schematic representation of the four steps that transport CO₂ to a surface adsorption site during a packed bed breakthrough experiment, (i) film diffusion, (ii) macropore diffusion, (iii) intraparticle diffusion and (iv) chemical reaction/adsorption.

Just as for the APS_{medium} material discussed in detail in chapter 3, the model predictions for the zeolite 13X and APS_{low} materials were relatively insensitive to the value of wall heat transfer coefficients, h , used. On the other hand, the temperature profiles were found to be sensitive to the effective bed thermal conductivity, K_z , whereas

the breakthrough curves were insensitive to this parameter, just as with the APS_medium material.

3.4.5. Necessity of using non-isothermal models

Similar to the parametric study carried out in the preceding chapter, the effect of heat removal and varying the linear driving force constant on CO₂ breakthrough was studied. For the zeolite 13X, APS_low, and APS-medium materials, heat removal has a negligible effect on CO₂ breakthrough, whereas lowering the linear driving force constant results in a significantly more disperse breakthrough compared to the experimentally measured curves. These results reinforce the conclusions from the previous chapter that under the experimental conditions used in this study, using the appropriate linear driving force constant, which represents the mass transfer rate in the adsorbent, is critical to accurately predicting breakthrough curves and that heat effects have an insignificant effect on breakthrough under these conditions.

3.4.6. Dynamics of high loading amine adsorbent, APS_high

Heat effects in packed beds have been widely studied and it is generally accepted that packed bed breakthrough experiments do not typically occur under strictly isothermal or adiabatic conditions.²⁸⁻³¹ Rather, there exists a finite rate of heat dissipation to the walls of the fixed bed adsorber, and this finite rate of heat transfer sometimes manifests itself in the form of a long tail in the breakthrough curve. This has been observed for the ethane-helium-zeolite 5A system,³⁰ ethylene –helium-zeolite 5A system,³² CO₂-helium-activated carbon system,²⁸ and the CO₂-N₂-zeolite 13X system.³³

The long tail in the breakthrough curve results in a smaller fraction of the total equilibrium capacity being realized before breakthrough, resulting in shorter breakthrough times and less efficient use of the adsorbent. As noted above, both mass diffusion limitations and heat transfer limitations can affect the breakthrough curve, but heat transfer effects often manifest themselves more prominently in the latter half of the breakthrough, in the form of a long tail, whereas mass diffusion effects typically cause significant spreading in both the initial and latter halves of the breakthrough curve.

As shown in the previous section, good fits were obtained between model predictions and experiments for zeolite 13X and the low and moderately loaded amine adsorbents using the linear driving force approximation. This, however, was not the case with the high loading adsorbent, APS_high. The best fit obtained by applying the linear driving force approximation to the breakthrough over this material is shown in Figure 3.10. Clearly, very poor prediction of the breakthrough shape was achieved using the model that was employed successfully for the other adsorbents.

There are two fundamental shortcomings in the best model prediction – the mass transfer rate was under-predicted and the long tail could not be captured. Increasing the linear driving force constant to increase the mass transfer rate sharpened the breakthrough curve significantly, but it also increased the breakthrough time by increasing the efficiency with which the adsorbent bed was utilized (Figure 3.11). This modeling approach could not capture simultaneously both the breakthrough time and degree of breakthrough spreading.

To attempt to simulate the long tail in the breakthrough, the heat transfer at the walls was adjusted. Using this approach, the optimal wall heat transfer coefficient (which is the value used to simulate the curve shown in Figure 3.10) was two orders of

magnitude lower than those obtained for the other three materials described above. Since all the packed bed breakthrough measurements reported here were carried out under similar experimental conditions, a heat transfer coefficient that is two orders of magnitude lower than the value used to successfully model the other adsorbents may be deemed physically unrealistic. Furthermore, even when using this unrealistically low heat transfer coefficient, the extremely long tail observed for the high loading material case could not be accurately captured. Figure 3.12 shows simulated breakthrough curves with wall heat transfer coefficients 0.1 and 0.01 times the optimum value, which itself is two orders of magnitude lower than the expected value. These data clearly show that adjusting the wall heat transfer characteristics cannot capture the breakthrough behavior over the APS_high material. This result, in addition to the fact that the tail was observed for the high loading material and not the moderately loaded material APS_medium material, which showed a larger temperature rise compared to the high loading material, leads to the conclusion that the tail cannot be a result of heat effects. On the contrary, this phenomenon must be a result of mass diffusion effects.

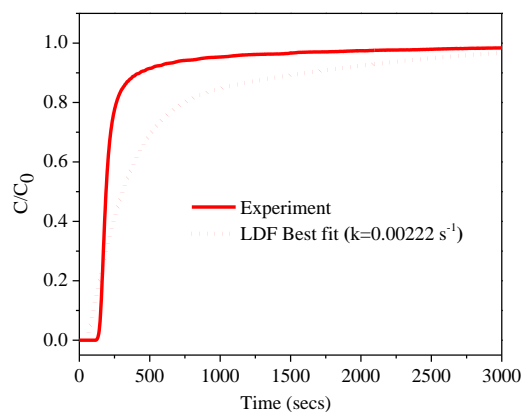


Figure 3.10: Best fit obtained for the breakthrough curve for the APS_high material using the linear driving force model.

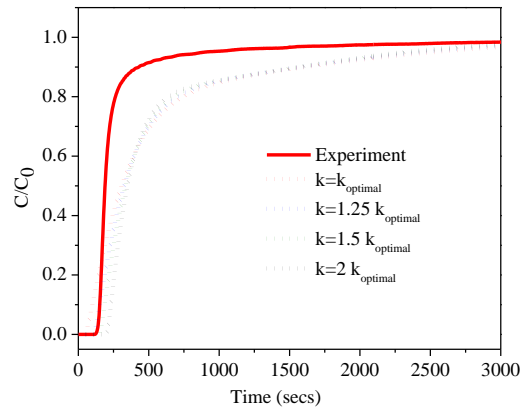


Figure 3.11: Effect of varying linear driving force constant, k , on simulated breakthrough curves for the homogeneous linear driving force model over the APS_high material.

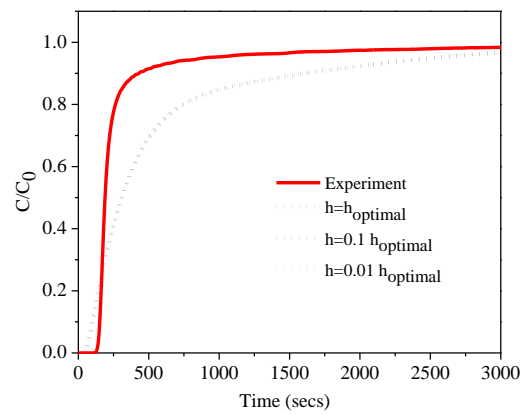


Figure 3.12: Effect of wall heat transfer coefficient on simulated breakthrough curves for the APS_high material.

The most obvious distinction between this APS_high material and the rest of the materials is that the APS-high material is the only adsorbent that has aminopolymer

present in the adsorbent material (produced by condensation/polymerization of APS moieties with each other, in addition to with the oxide support). It is hypothesized here that the diffusion resistance introduced by the aminopolymer causes the unusual breakthrough behavior of the APS_high material. To test this hypothesis, diffusion was modeled in the adsorbent not as a homogeneous process represented by a single linear driving force constant (as for the materials above) but as a heterogeneous process consisting of two components: (i) fast diffusion through the pores of the adsorbent and (ii) relatively slow diffusion through the aminopolymer phase. Figure 3.13 depicts this idea schematically. The equation that results from this treatment is:

$$\frac{\partial q}{\partial t} = k_1 (\eta q_e - q_1) + k_2 ((1 - \eta)q_e - q_2) \quad (3.9)$$

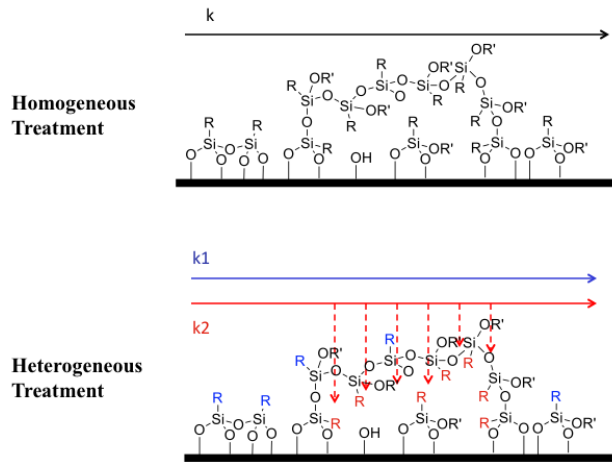


Figure 3.13: Schematic representation of the homogeneous and heterogeneous models used for modeling mass transfer in amine adsorbents.

In this heterogeneous treatment, three parameters are fitted, (i) the linear driving force constant for pore diffusion (k_1), (ii) the linear driving force constant for diffusion through the aminopolymer phase (k_2), and (iii) the fraction of total amine adsorption sites

that are readily accessible to the CO₂ molecules (η). Figure 3.14 shows that a reasonably good fit of the breakthrough behavior of the adsorbent APS_high can be obtained using the heterogeneous model. Also, isothermal models give sufficiently accurate predictions, similar to the rest of the materials evaluated in this study, as discussed above.

The optimal values of all 5 fitting parameters are shown in Table 3.4. The values of axial bed thermal conductivity and wall heat transfer coefficients were very close to those obtained with the homogeneous model for the other three adsorbents. The values for the other three parameters differ and the differences are intriguing. The models for the zeolite 13X and the APS_low material converge to the same solution as the homogeneous model. For zeolite 13X, even though the value of η is 0.48, both linear driving force constant values are the same as the value obtained using the homogeneous model, implying that the optimal model prediction is still a result that corresponds to a material where the diffusion process is relatively homogeneous. In case of the APS_low material, $\eta=1$, implying that there is only one type of diffusion resistance that corresponds to a linear driving force constant value of 0.061 s⁻¹ (the same as the value obtained for the homogeneous treatment). Thus, for both these materials, the homogeneous model represents the best solution to characterize the experimental data. In contrast, for the APS_medium and the APS_high materials, this convergence was not observed. For the APS_high material, for which the homogeneous treatment proved to be insufficient, the experimental concentration breakthrough and temperature profile were adequately explained by the heterogeneous model, which suggested that 35% of the amine adsorption sites were readily accessible to the adsorbate ($k=0.0163$ s⁻¹) with the rest of the amine adsorption sites only accessed after encountering significant diffusion resistances ($k=0.000164$ s⁻¹). The best fit for the

APS_medium material, on the other hand, was obtained when 28% of the amine sites were deemed to be highly accessible, with a linear driving force constant of 0.02 s^{-1} , with 72% of the amine sites being only slightly less accessible, with a linear driving force constant of 0.011 s^{-1} . The major difference between the results for these two materials is that for the moderately loaded material, the ratio of the two linear driving force constants is approximately 2, whereas for the highly loaded material, that ratio is 100. These results suggest that while both materials may exhibit heterogeneous characteristics, in case of the APS_high material, the degree of heterogeneity is so high that it becomes necessary to use a heterogeneous model to capture the experimental data. In the case of the APS_medium material, however, the degree of heterogeneity is small enough that a homogeneous model can adequately capture the adsorption characteristics. In the case of the APS_medium adsorbent, the agreement of the heterogeneous model with the experimental data is marginally better than that of the homogenous model, but not sufficiently better to justify the use the a heterogeneous modeling treatment.

The likely reason for heterogeneity in the APS_high material, as depicted in Figure 3.13, is hindered diffusion through the aminopolymer phase within the adsorbent. In the case of the APS_medium material, however, the source of heterogeneity is less obvious. Figure 3.2 is an attempt to depict an ideal silica surface with the aminosilane present in the form of an almost perfect monolayer. However, it appears that the physical form of the material does not conform with this ideal scenario because if that were the case, the adsorbent should behave as a perfectly homogeneous material. Instead, we hypothesize that the aminosilanes form clusters on the surface, resulting in a surface where some amines are readily accessible to the CO_2 molecules and others are not.

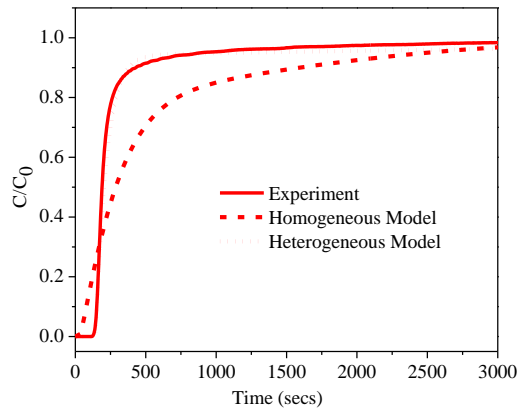


Figure 3.14: Comparison of the optimal predictions obtained using the homogeneous and heterogeneous linear driving force models for breakthrough over the APS_high adsorbent bed.

Table 3.4: Optimal values of fitting parameters obtained using the heterogeneous model

Material	η	k_1 (s ⁻¹)	k_2 (s ⁻¹)	K_z (W/m. °C)	h (W/m ² . °C)
13X	0.48	0.0051	0.0051	0.85	0.48
APS_low	1	0.06	-	3.84	1.92
APS_medium	0.28	0.02	0.011	1.77	0.88
APS_high	0.35	0.0163	0.000164	1.81	1.91

One may now revisit the batch uptake data to probe for evidence of diffusion limitations in hypothetical polymer phases. One way of increasing diffusion rates in the polymer phase, if indeed such a phase is present, is to increase the temperature of adsorption. To this end, uptake rates were measured at three different temperatures: 25,

45, and 65°C. Figure 3.15 shows the uptake curves for APS_medium and APS_high materials as a function of adsorption temperature. Though temperature has a favorable effect on the uptake rates on both materials, this effect was found to be much more pronounced in case of the APS_high material (Figure 3.15), in agreement with the hypothesis that CO₂ diffusion through the aminopolymer phase, which is much slower than diffusion through the open pore space in the pellet, results in severe diffusion limitations, and higher temperatures can help overcome these diffusion limitations, leading to more efficient utilization of the adsorbent. Earlier, when fractional uptakes for the APS_high material were plotted as a function of the square root of time, non-linear behavior was observed (vide supra) and it was not clear whether this non-linearity was a result of heat effects or mass diffusion effects. If this non-linearity was caused by mass diffusion effects, it should decrease as the adsorption temperature increases, and this is what was observed in the experiments (Figure 3.16: top). When the total CO₂ uptake is plotted as a function of time, as the adsorption temperature is increased, the total uptake increased (Figure 3.16: bottom). The fact that as the adsorption temperature is increased the plots (Figure 3.16: top) approached linearity even though the total CO₂ uptake increased strongly indicates that the non-linearity was indeed a result of mass diffusion effects and not heat effects.

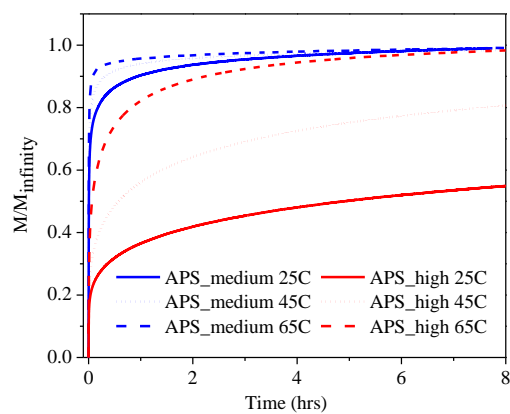


Figure 3.15: Effect of temperature on uptake rates of APS_medium and APS_high adsorbents.

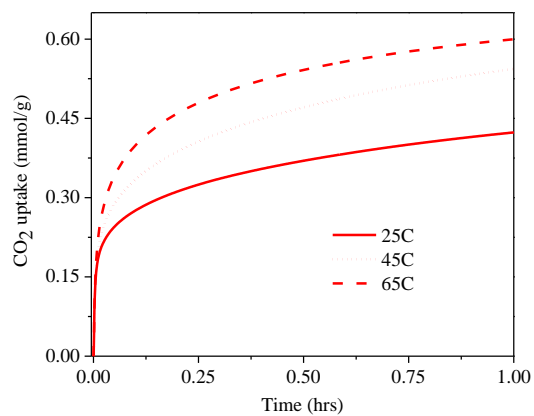
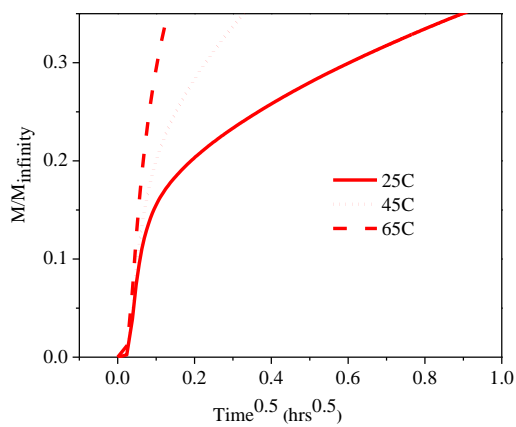


Figure 3.16: Effect of temperature on linearity of the plot of fractional uptake plotted as function of the square root of time (top) and the total CO₂ uptake plotted as function of time (bottom).

The results of this first comprehensive study of heat and mass diffusion effects in an array of supported amine CO₂ adsorbents suggest that the breakthrough shape for adsorbents with high amine loadings can be explained if the adsorbent is treated as a heterogeneous combination of sites that are highly accessible (high k) and other sites that are relatively less accessible (lower k). It is important to note that the materials Sayari and coworkers reported in their first of its kind study were synthesized using water in the reaction mixture, implying that there may be aminopolymer present in their adsorbents as well.²³ It would be interesting to see if the heterogeneous models described in this study can predict breakthrough shapes accurately for those materials as well.

3.5. Conclusions

Packed bed heat and mass transfer data measured on commercial zeolite 13X and amine functionalized SBA-15 materials with three different amine loadings were modeled successfully. The results indicate that the low and moderately loaded amine adsorbents tested in this study have better CO₂ diffusion properties compared to commercial zeolite 13X on account of their open mesopores. However, when the support is loaded excessively with amines via incorporation of a high loading of aminopolymer, adsorption kinetics were adversely affected. Poor adsorption kinetics were found to be manifested in the form of premature CO₂ breakthrough and a long tail on the end of breakthrough. Modeling results show that unlike conventional

physisorbants, this long tail is not associated with heat effects. Rather, the tail is associated with diffusion limitations induced by the presence of the aminopolymer. A rate model that accounts for heterogeneity in mass diffusion was found to give accurate predictions of the breakthrough shape for the high loading aminosilica material. The results of this study point to the fact that merely incorporating more amines into the support does not necessarily lead to high performing adsorbents for CO₂ capture applications. Instead, adsorbent design must focus on either incorporating more amines that are easily accessible to CO₂ molecules or finding a strategy to make the limited number of amines that can indeed be incorporated into the support (without introducing diffusion limitations) more efficient in terms of CO₂ adsorption.

3.6. Notation

n_s : Saturation capacity (Langmuir site 1)/ amine adsorbent saturation capacity

m_s : Saturation capacity (Langmuir site 2)

b : Langmuir affinity parameter (site 1)/ amine adsorbent affinity parameter

d : Langmuir affinity parameter (site 2)

b_0 : affinity parameter (site 1)/ amine adsorbent at reference temperature

d_0 : affinity parameter (site 1) at reference temperature

t' : Toth heterogeneity parameter

H_{ads} : Heat of adsorption (site 1)

H_{ads}' : Heat of adsorption (site 2)

Z: Distance in the axial direction (m)

t: Time (s)

ε : Bed void fraction

R: Radius of the pellet (m)

ρ_B : Adsorbent bulk density (kg/m^3)

ρ_S : Solid density (kg/m^3)

C_g : Gas phase specific heat capacity ($\text{J/kg}\cdot^\circ\text{C}$)

C_S : Solid phase specific heat capacity ($\text{J/kg}\cdot^\circ\text{C}$)

C_A : Adsorbate gas phase concentration (mol/m^3)

q: Adsorbed phase concentration (mol/kg)

q_e : Equilibrium adsorbed phase concentration (mol/kg)

Γ : Gas temperature ($^\circ\text{C}$)

Γ_0 : Ambient temperature ($^\circ\text{C}$)

T: Gas temperature (K) ($\Gamma+273.15$)

T_0 : Ambient temperature (K) ($\Gamma_0+273.15$)

P: Gas pressure (N/m^2)

U: Gas superficial velocity (m/s)

D_L : Axial dispersion coefficient (m^2/s)

K_z : Effective bed thermal conductivity in the axial direction (W/m.°C)

k : Linear driving force constant (s^{-1})

D : CO₂ diffusivity m²/s

M_t : CO₂ uptake (mol/kg)

M_∞ : Final CO₂ uptake (mol/kg)

q_1 : Adsorbed phase concentration on site 1 (mol/kg)

q_2 : Adsorbed phase concentration on site 2 (mol/kg)

Q_{ads} : Heat of adsorption at zero surface coverage (J/mol)

h : Wall heat transfer coefficient (W/m². °C)

η : Fraction of amine adsorption sites easily accessible to amine molecules
(corresponding to the linear driving force constant k_1)

k_1 : Linear driving force constant for amines easily accessible to CO₂ molecules (s^{-1})

k_2 : Linear driving force constant for amines not easily accessible to CO₂ molecules (s^{-1})

3.7. References

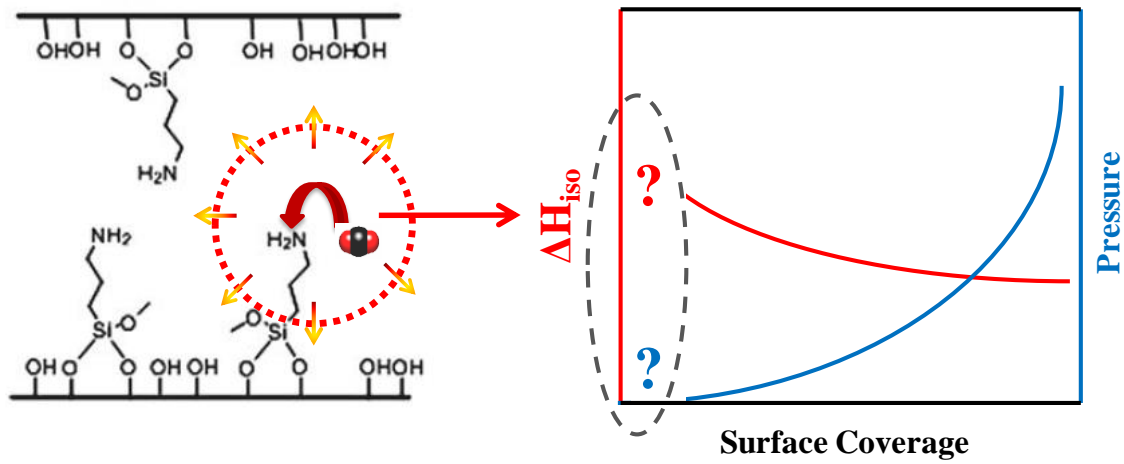
- (1) Bollini, P.; Didas, S. A.; Jones, C. W. Amine-oxide Hybrid Materials for Acid Gas Separations. *J. Mater. Chem.* **2011**, *21*, 15100.
- (2) Choi, S.; Drese, J. H.; Jones, C. W. Adsorbent Materials for Carbon Dioxide Capture from Large Anthropogenic Point Sources. *ChemSusChem* **2009**, *2*, 796.
- (3) Rezaei, F.; Grahn, M. Thermal Management of Structured Adsorbents in CO₂ Capture Processes. *Ind. Eng. Chem. Res.* **2012**, *51*, 4025.
- (4) Li, G.; Xiao, P.; Webley, P. A.; Zhang, J.; Singh, R. Competition of CO₂/H₂O in Adsorption based CO₂ Capture. *Energy Procedia* **2009**, *1*, 1123.
- (5) Xiao, P.; Zhang, J.; Webley, P.; Li, G.; Singh, R.; Todd, R. Capture of CO₂ from Flue Gas Streams with Zeolite 13X by Vacuum-pressure Swing Adsorption. *Adsorption* **2008**, *14*, 575.
- (6) Hashemifard, S. A.; Ismail, A. F.; Matsuura, T. Prediction of Gas Permeability in Mixed Matrix Membranes using Theoretical Models. *J. Membr. Sci.* **2010**, *347*, 53.
- (7) Brandani, F.; Ruthven, D. Measurement of Adsorption Equilibria by the Zero Length Column (ZLC) Technique Part 2: Binary Systems. *Ind. Eng. Chem. Res.* **2003**, *42*, 1462.
- (8) Ritter, J. A.; Bhadra, S. J.; Ebner, A. D. On the Use of the Dual-process Langmuir Model for Correlating Unary Equilibria and Predicting Mixed-gas Adsorption Equilibria. *Langmuir* **2011**, *27*, 4700.

- (9) Harlick, P. J. E.; Sayari, A. Applications of Pore-Expanded Mesoporous Silica . 5 . Triamine Grafted Material with Exceptional CO₂ Dynamic and Equilibrium Adsorption Performance. *Ind. Eng. Chem. Res.* **2007**, *46*, 446.
- (10) Jones, C. W. CO₂ Capture from Dilute Gases as a Component of Modern Global Carbon Management. *Annu. Rev. Chem. Biomol. Eng.* **2011**, *2*, 31.
- (11) S.A. Didas, A.R. Kulkarni, D.S. Sholl, C. W. J. Role of Amine Structure on CO₂ Adsorption from Ultra-dilute Gas Streams such as Ambient Air. *ChemSusChem* **2012**, *5*, 2058.
- (12) Gebald, C.; Wurzbacher, J. A.; Tingaut, P.; Zimmermann, T.; Steinfeld, A. Amine-based Nanofibrillated Cellulose as Adsorbent for CO₂ Capture From Air. *Environ. Sci. Technol.* **2011**, *45*, 9101.
- (13) Wurzbacher, J. A.; Gebald, C.; Steinfeld, A. Separation of CO₂ from Air by Temperature-vacuum Swing Adsorption Using Diamine-functionalized Silica Gel. *Energy Environ. Sci.* **2011**, *4*, 3584.
- (14) Chaikittisilp, W.; Lunn, J. D.; Shantz, D. F.; Jones, C. W. Poly(L-lysine) Brush-Mesoporous Silica Hybrid Material as a Biomolecule-Based Adsorbent for CO₂ Capture from Simulated Flue Gas and Air. *Chem. Eur. J.* **2011**, *17*, 10556.
- (15) Chaikittisilp, W.; Khunsupat, R.; Chen, T. T.; Jones, C. W. Poly(allylamine) - Mesoporous Silica Composite Materials for CO₂ Capture from Simulated Flue Gas or Ambient Air. *Ind. Eng. Chem. Res.* **2011**, *50*, 14203.

- (16) Chaikittisilp, W.; Kim, H. J.; Jones, C. W. Mesoporous Alumina-Supported Amines as Potential Steam-Stable Adsorbents for Capturing CO₂ from Simulated Flue Gas and Ambient Air. *Energy Fuels* **2011**, *25*, 5528.
- (17) Stuckert, N. R.; Yang, R. T. CO₂ Capture from the Atmosphere and Simultaneous Concentration Using Zeolites and Amine-grafted SBA-15. *Environ. Sci. Technol.* **2011**, *45*, 10257.
- (18) Belmabkhout, Y.; Serna-Guerrero, R.; Sayari, A. Amine-bearing Mesoporous Silica for CO₂ Removal from Dry and Humid Air. *Chem. Eng. Sci* **2010**, *65*, 3695.
- (19) Choi, S.; Drese, J. H.; Eisenberger, P. M.; Jones, C. W. Application of Amine-tethered Solid Sorbents for Direct CO₂ Capture from the Ambient Air. *Environ. Sci. Technol.* **2011**, *45*, 2420.
- (20) Choi, S.; Gray, M. L.; Jones, C. W. Amine-tethered Solid Adsorbents Coupling High Adsorption Capacity and Regenerability for CO₂ Capture from Ambient Air. *ChemSusChem* **2011**, *4*, 628.
- (21) Serna-Guerrero, R.; Belmabkhout, Y.; Sayari, A. Modeling CO₂ Adsorption on Amine-functionalized Mesoporous Silica: 1. A Semi-empirical Equilibrium Model. *Chem. Eng. J.* **2010**, *161*, 173.
- (22) Ruthven, D. M. *Principles of Adsorption & Adsorption Processes*; pp. John Wiley & Sons: New York, 1984.
- (23) Serna-Guerrero, R.; Sayari, A. Modeling Adsorption of CO₂ on Amine-functionalized Mesoporous Silica. 2: Kinetics and Breakthrough Curves. *Chem. Eng. J.* **2010**, *161*, 182.

- (24) Farooq, S.; Ruthven, D. M. Heat Effects in Adsorption Column Dynamics. 2. Experimental Validation of the One-Dimensional Model. *Ind. Eng. Chem. Res.* **1990**, *29*, 1084.
- (25) Hicks, J. C.; Jones, C. W. Controlling the Density of Amine Sites on Silica Surfaces Using Benzyl Spacers. *Langmuir* **2006**, *22*, 2676.
- (26) Hicks, J. C.; Dabestani, R.; Ili, A. C. B.; Jones, C. W.; Division, C. S.; Ridge, O.; Box, P. O. Spacing and Site Isolation of Amine Groups in 3-Aminopropyl-Grafted Silica Materials: The Role of Protecting Groups. *Chem. Mater.* **2006**, *18*, 5022.
- (27) Bass, J. D.; Katz, A. Bifunctional Surface Imprinting of Silica: Thermolytic Synthesis and Characterization of Discrete Thiol–Amine Functional Group Pairs. *Chem. Mater.* **2006**, *18*, 1611.
- (28) Kim, J.; Chue, K.; Kim, K.; Choi, S. Non-isothermal Adsorption of Nitrogen-Carbon Dioxide Mixture in a Fixed Bed of Zeolite-X. *J. Chem. Eng. Jpn.* **1994**, *27*, 45.
- (29) Hwang, K.; Jun, J.; Lee, W. Fixed-Bed Adsorption for Bulk Component System. Non-equilibrium, Non-isothermal and Non-adiabatic Model. *Chem. Eng. Sci.* **1995**, *50*, 813.
- (30) Rezaei, F.; Mosca, A.; Webley, P.; Hedlund, J.; Xiao, P. Comparison of Traditional and Structured Adsorbents for CO₂ Separation by Vacuum-Swing Adsorption. *Ind. Eng. Chem. Res.* **2010**, *49*, 4832.
- (31) Sircar, S.; Kumar, R.; Anselmo, K. Effects of Column Nonisothermality or Nonadiabaticity on the Adsorption Breakthrough Curves. *Ind. Eng. Chem. Process Des. Dev.* **1983**, *22*, 10.

- (32) Belmabkhout, Y.; De Weireld, G.; Sayari, A. Amine-Bearing Mesoporous Silica for CO₂ and H₂S Removal from Natural Gas and Biogas. *Langmuir* **2009**, *25*, 13275.
- (33) White, L. D.; Tripp, C. P. An Infrared Study of the Amine-Catalyzed Reaction of Methoxymethylsilanes with Silica. *J. Colloid Interface Sci.* **2000**, *227*, 237.



CHAPTER 4

AN ADSORPTION CALORIMETRY APPARATUS TO STUDY CO₂-SUPPORTED AMINE INTERACTIONS

4.1. Background

Isosteric adsorption enthalpies (commonly referred to as isosteric heats of adsorption) represent a fundamental thermodynamic function of immense practical importance. They are necessary input variables in the simulation and design of adsorption separation processes. Isosteric heats of adsorption determine the degree of non-isothermality of an adsorption process, which in turn affects the local adsorption equilibria and kinetics. Also, in the case of temperature swing adsorption processes, the enthalpy of sorption impacts how much heat needs to be supplied to the adsorbent bed during the desorption step. Isosteric heats of adsorption, generally assumed to be temperature-independent functions, can be directly incorporated into the heat balance of an adsorption column described using the Gibbsian Surface Excess dynamic model.¹⁻³

In addition to its practical utility, isosteric heat of adsorption data can also be used to better understand adsorption thermodynamics. They are of fundamental importance from the point of view of testing the thermodynamic consistency of adsorption isotherm models. The nature of the isosteric heat of adsorption-surface coverage curve (referred to hereon as the heat-coverage curve) is a more stringent test for model validity compared to merely fitting equilibrium isotherm data at multiple temperatures to isotherm models.⁴ Apart from testing the physical consistency of

isotherm models used, heat-coverage data can provide extremely valuable information about the extent and nature of adsorbent surface heterogeneity.

There are several reports in the literature of indirect calculations of the isosteric heat of CO₂ adsorption as a function of amount of CO₂ adsorbed for supported amine materials.⁵⁻⁹ The heats of adsorption values calculated using the Clausius-Clayperon equation were not, however, compared to experimentally measured ones. In the case of supported amine adsorbent materials, the Toth model has been used most commonly to describe equilibrium CO₂ adsorption data.¹⁰⁻¹³ Whether the Toth model is capable of providing a satisfactory description of the CO₂-amine surface adsorption thermodynamics because the model is consistent with the adsorption process or merely as a result of an empirical fit, is a question that has not been explored. In addition, small errors in adsorption isotherm measurements at low pressures can lead to large errors in the isosteric heats calculated using the Clausius-Clayperon equation.¹⁴⁻¹⁷

The role of amine clustering and amine polymerization on diffusion heterogeneity was discussed in chapter 3. The heterogeneity in terms of CO₂ adsorption equilibrium, however, was treated purely on the basis of Toth isotherm parameters obtained from fitting adsorption data at multiple temperatures. A fundamental analysis of surface heterogeneity through rigorous calorimetry measurements and correlation of isosteric heats with different types of adsorption sites can potentially enable design of amine adsorbents with improved equilibrium CO₂ adsorption properties.

Recently, researchers in the supported amine adsorbent community, have begun investigating non-silica mesoporous oxide materials as supports for CO₂ capture.¹⁸⁻²¹ Some of the non-silica supports used in these studies were shown to have a favorable impact on amine efficiency (moles CO₂ adsorbed/moles amine) relative to the silica

support. Kuwahara et al.^{19,20} found that incorporation of an optimal amount of transition metal into the silica support resulted in a significant enhancement in the amine efficiency of PEI-impregnated adsorbents. The authors hypothesized that the observed enhancement in CO₂ capture efficiency may be a result of more optimal amine polymer–surface interaction. This polymer-surface interaction could potentially result in a modification of either 1) the physical configuration of the polymer or 2) electronic properties of the amine-polymer, or both. Modification of the physical configuration of the amine polymer can be probed by measuring the physical characteristics of the polymer impregnated material using techniques like N₂ physisorption (although the physical characteristics may be significantly different at liquid nitrogen temperatures versus close to room temperatures) and transport of non-chemisorbing gases through the pores of the support. On the other hand, a change in the electronic properties of the amine-polymer can be probed by measuring the strength of interactions (isosteric heat of adsorption) between CO₂ and amine adsorption sites. To this end, Llewellyn and co-workers²¹ have compared the adsorption isotherms and heat-coverage curves up to a pressure of 1 bar for aminopropylsilyl functionalized mesoporous silica and titania supports. Under the experimental conditions used in their study, the mesoporous titania supported amine adsorbent showed higher amine efficiencies compared to the mesoporous silica support. Below 0.1 bar, which is the pressure range relevant to post-combustion CO₂ capture applications, and also the pressure range in which we expect the contribution from CO₂ physisorption onto the bare mesoporous support to be negligibly small compared to chemisorption onto amine sites,¹³ the isosteric enthalpy of CO₂ sorption onto the titania supported material was higher than that onto the silica supported material at the same amine efficiency values (which may be considered a proxy for surface coverage). At the lowest amine efficiency value where isosteric sorption enthalpy values were reported for both materials, however, the adsorption enthalpy value for the mesoporous titania

supported aminopropyl material was approximately 10 KJ/mol higher than the value for the silica supported material. Even though the bare mesoporous titania support showed significant adsorption under the conditions of their study, the CO₂ adsorption enthalpy onto the bare titania support was lower than that for both amine functionalized supports at all surface coverages. The fact that the data for isosteric heat of CO₂ adsorption onto the APS-titania material was above that for the APS-silica material despite the lower enthalpies of CO₂ sorption onto the titania support suggests that the heat of CO₂ adsorption onto the amine sites on the APS-titania material is higher than for CO₂ adsorption onto the amine sites on the APS-silica material. This study strongly supports the hypothesis that modification of the support used to synthesize the supported amine adsorbent can indeed be used as a strategy to tune the chemical nature of the CO₂ capturing amine sites, thereby increasing the isosteric heat of CO₂-amine adsorption and potentially improving amine efficiencies. Whether or not this approach can be extended to non-titania supports has not been tested yet.

In other studies, Llewellyn and co-workers reported isosteric enthalpy of CO₂ adsorption data on supported amine adsorbents over pressures ranging from 0-6 bar for 3-(trimethoxysilyl)-propylethylenediamine functionalized silica²² and 0-2.5 bar on 3-aminopropylsilyl functionalized silica.²³ More recently, Azevedo and co-workers²⁴ measured the increase in CO₂ adsorption enthalpy on impregnating zeolite 13X with monoethanolamine.

Each of these measurements of isosteric heats of adsorption for supported amine materials have been reported for pressures up to a few bar, whereas the partial pressure range of interest for post-combustion CO₂ capture applications is 0-0.1 bar and that for air capture is 0-0.0004 bar. In the case of amine materials, it is not uncommon for the isotherm to be out of the Henry's law region even at a pressures as low as 0.001

bar.¹⁰⁻¹² To further emphasize the lack of isosteric adsorption enthalpy measurements in the ultra low pressure region of the isotherms, the number of data points reported corresponding to a pressure lower than 0.01 bar CO₂ adsorption for studies in the literature are reported in Table 4.1. Clearly, the focus of studies in the literature has been on measuring isosteric heats over a wide range of pressures, rather than measuring them accurately in the important low pressure range. Note that there is an intrinsic tradeoff between the pressure range of measurement and the accuracy of measurements at ultra-low pressures, due to limitations on the accuracy of high pressure transducers. To test physical consistency of isotherm models in the pressure range of interest, there is a need to collect more data points in the low pressure region of the isotherm compared to studies reported in the literature. In addition, since the most energetically favorable sites are filled in the low pressure region, this is the region that can be expected to yield the most interesting information with respect to CO₂-amine interactions. Arguably, the strongest motivation behind the study of heats of adsorption at very low coverages/pressures is the increasing influence of physisorption onto the bare oxide support as a function of pressure.¹³ Isosteric heat of adsorption data at low coverages can potentially enable direct investigation of CO₂-supported amine interactions without the need to deconvolute effects of CO₂-support physisorption and CO₂-amine chemisorption.

Table 4.1: Pressure range for measurement and number of low pressure data points for literature reports on CO₂-supported amine isosteric enthalpies of adsorption

Reference	Pressure range (bar)	Number of data points below 0.01 bar
22	0-6	0
21	0-1	1
23	0-2.5	0
24	0-1	1

Unlike the case of physisorbents, the detailed and systematic study of CO₂ chemisorption onto supported amine materials in the pressure range of interest requires the use of an adsorption calorimeter capable of measuring isosteric heats of adsorption accurately at low pressures (< 0.1 bar). Also, as mentioned before, the lower the pressure, the more significant one may expect errors in indirectly calculated isosteric heats of adsorption values to be. With this end in mind, I set out to design and validate an adsorption calorimeter apparatus that operates in the low pressure region (0-0.1 bar) and is capable of accurately measuring isosteric heats at pressures as low as 10⁻⁴ bar.

4.2. Theory

Figure 4.1 shows a closed system comprised of three phases: the solid adsorbent phase, the bulk gas phase, and the adsorbed phase. Using the Gibbsian surface excess model, one can define the isosteric heat of adsorption (which is in reality

the isosteric enthalpy of adsorption) as the negative of the differential change in system enthalpy with respect to adsorbate surface excess at constant temperature.

$$q_i = - \left[\frac{\partial H^{sys}}{\partial n^a} \right]_T \quad (4.1)$$

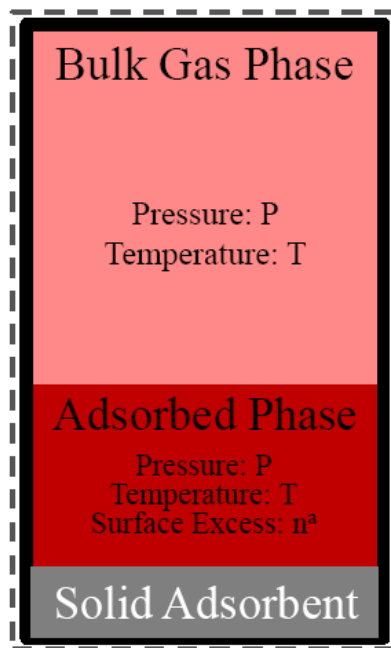


Figure 4.1: Schematic of the various phases according to the Gibbsian surface excess model (Illustration adapted from ref ¹)

In practice, it is not the system enthalpy change that is measured experimentally, but the heat evolved during the adsorption process. Since heat, unlike enthalpy change, depends on the path taken by the system during a process, one has to use the appropriate thermodynamic relation between heat measured and the enthalpy change

for a particular process. Applying the first law of thermodynamics and mole balances on the three phases of the open system (which is our sample cell, into which the adsorptive gas is dosed from a gas reservoir), the correlation between the experimentally measured heat and the isosteric heat of adsorption for a gas that behaves ideally under the conditions of the experiment can be shown to be as follows:²⁵

$$-\left[\frac{\partial Q^{\text{exp}}}{\partial n^a}\right]_{\text{T}} = q_i - (h^{\text{g,in}} - h^{\text{g}}) - (h^{\text{g,in}} - u^{\text{g}}) \left[\frac{\partial n^{\text{g}}}{\partial n^a}\right]_{\text{T}} \quad (4.2)$$

The same approach is taken for a system without the adsorbent or with a non-adsorbing solid, yields equation 4.3.

$$-\left[\frac{\partial Q'}{\partial n^a}\right]_{\text{T}} = - (h^{\text{g,in}} - u^{\text{g}}) \left[\frac{\partial n^{\text{g}}}{\partial n^a}\right]_{\text{T}} \quad (4.3)$$

Subtracting equation 4.3 from equation 4.2, gives:

$$-\left[\frac{\partial(Q^{\text{exp}} - Q')}{\partial n^a}\right]_{\text{T}} = q_i - (h^{\text{g,in}} - h^{\text{g}}) \quad (4.4)$$

Equation 4.4 implies there that are 2 ways to avoid calculating the third term on the right hand side of equation 4.2, which would require computing the slope of the adsorption isotherm. The first method is to run background measurements without the

sample for each set of expansions and obtain the heat released as a function of pressure. The second method is to use a twin cell arrangement and calculate the difference between the heat measurement in the sample cell (containing the adsorbent: Q_{exp}) and the reference cell (empty : Q'). For the sake of convenience of measurement and other factors discussed in the section 4.3, the second approach with a twin-cell arrangement was chosen. The second term on the right hand side of equation 4.4 is merely the difference in molar enthalpy between the incoming gas and the gas in the sample cell. For an ideal gas, this term can be eliminated if the incoming gas and the gas in the sample cell are at maintained at the same temperature. Hence, for a twin cell calorimeter with the gas reservoir maintained at the same temperature as the sample chamber, the differential of the heat measured experimentally with respect to the surface excess at constant temperature yields the isosteric heat of adsorption (equation 4.5).

$$-\left[\frac{\partial(Q^{\text{exp}} - Q')}{\partial n^a}\right]_T = q_i \quad (4.5)$$

4.3. Experiments

4.3.1. Dosing system design considerations

The two variables that need to be monitored accurately during the course of the experiments are the gas pressure above the adsorbent at a certain adsorbate loading and the amount of heat evolved during the adsorption process. Lessons learned and design considerations implemented in a number of previous reports in the literature^{14,26-30} were incorporated in the design of the instrument. Here are some of the practical constraints under which the system needs to be operated.

The adsorption process needs to be relatively fast, ideally equilibrating in less than an hour, to enable accurate estimation of heat evolved by integrating the thermopile signal. To make sure adsorption equilibration is achieved on a short time scale, it is not sufficient merely to have an adsorbent material that equilibrates rapidly. Equilibration inside the void space in the sample cell must also be relatively fast. As an example, for a sample having a pore size of 5 nm, at room temperature, Knudsen diffusion coefficients are on the order of $0.01 \text{ cm}^2/\text{s}$. For a particle 500 micron in size, the time scale for diffusion is approximately 0.25 seconds. Also, at room temperature and 0.1 bar, the gas phase bulk diffusion coefficient is on the order of $1 \text{ cm}^2/\text{s}$. If the longest dimension in the cell is 15 cm, the time scale for gas diffusion is 225 seconds. Hence, unless the material has significant diffusion limitations, it is diffusion within the sample cell that will determine equilibration time. Obviously, reducing the size of the sample cell will result in a reduction in equilibration time, but other system requirements that determine a lower limit on the reduction in sample chamber volume that can be achieved.

For chemisorbants like supported amines, in the initial doses, a significant fraction of the gas that gets transferred from the gas reservoir to the sample chamber is adsorbed onto the amine adsorbent, thereby increasing the surface coverage significantly. Given the steep nature of the CO_2 isotherm at low pressures, measuring isosteric heats at low coverages necessitates the ability to 1) dose small amounts of gas into the sample cell and 2) measure minute changes in gas phase pressure. The second requirement can be met by a sufficiently accurate pressure transducer. The first requirement, which is one of small dose sizes, is achieved by using an apparatus with a high ratio of sample chamber volume to gas reservoir volume. For specific initial pressures in the sample chamber and gas reservoir, the higher the sample chamber to gas reservoir volume, the lower the final pressure in the sample chamber, thus enabling

multiple doses at low pressures. The sample chamber volume cannot, however, be increased indefinitely because of the limitation on the largest length scale for gas diffusion (discussed above). As a result of this tradeoff, a sample chamber volume of 16.3 ml and a reservoir volume of 5.68 ml was used for the instrument. The length of the maximum dimension for the sample chamber is ~30 cm, which corresponds to an approximate equilibration time of 900 seconds, well below the 1 hour limit on the equilibration time set by the sensitivity of the thermopiles. As will be shown later in this chapter as well as the next, these parameters allowed for multiple doses to be carried out at low coverages/pressures.

A low-pressure, high-accuracy pressure transducer (range: 0-0.1 bar) was used on the sample side (which had a large volume and hence small pressure changes) and a high-pressure transducer (0-3.5 bar) was used on the reservoir side (which had a small volume and hence large pressure changes).

4.3.2. *Calorimeter description*

There are three different ways to measure heat evolution corresponding to a certain physical/chemical process: adiabatic calorimetry, isoperibol calorimetry, and conduction calorimetry (also referred to as Tian-Calvet calorimetry).³¹ In the case of adiabatic calorimetry, as the name suggests, the sample cell wall is insulated from the inner wall of the surrounding cavity. Knowing the specific heat capacity of the sample cell, the rise in temperature of the sample cell is correlated with the amount of heat released. In practice, it is extremely hard if not impossible, to insulate the sample cell completely from the surrounding block, thus resulting in heat leakage. Also, stirring the contents of the cell is necessary to maintain temperature uniformity, adding complexity

to the cell and rendering it hard to measure small quantities of heat. In the case of the isoperibol calorimeter, the temperature of the jacket surrounding the sample cell is kept constant. A large thermal conductivity of the medium between the sample cell and the outer vessel is needed to maintain a small temperature difference between the sample and the outer vessel. A major hurdle in using this type of calorimeter is its high thermal inertia.³¹ The third type of calorimeter, which is the one used in this study, is a conduction calorimeter, or a Tian-Calvet heat flux microcalorimeter.

A Sensys Evo DSC purchased from Setaram Inc. is used to measure the heat evolved in the sample cell. The basic principle of operation is shown in Figure 4.2. A and B are two different conductors. If the junctions A/B and B/A are at different temperatures T_1 and T_2 , and the number of conductor wires is n , then an electromotive force proportional to both the number of junctions as well as the temperature difference $T_1 - T_2$ is produced and this can be measured by a voltmeter in the circuit. This phenomenon is known as the Seebeck effect. As a corollary to this effect (known as the Peltier effect), if there is instead, a battery connected to these conductors in series and a current I is passed through them, one junction becomes hot and the other cold. The direction of the temperature gradient can be reversed by passing current in the opposite direction. In the calorimeter block, there are several hundred thermocouples located around the sample area, which enable accurate measurement of the heat released on adsorption. It can be shown that the electromotive force (emf) developed in each thermocouple is proportional to the heat flowing through the wall area, irrespective of the temperature of the sample cell wall. This means that the total heat generated is directly proportional to the total emf developed. This is extremely advantageous, since, even when the contents of the sample are in a state of non-equilibrium, thus leading to a non-uniform temperature distribution in the sample cell wall, the total heat flux can be measured accurately. In

practice, the heat generated in the sample cell is compensated for by passing a current through the thermopile such that as a result of Peltier cooling, no net temperature gradient exists between the inner and outer walls. This helps keep the sample at a constant temperature throughout the run. For experiments reported in this chapter and the next, it was found that the temperature of the sample varied by less than a hundredth of a degree. In addition to enabling direct calculation of isosteric heats of adsorption (read above), the twin cell design also allowed for direct accounting of any thermal fluctuations in the calorimeter block.

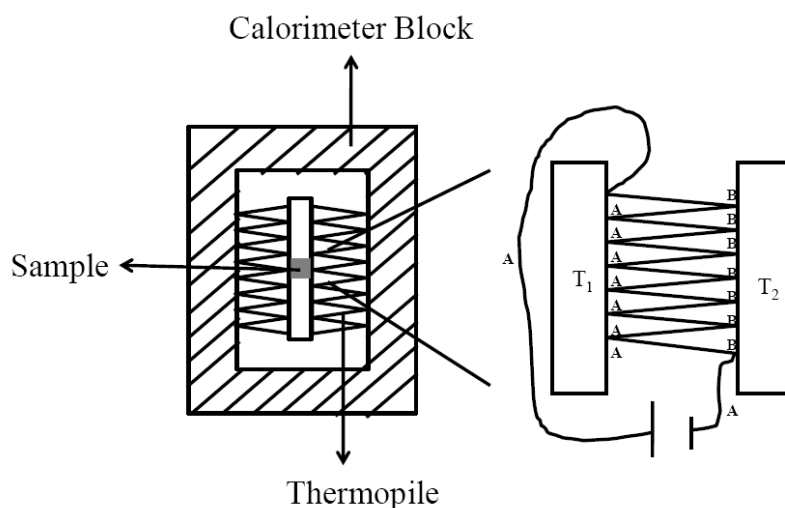


Figure 4.2: Schematic describing measurement of heat evolution in the calorimeter.

Illustration adapted from the description in ³¹

4.3.3. Experimental setup

Figure 4.3 shows a schematic of the experimental apparatus. The vacuum pump and gas tank are connected to the gas reservoir, with the option of venting the reservoir

to atmospheric conditions. The gas reservoir is connected to the sample chamber, which has two prongs, one going to the sample cell and the other going to the reference cell. The entire assembly is maintained at the same temperature, using the calorimeter heating/cooling block for the sample cell and heating tape combined with cotton wool insulation for the rest of the apparatus (shown using the dashed line in Figure 4.3). A fritted VCR gasket is used to prevent the sample from being pulled out of the sample cell. The dead volume in the sample chamber is calculated using helium expansion measurements.

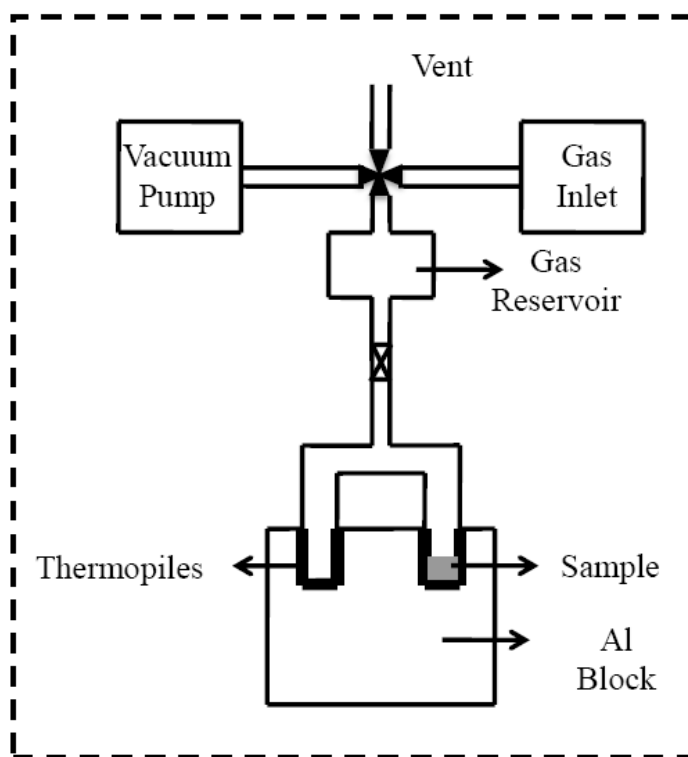


Figure 4.3: Schematic of the experimental setup used to measure isosteric heats of adsorption

4.3.4. *Experimental procedure*

The powder adsorbent sample was first pressed into pellets under a pressure of 4000 psi, after which they were sieved between 500 and 1500 microns. Then, 30-70 mg of the sample were loaded into the sample cell (on the sample side and not on the reference side). The sample tube was attached to the dosing system and carefully inserted into the calorimeter block. Slowly, vacuum was pulled on the sample by inducing static vacuum in the gas reservoir and the sample chamber until the pressure fell to a value of 5 mbar, below which the sample was exposed to dynamic vacuum. At this point the system was purged with helium 3 times to make sure the residual gas pressure in the system was due to non-adsorbing helium and not some other adsorbing gas. After vacuum was pulled on the sample once more, the sample chamber was heated to 120°C using a ramp rate of 5°C/min and held at that temperature for 3 hours, after which the temperature was brought down to 30°C. It took approximately 3 hours for the sample chamber to cool down to and equilibrate at 30°C, after which the sample chamber was isolated from vacuum, allowed to stabilize, and the adsorption measurement started. The regeneration protocol described here was found to produce highly reproducible results for zeolites and supported amine adsorbents.

After regeneration was complete and the system stabilized at 30°C, the appropriate amount of gas was dosed into the gas reservoir and allowed to equilibrate for 15 minutes. The valve between the gas reservoir and the sample chamber was opened briefly and closed back while monitoring the heat signal from the thermopiles and the pressure in both the reservoir and the sample chamber. A mole balance applied on the system (sample chamber + gas reservoir) using the initial and final pressures is used to calculate the amount adsorbed and integration of the thermopile signal obtained as a function of time yields the total heat evolved. All data reported in this chapter and

chapter 5 is for materials that equilibrated in less than an hour per dose. In practice, the adsorption rate does not go all the way to zero and one needs to define an adsorption rate that is sufficiently low to justify the assumption of reaching adsorption equilibrium. A cutoff rate of change of 0.15 Pa/min was used in the experiments, which translates to an adsorption rate of 0.028 mmol/(g.day) for 50 mg of sample loaded into the apparatus. The heat versus adsorbed amount curve, which is a plot of the integral heat of adsorption, was obtained after all the doses were completed. The isosteric heat is then obtained by differentiating this integral enthalpy of adsorption curve.

4.4. Results & Discussion

To validate the adsorption calorimeter apparatus, a material that satisfies several criteria is needed. Ideally, a material is needed for which there is good agreement on both the isosteric heat of adsorption at zero coverage and the trend for CO₂ isosteric heat of adsorption as a function of coverage. Also, since the glass to metal connection in the apparatus is sealed using an epoxy resin that can only withstand temperatures up to 120°C, the adsorbent material must be capable of being regenerated at or below a temperature of 120°C. Based on these criteria, silicalite-1 was chosen to test the system against literature data. Its adsorption properties have been studied by many different research groups.^{14,32-37} The isosteric heats of CO₂ adsorption on silicalite have been estimated by several groups using indirect^{34,37,38} and direct (calorimetric)^{14,33} methods. Its hydrophobic surface properties compared to other zeolites like 13X makes it suitable for regeneration at 120°C.

Figure 4.4 shows the data for CO₂ adsorption on silicalite measured using the system described in this chapter. The figure shows three separate runs on the

instrument. The first two runs have approximately the same dose size, whereas the third run has almost twice the dose size as the first two runs. It is clear that the measured value of isosteric heat of adsorption is independent of dose size, which is a critical result to obtain. Even though the isosteric heat of adsorption is a differential quantity, in practice, it is calculated from heat measurements resulting from finite doses. According to Myers et al.,²⁶ the error associated with finite doses is generally negligible below doses of the size 1 mol/kg. There is, however, no theoretical basis for this limit and hence, the effect of dose size on measured isosteric heats must be evaluated for every adsorbent to ensure that the reported heats are truly differential quantities. In the case for the silicalite runs shown in Figure 4.4, clearly, the dose sizes are small enough to measure isosteric heats of adsorption. The reproducibility is excellent for both the adsorption isotherms as well as the heat-coverage curves.

Sircar and co-workers¹⁴ have compiled a list of isosteric heats of CO₂ adsorption at zero coverage calculated using different techniques. In Table 4.2, we compare the value of isosteric heat of adsorption at zero coverage in this study with values reported in the literature. We see that the value for this study (25.4 KJ/mol) lies within the range of values reported in the literature. The nature of the heat-coverage curve is also consistent with literature reports.¹⁴ The silicalite surface is highly homogeneous, resulting in a very slight increase in isosteric heat as a function of coverage as a result of lateral CO₂-CO₂ interactions. Note that a direct comparison of the data points in this study with those in the literature is not provided here, since, except for a few data points in the literature, all the rest are at higher pressures than the pressure range of this instrument. The fact that the apparatus described in this chapter yields consistent results for CO₂ adsorption on silicalite in terms of both the isosteric heat at zero coverage as well as the nature of the heat-coverage curve is promising for future studies on CO₂-amine adsorption, as the

expected values of isosteric heats for the latter are expected to be approximately 4 times the former. Overall, the sensitivity, reproducibility, and accuracy of the instrument are sufficiently high insofar as it promises to enable fundamental studies of CO₂-supported amine adsorption at low pressures/surface coverages.

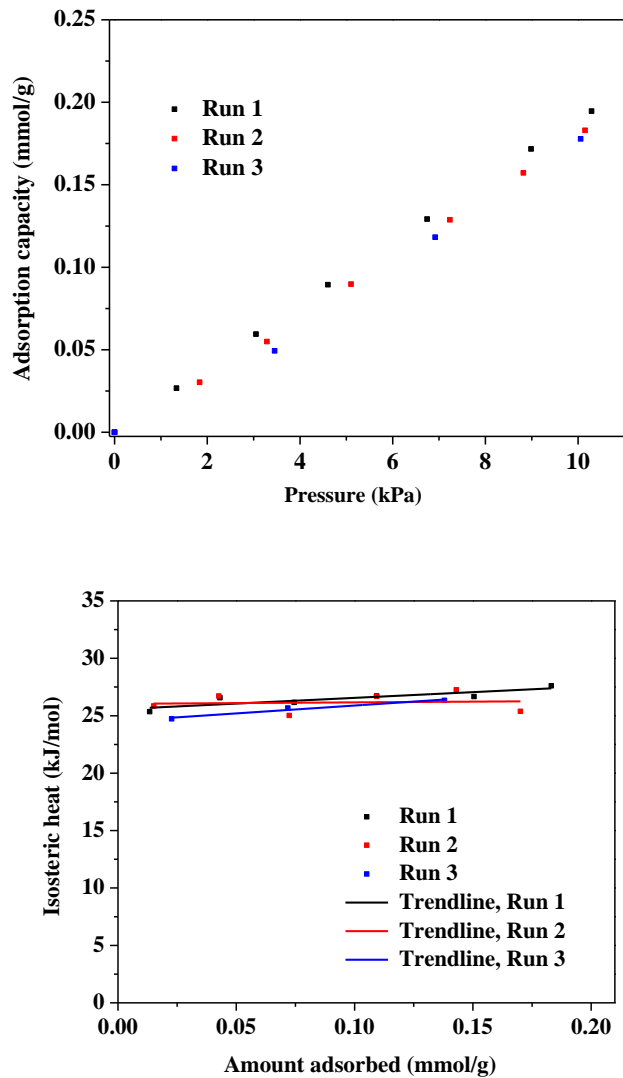


Figure 4.4: Adsorption isotherm (top) and isosteric heat of adsorption (bottom) for CO₂ adsorption onto silicalite

Table 4.2: Isosteric heats at zero coverage for CO₂ adsorption on Silicalite-1

Reference	Method Used	Isosteric heat at 0 coverage (kJ/mol)
This study	Calorimetric	25.4
14	Calorimetric	27.2
33	Calorimetric	29.0
34	Volumetric	24.1
38	Isosteric	24.6
37	GC Pulse	21.7

4.5. Conclusions

Isosteric heat of adsorption data obtained at low pressures (<0.1 bar) can potentially enhance the fundamental understanding of CO₂ adsorption onto supported amine materials. This chapter describes the underlying theory, experimental setup, and validation of an adsorption calorimeter capable of measuring these quantities at low pressures/coverages. Silicalite-1, a well-studied material in terms of CO₂ isosteric heats of adsorption, has been tested to assess the performance of the setup. The isosteric heat of sorption at zero coverage was found to be within the bounds of values reported in the literature. In addition, the expected trend for isosteric heat of adsorption with increasing surface coverage for a homogenous adsorbent was obtained. This apparatus has the potential to enable a better overall understanding of CO₂-amine adsorption thermodynamics and provide new insights into supported amine adsorbent surface heterogeneity.

4.6. Notation

q_i : Isosteric enthalpy (heat of adsorption)

H^{sys} : Total system enthalpy

n^{a} : Gibbsian surface excess

P : Pressure

T : Temperature

Q^{exp} : Experimentally measured heat (with sample)

Q' : Experimentally measured heat (without sample)

n^{g} : number of moles in the gas phase

u^{g} : gas phase molar internal energy

h^{g} : gas phase molar enthalpy

$h^{\text{g, in}}$: molar enthalpy of incoming (dosed) gas

4.7. References

- (1) Sircar, S.; Mohr, R.; Ristic, C.; Rao, M. B. Isotheric heat of adsorption: Theory and experiment. *J. Phys. Chem. B* **1999**, *103*, 6539-6546.
- (2) Sircar, S. Excess properties and thermodynamics of multicomponent gas adsorption. *J. Chem. Soc., Faraday Trans.* **1985**, *81*, 1527.
- (3) Sircar, S. Excess properties and column dynamics of multicomponent gas adsorption. *J. Chem. Soc., Faraday Trans.* **1985**, *1541*, 1541-1545.
- (4) Rudzinski, W.; Narkiewicz-Michalek, J.; Szabelski, P.; Chiang, A. S. T. Adsorption of aromatics in zeolites ZSM-5 : A thermodynamic-calorimetric study based on the model of adsorption on heterogeneous adsorption sites. *Langmuir* **1997**, *13*, 1095-1103.
- (5) Leal, O.; Bolivar, C.; Ovalles, C.; Jos, J.; Espidel, Y. Reversible adsorption of carbon dioxide on amine surface-bonded silica gel. *Inorganica Chimica Acta* **1995**, *240*, 183-189.
- (6) Wang, L.; Yang, R. T. Increasing selective CO₂ adsorption on amine-grafted SBA-15 by increasing silanol density. *J. Phys. Chem. C* **2011**, *115*, 21264-21272.
- (7) Zúkal, A.; Jagiello, J.; Mayerová, J.; Čejka, J. Thermodynamics of CO₂ adsorption on functionalized SBA-15 silica. NLDFT analysis of surface energetic heterogeneity. *Phys. Chem. Chem. Phys.* **2011**, *13*, 15468-75.

- (8) Zukal, A.; Dominguez, I.; Mayerová, J.; Cejka, J. Functionalization of delaminated zeolite ITQ-6 for the adsorption of carbon dioxide. *Langmuir* **2009**, *25*, 10314-21.
- (9) Belmabkhout, Y.; Sayari, A. Effect of pore expansion and amine functionalization of mesoporous silica on CO₂ adsorption over a wide range of conditions. *Adsorption* **2009**, *15*, 318-328.
- (10) Bollini, P.; Brunelli, N. A.; Didas, S. A.; Jones, C. W. Dynamics of CO₂ adsorption on amine adsorbents. 1. Impact of heat effects. *Ind. Eng. Chem. Res.* **2012**, *51*, 15145-15152.
- (11) Bollini, P.; Brunelli, N. A.; Didas, S. A.; Jones, C. W. Dynamics of CO₂ adsorption on amine adsorbents. 2. Insights Into adsorbent design. *Ind. Eng. Chem. Res.* **2012**, *51*, 15153-15162.
- (12) S.A. Didas, A.R. Kulkarni, D.S. Sholl, C. W. J. Role of Amine Structure on CO₂ Adsorption from Ultra-dilute Gas Streams such as Ambient Air. *ChemSusChem* **2012**, *5*, 2058.
- (13) Serna-Guerrero, R.; Belmabkhout, Y.; Sayari, A. Modeling CO₂ Adsorption on Amine-functionalized Mesoporous Silica: 1. A Semi-empirical Equilibrium Model. *Chem. Eng. J.* **2010**, *161*, 173.

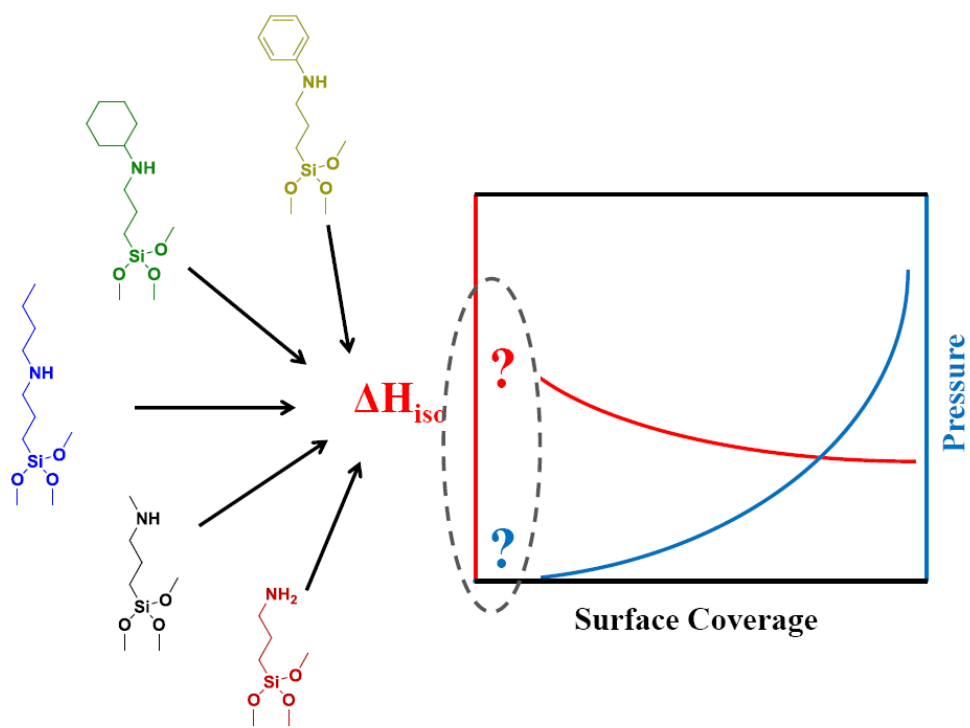
- (14) Dunne, J. A.; Mariwala, R.; Rao, M.; Sircar, S.; Gorte, R. J.; Myers, A. L. Calorimetric heats of adsorption and adsorption isotherms. 1. O₂, N₂, Ar, CO₂, CH₄, C₂H₆, and SF₆ on silicalite. *Langmuir* **1996**, *12*, 5888-5895.
- (15) Rouquerol, F.; Rouquerol, J.; Della Gatta, G.; Letoquart, C. Use of isothermal microcalorimetry data for the determination of integral molar entropies of adsorption at the gas-solid interface by a quasi-equilibrium procedure. *Thermochim. Acta* **1980**, *39*, 151-158.
- (16) Mohlin, U.-B.; Gray, D. . Gas chromatography on polymer surfaces: Adsorption on cellulose. *J. Colloid Int. Sci.* **1974**, *47*, 747-754.
- (17) Rhodin, T. N. The anisotropy of nitrogen adsorption on single crystal copper surfaces. *J. Am. Chem. Soc.* **1950**, *8*.
- (18) Chaikittisilp, W.; Kim, H. J.; Jones, C. W. Mesoporous Alumina-Supported Amines as Potential Steam-Stable Adsorbents for Capturing CO₂ from Simulated Flue Gas and Ambient Air. *Energy Fuels* **2011**, *25*, 5528.
- (19) Kuwahara, Y.; Kang, D.-Y.; Copeland, J. R.; Bollini, P.; Sievers, C.; Kamegawa, T.; Yamashita, H.; Jones, C. W. Enhanced CO₂ adsorption over polymeric amines supported on heteroatom-incorporated SBA-15 silica: impact of heteroatom type and loading on sorbent structure and adsorption performance. *Chem. Eur. J.* **2012**, *18*, 16649-64.

- (20) Kuwahara, Y.; Kang, D.-Y.; Copeland, J. R.; Brunelli, N. a; Didas, S. a; Bollini, P.; Sievers, C.; Kamegawa, T.; Yamashita, H.; Jones, C. W. Dramatic enhancement of CO₂ uptake by poly(ethyleneimine) using zirconosilicate supports. *J. Am. Chem. Soc.* **2012**, *134*, 10757-60.
- (21) Knöfel, C.; Martin, C.; Hornebecq, V.; Llewellyn, P. L. Study of Carbon Dioxide Adsorption on Mesoporous Aminopropylsilane-Functionalized Silica and Titania Combining Microcalorimetry and in Situ Infrared Spectroscopy. *J. Phys. Chem. C* **2009**, *113*, 21726.
- (22) Knöfel, C.; Descarpentries, J.; Benzaouia, A.; Zeleňák, V.; Mornet, S.; Llewellyn, P. L.; Hornebecq, V. Functionalised micro-/mesoporous silica for the adsorption of carbon dioxide. *Microporous Mesoporous Mater.* **2007**, *99*, 79-85.
- (23) Mello, M. R.; Phanon, D.; Silveira, G. Q.; Llewellyn, P. L.; Ronconi, C. M. Amine-modified MCM-41 mesoporous silica for carbon dioxide capture. *Microporous Mesoporous Mater.* **2011**, *143*, 174-179.
- (24) da Silva, F. W. M.; Maia, D. a. S.; Oliveira, R. S.; Moreno-Piraján, J. C.; Sapag, K.; Cavalcante, C. L.; Zgrablich, G.; Azevedo, D. C. S. Adsorption microcalorimetry applied to the characterisation of adsorbents for CO₂ capture. *Can. J. Chem. Eng.* **2012**, *90*, 1372-1380.

- (25) Cardona-Martinez, N.; Dumesic, J. A. Applications of adsorption microcalorimetry to the study of heterogeneous catalysis. *Adv. Catal.* **1992**, *38*, 149-237.
- (26) Siperstein, F.; Gorte, R. J.; Myers, A. L. A new calorimeter for simultaneous measurements of loading and heats of adsorption from gaseous mixtures. *Langmuir* **1999**, *15*, 1570-1576.
- (27) Parrillo, D. J.; Gorte, R. J. Design parameters for the construction and operation of heat-flow calorimeters. *Thermochim. Acta* **1998**, *312*, 125-132.
- (28) Handy, B. E.; Sharma, S. B.; Spiewak, B. E.; Dumesic, J. A. A Tian-Calvet heat-flux microcalorimeter for measurement of differential heats of adsorption. *Meas. Sci. Technol.* **1993**, *4*, 1350-1356.
- (29) Garcia-Cuello, V.; Moreno-Piraján, J. C.; Giraldo-Gutiérrez, L.; Sapag, K.; Zgrablich, G. A new microcalorimeter of adsorption for the determination of differential enthalpies. *Microporous Mesoporous Mater.* **2009**, *120*, 239-245.
- (30) Garcia-Cuello, V.; Moreno-Pirajan, J. C.; Giraldo-Gutierrez, L.; Sapag, K.; Zgrablich, G. Design, calibration, and testing of a new Tian-Calvet Heat-Flow Microcalorimeter for measurement of differential heats of adsorption. *Instrum. Sci. Technol.* **2008**, *36*, 455-475.

- (31) Calvet, E.; Prat, H.; Skinner, H. A. *Recent progress in microcalorimetry*, The Macmillan Company: New York, 1963; Vol. 39, pp. 183-189.
- (32) Chaudhary, V. R.; Mayadevi, S. Adsorption of methane, ethane, ethylene, and carbon dioxide on silicalite-I. *Zeolites* **1996**, *17*, 501-507.
- (33) Dubinin, M. M.; Rakhmatkariev, G. U.; Isirikiyan, A. A. Heats of adsorption of CO₂ on high-silicon zeolites and silicalite. *Izv. Akad. Nauk SSSR, Ser. Khim.* **1989**, *11*, 2636-2638.
- (34) Golden, T. C.; Sircar, S. Gas adsorption on silicalite. *J. Colloid Int. Sci.* **1994**, *162*, 182-188.
- (35) Delgado, J. A.; Uguina, M. A.; Sotelo, J. L.; Ruíz, B. Fixed-bed adsorption of carbon dioxide–helium, nitrogen–helium and carbon dioxide–nitrogen mixtures onto silicalite pellets. *Sep. Purif. Technol.* **2006**, *49*, 91-100.
- (36) Lee, S. C. Prediction of permeation behavior of CO₂ and CH₄ through silicalite-1 membranes in single-component or binary mixture systems using occupancy-dependent Maxwell–Stefan diffusivities. *J. Membr. Sci.* **2007**, *306*, 267-276.
- (37) Chaoudhary, V. R.; Mayadevi, S. Adsorption of methane, ethane, ethylene, and carbon dioxide on high silica pentasil zeolites and zeolite-like materials using gas chromatography pulse technique. *Sep. Sci. Technol.* **1993**, *28*, 2197-2209.

- (38) Rees, L. V. C.; Hampson, J.; Brückner, P. Sorption of single gases and their binary mixtures in zeolites. *Zeolite Microporous Solids: Synthesis, Structure, and Reactivity* **1992**, 352, 133-149.



CHAPTER 5

EFFICIENCY OF SUPPORTED AMINE ADSORBENTS FOR CO₂ CAPTURE: ROLE OF AMINE STRUCTURE & DENSITY

5.1. Background

In chapter 3, strong evidence was presented supporting the idea that overloading of mesoporous oxide supports with amine containing organic groups can induce CO₂ diffusion limitations in supported amine adsorbents, thereby reducing breakthrough capacities. In principle, there are two approaches to synthesizing more attractive adsorbents from a practical application perspective, where breakthrough capacities are of paramount importance. The first is to try to increase the fraction of highly accessible amine groups at high amine loadings. The second approach is to increase the efficiency with which amines adsorb CO₂ in the first place. The first approach is one where new materials with improved adsorption kinetics are synthesized, and the second, one where materials with better thermodynamic CO₂ adsorption properties are synthesized. In the amine adsorbent literature, the metric 'amine efficiency' is commonly used to denote the overall utility of amine sites in terms of CO₂ adsorption.

Although many studies in the literature report amine efficiency values (for a list of amine efficiencies, see ¹), there is a need for better understanding of the factors that impact amine efficiencies. Two characteristics of the amine supported adsorbents that are consistently correlated with amine efficiencies are amine type and amine density/proximity. Several groups have found that at similar amine loadings, primary amines are more efficient at capturing CO₂ than secondary amines. Didas et al.²

reported amine efficiency values for aminopropylsilyl functionalized mesocellular foam silica (a primary amine containing material abbreviated as APS) that were 2.4 times those for the methylaminopropylsilyl functionalized material (a secondary amine functionalized material abbreviated as MAPS) at 0.0004 bar CO₂ and room temperature and 1.4 times that of the MAPS material at 0.1 bar. The authors noted that the higher isosteric heats of CO₂ adsorption on the APS material relative to the MAPS material obtained using the Toth model suggested that higher isosteric heats of CO₂ adsorption correlated with higher amine efficiencies. Choi et al.³ reported amine efficiencies for APS functionalized SBA-15 that are 16% higher than those for MAPS functionalized ones at similar amine loadings. Their measurements, however, were carried out at 1 bar CO₂, a pressure at which the contribution from CO₂ physisorption to overall adsorption can be significant.⁴ Despite the higher pressures, they observed a higher amine efficiency for the APS functionalized SBA-15 material relative to the MAPS functionalized one. Zelenak et al.⁵ reported amine efficiencies at 0.1 bar for the APS functionalized SBA-12 that were 9% higher than those for the MAPS functionalized material at very similar amine loadings. The consistency of these reports from different research groups suggests that primary amines are more efficient at adsorbing CO₂ compared to secondary amines. Chaikittisilp et al.⁶ attempted to exploit this higher efficiency of primary amines by impregnating an all primary amine polymer polyallylamine (PAA) into a mesocellular foam silica support. At low organic loadings, the PAA materials exhibited similar amine efficiencies as the branched polyethyleneimine (PEI) adsorbents. Also, both the PAA and the branched PEI impregnated adsorbents showed higher amine efficiencies compared to the linear PEI impregnated MCF materials, which had the lowest fraction of primary amines amongst the amine-polymers used in the study. It was hypothesized that the difference in backbone structures of the

PAA and PEI impregnated adsorbents was a possible cause of similar amine efficiencies measured for the PAA and branched PEI impregnated MCF materials.

The impact of amine density on amine efficiency is also well accepted. Several authors have reported increasing amine efficiencies with increasing amine loadings for both impregnated materials as well as adsorbents with covalently tethered amines.^{7,8} Increasing amine efficiency as a function of amine density/proximity can be interpreted as a direct consequence of the proposed CO₂-amine reaction mechanism. Under dry conditions, two amine groups are required to adsorb one molecule of CO₂, (see chapter 1) and hence, the greater the proximity of amines, the more efficient they are at adsorbing CO₂.

The theoretical maximum amine efficiency of 0.5 applies only to the ideal case where there is no physisorption of CO₂ onto the bare support. In practice, there is always some CO₂ physisorption on a supported amine material as long as there is a certain fraction of the bare surface left exposed post amine-functionalization. Serna-Guerrero et al.⁴ carried out a detailed modeling study of both physisorption and chemisorption onto triamine functionalized pore expanded MCM-41. The study was carried out in the pressure range 0-20 bar. It was concluded that for the materials tested in that study, CO₂ physisorption did not contribute significantly to overall adsorption below 0.2 bar. Their results suggest that studying adsorption at low pressures (< 0.1 bar) can potentially enable study of amine efficiencies in the absence of physisorption, where the expected maximum amine efficiency is 0.5.

From a thermodynamic standpoint, there are two factors that can potentially affect the efficiency of a supported amine adsorbent: the enthalpy change associated with the adsorption process and the entropy change associated with the adsorption

process. The enthalpy change or the isosteric enthalpy of adsorption can be interpreted as a direct measure of the strength of the chemical interaction between the amine group/groups and the adsorbed CO₂ molecule. The entropy change, on the other hand, is representative of the loss in degrees of freedom associated with the transfer of molecules from the gas phase to the adsorbed phase. To the best of the author's knowledge, there are no reports in the literature that attempt to rationalize amine efficiencies of various supported amine structures from an enthalpic and entropic perspective. The adsorption calorimeter described in the previous chapter can be used for this purpose. In this study, experimentally measured isosteric enthalpies of CO₂ adsorption are reported as a function of amount adsorbed for an array of supported amine adsorbents in which the alkyl group attached to the nitrogen atom and the amine density are varied in a systematic fashion. The study provided novel insights into amine efficiency trends consistent with those observed in the literature.

5.2. Experiments

Materials synthesis and characterization techniques used in this study are described in detail in chapter 2. The procedure for calorimetry experiments has been described in the previous chapter.

5.3. Results & Discussion

5.3.1. Effect of amine density

To study the effect of amine density on isosteric heats of adsorption, a series of aminopropylsilyl functionalized SBA-15 materials was synthesized with progressively increasing loadings of aminopropylsilane. Figure 5.1 shows the isosteric heat of adsorption and adsorption isotherm data for this series of materials. The isosteric heat of adsorption for the material with the lowest amine loading (0.87 mmol N/g) is almost indistinguishable from that of the silica support. As the amine loading is increased, the isosteric heat of adsorption close to zero coverage also increases with loading, reaching a value of 92 kJ/mol for the material with a loading of 1.87 mmol N/g SiO₂. All of the materials tested were found to be highly heterogeneous, with large variations in isosteric heat of adsorption with coverage. As explained in the previous section, there is evidence in the literature of increasing amine efficiencies with amine loading. The same factors that lead to an increase in amine efficiency with loading can be hypothesized to explain the increasing isosteric heats of adsorption at low surface coverages observed in Figure 5.1. But there is another additional factor that would lead to an increasing trend in CO₂ isosteric heat as a function of amine loading. Increasing the amine loading not only increases the number of sites available for CO₂ chemisorption, but also reduces the amount of bare unfunctionalized surface available for CO₂ physisorption. As can be seen in Figure 5.1 (bottom), the amount of CO₂ physisorbed onto the bare support is significant compared to the overall amount adsorbed at low amine loadings.

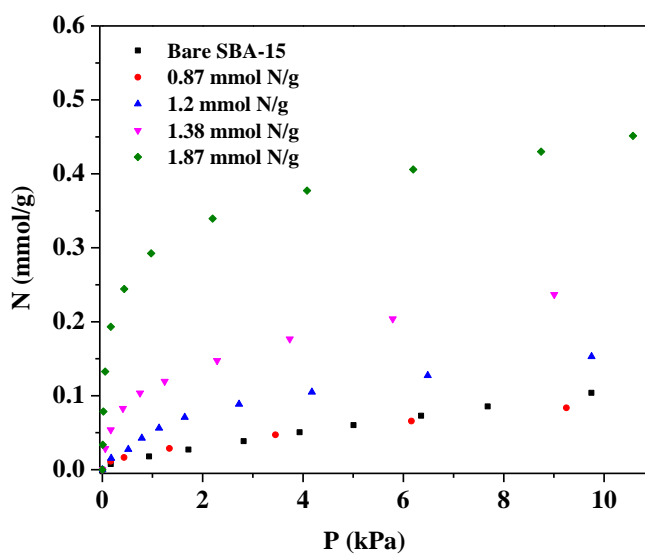
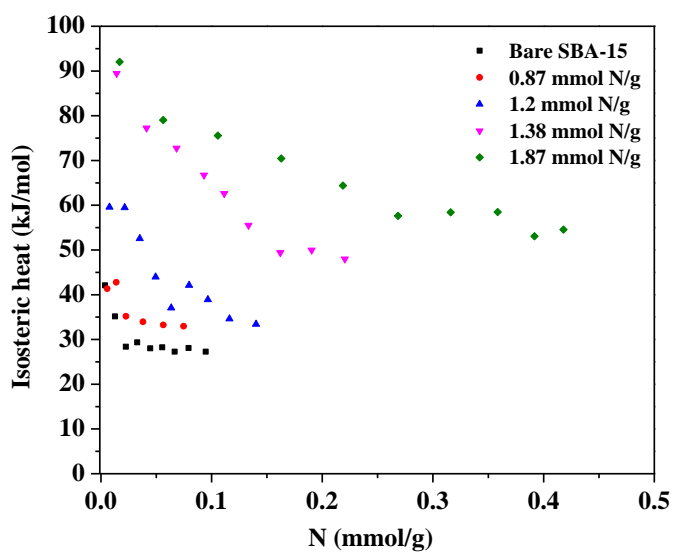


Figure 5.1: Heat-coverage curves (top) and adsorption isotherms (bottom) for the aminopropylsilyl functionalized SBA-15 materials

To deconvolute these two effects, the amount physisorbed onto the exposed silica surface of the aminopropylsilyl SBA-15 materials is calculated by taking into

account the ratio of the BET surface areas of the bare silica support and the aminopropylsilyl functionalized materials. The amount of chemisorbed CO₂ can then be calculated from the difference between the total adsorption capacity and the physisorption capacity. This approach has been applied successfully to other adsorbent materials in the literature.⁴ Having obtained an estimate of the relative amounts of CO₂ physisorbed and chemisorbed, we can then estimate the isosteric heat of adsorption associated purely with chemisorption. The APS material with an amine loading with an amine loading of 1.2 mmolN/g is ideally suited for this calculation, since it has an isosteric heat approximately midway between that of the silica support and the adsorbent with the highest initial isosteric heat of adsorption (92 kJ/mol). The initial isosteric heat of CO₂ chemisorption onto this particular material is 65.3 kJ/mol, which is higher than the value of 59.6 kJ/mol obtained for overall adsorption (physisorption + chemisorption) onto the same material, but lower than that for APS materials that are more heavily loaded. The results of this analysis strongly suggest that both the decreasing relative contribution of physisorption to the overall adsorbed amount as well as the favorable impact of amine density on isosteric heat of chemisorption contribute to the increasing isosteric heats of adsorption as a function of coverage.

5.3.2. Effect of amine structure

As discussed in section 5.1, the role of amine structure on amine efficiency is not very well understood, apart from the enhanced amine efficiency of aminopropylsilyl functionalized materials compared to methylaminopropylsilyl functionalized materials. To systematically investigate the effect of amine structure on CO₂ adsorption efficiency through isosteric heats of adsorption measurements, a series of materials with different

alkyl groups attached to the nitrogen atom were synthesized. The materials are depicted in Figure 5.2, with the nomenclature used in this chapter. The physical characteristics of the materials are reported in Table 5.1. The hydrogen atom in the case of the aminopropylsilyl material is replaced with a methyl, n-butyl, cyclohexyl, and phenyl group to obtain the MAPS, NBAPS, CHAPS, and PHAPS materials respectively.

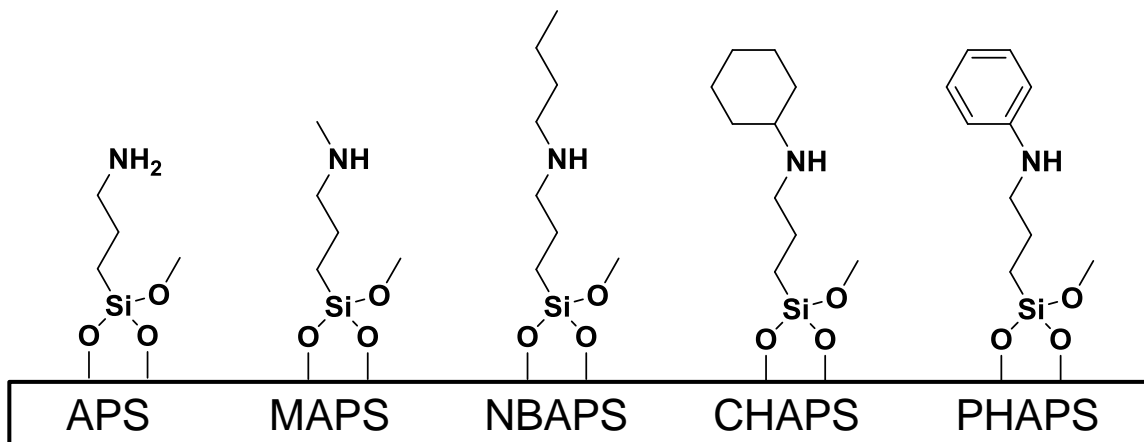


Figure 5.2: Amine adsorbent structures used in this study and their nomenclature

Table 5.1: Surface areas and amine loadings of materials tested in this study

Material	Amine loading (mmol N/ g SiO ₂)	BET surface area (m ² /g)
SBA-15	-	937
SBA_APS	1.87	295
SBA_MAPS	1.77	362
SBA_NBAPS	2.3	244
SBA_CHAPS	1.97	285
SBA_BZAPS	1.28	450

Figure 5.3 shows the isosteric heat of adsorption data for the amine structures depicted in Figure 5.2. The initial isosteric heats for the APS, MAPS, and NBAPS materials fall in the same range ~85-95 kJ/mol. The degree of heterogeneity for the NBAPS material though, is slightly lower than that for the APS and MAPS materials. The isosteric heat starts out ~3 kJ/mol below that for the APS material, and ends up 11 kJ/mol higher than the APS material at the loading corresponding to 0.1 bar CO₂. The relatively less heterogeneous NBAPS surface manifests itself in the adsorption isotherm in terms of a worse performance compared to the APS and MAPS materials at ultra-low pressures (< 0.01 bar), but better than both at higher pressures (close to 0.1 bar). This enhancement in performance at higher pressures cannot be a result of differences in degrees of physisorbed CO₂, since the NBAPS material has the lowest surface area of the three materials in this set discussed so far (Table 5.1). The relative homogeneity of the NBAPS material relative to the APS and MAPS material can be a result of better amine spacing as a result of the bulkier n-butyl group attached to the amine. The isosteric heats for the CHAPS material are lower than the APS, MAPS, and NBAPS material. More specifically, the isosteric heat for the CHAPS material is 52 kJ/mol lower than that for the APS material close to zero loading of adsorbate. This can be attributed to significant contributions of CO₂ physisorption onto the support to the overall amount of CO₂ adsorbed. The PHAPS material has the lowest isosteric heat of adsorption of all the materials tested in this study. The isosteric heat is even lower than that of the bare SBA-15 silica support. This may be due to reduced basicity of the amine group to which the electron withdrawing benzene ring is attached. Perhaps, the most important result to come out of this study of isosteric heats of adsorption as a function of amine structure is that amine efficiencies cannot purely be understood from the standpoint of adsorption enthalpies. The APS and MAPS materials discussed here have very similar isosteric adsorption enthalpies throughout the range of coverages reported in this study, but still

have significantly different amine efficiencies. These results suggest that the observed trend in the literature (read above) of higher amine efficiencies for APS materials compared to MAPS materials are not necessarily a consequence of enthalpic factors but instead, likely a result of entropic factors.

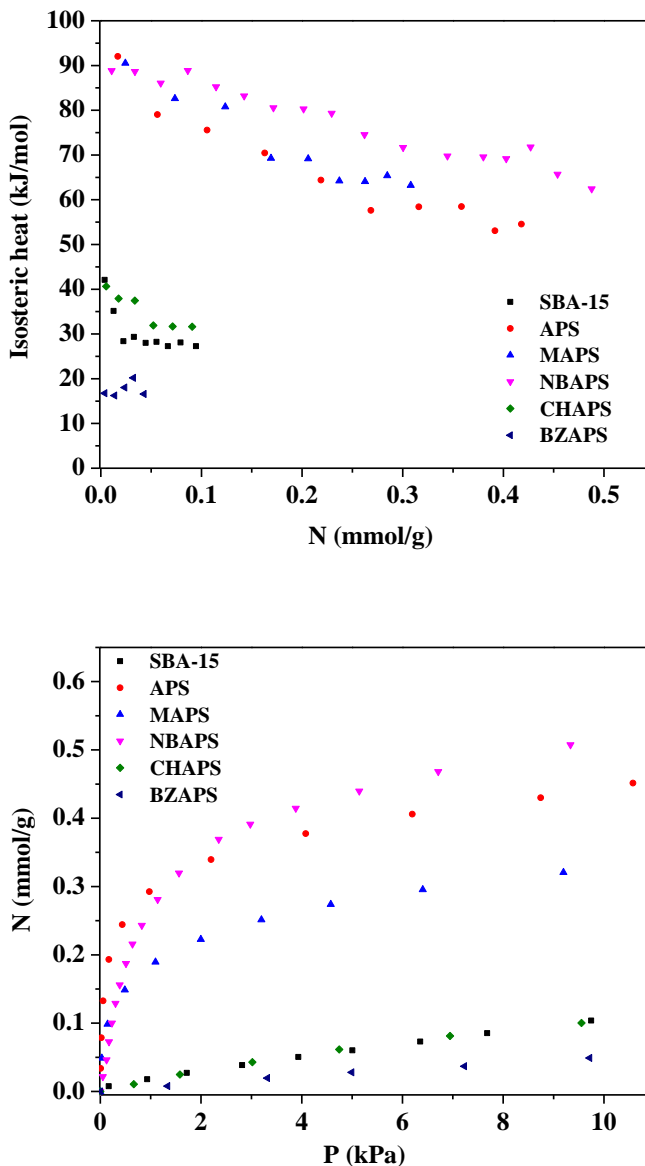


Figure 5.3: Isothermic heats of adsorption and adsorption isotherms for amine materials with structures shown in Figure 5.2.

5.3.3. Accuracy of isosteric heats derived from isotherms

Figure 5.2 shows the comparison between isosteric heats of adsorption obtained from fitting CO₂ adsorption isotherms at multiple temperatures (30-60°C) to the Toth model for an aminopropylsilyl and methylaminopropylsilyl functionalized material. Clearly, the fits are not very good for both materials. The Toth model predictions do match up well with experiments at high coverages for the APS material. The fits for the MAPS material, on the other hand, are poor throughout the range of coverages reported in this study. This misfit between experimental and predicted values of isosteric heats points to a fundamental deficiency in the utilization of the Toth isotherm model for modeling isotherms for supported amine materials. Note that the data in Figure 5.3 are for very simple class 2 model adsorbents and not for more structurally complex class 1 and 3 materials. The partial pressure range of the data is also relatively small compared to what one would need to model for a real adsorption-desorption process, in which CO₂ pressures in the desorption step will rise significantly above 0.1 bar. The limited fit between predicted and experimental heat-coverage curves points to the need for improved models and the necessity of comparing experimentally measured isosteric heats of adsorption data to model predicted values when assessing suitability of adsorption isotherm models.

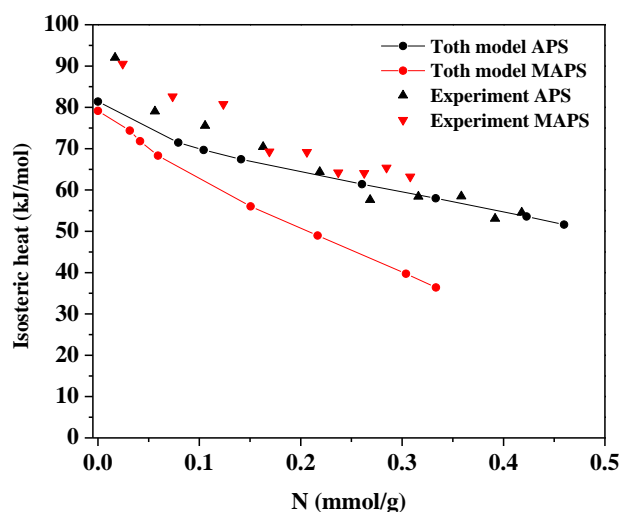


Figure 5.4: Comparison of experimentally measured isosteric heats with those derived from the Toth model for the APS & MAPS materials.

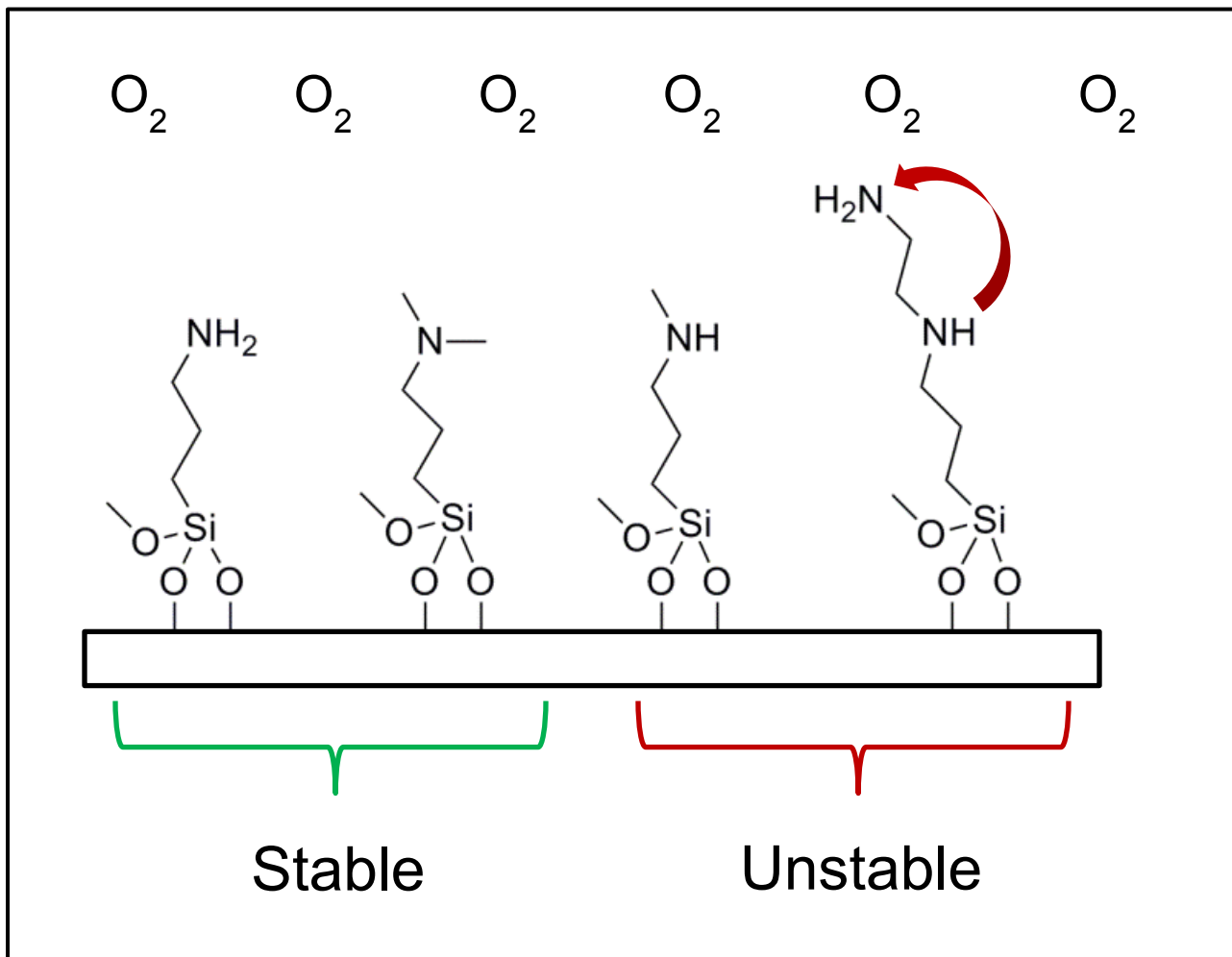
5.4. Conclusions

In conclusion, isosteric heats of adsorption measurements were carried out on an array of supported amine adsorbents in which amine density and amine structure were systematically varied. Unlike Sayari's report,⁴ where CO₂ physisorption onto the bare support was found to be negligible below 0.2 bar, in this study, physisorption was found to have a significant impact on both amine efficiencies and isosteric heats of CO₂ adsorption below 0.1 bar. Higher amine densities were found to have result in higher isosteric heats of adsorption, suggesting that amine proximity is a key factor influencing amine efficiency. Introduction of bulky groups onto the nitrogen atom reduced amine efficiencies drastically, suggesting that entropic factors are important to consider in addition to enthalpic factors when designing amine adsorbents with improved amine efficiencies for CO₂ capture.

5.5. References

- (1) Choi, S.; Drese, J. H.; Jones, C. W. Adsorbent Materials for Carbon Dioxide Capture from Large Anthropogenic Point Sources. *ChemSusChem* **2009**, *2*, 796.
- (2) S.A. Didas, A.R. Kulkarni, D.S. Sholl, C. W. J. Role of Amine Structure on CO₂ Adsorption from Ultra-dilute Gas Streams such as Ambient Air. *ChemSusChem* **2012**, *5*, 2058.
- (3) Ko, Y. G.; Shin, S. S.; Choi, U. S. Primary, secondary, and tertiary amines for CO₂ capture: Designing for mesoporous CO₂ adsorbents. *J. Colloid Int. Sci.* **2011**, *361*, 594-602.
- (4) Serna-Guerrero, R.; Belmabkhout, Y.; Sayari, A. Modeling CO₂ Adsorption on Amine-functionalized Mesoporous Silica: 1. A Semi-empirical Equilibrium Model. *Chem. Eng. J.* **2010**, *161*, 173.
- (5) Zelenak, V.; Halamova, D.; Gaberova, L.; Bloch, E.; Llewellyn, P. Amine-modified SBA-12 mesoporous silica for carbon dioxide capture: Effect of amine basicity on sorption properties. *Microporous Mesoporous Mater.* **2008**, *116*, 358-364.
- (6) Chaikittisilp, W.; Khunsupat, R.; Chen, T. T.; Jones, C. W. Poly(allylamine)-Mesoporous Silica Composite Materials for CO₂ Capture from Simulated Flue Gas or Ambient Air. *Ind. Eng. Chem. Res.* **2011**, *50*, 14203.

- (7) Hiyoshi, N.; Yogo, K.; Yashima, T. Adsorption characteristics of carbon dioxide on organically functionalized SBA-15. *Microporous Mesoporous Mater.* **2005**, *84*, 357-365.
- (8) Harlick, P. J. E.; Sayari, A. Applications of pore-expanded mesoporous silicas . 3 . Triamine silane grafting for enhanced CO₂ adsorption. *Ind. Eng. Chem. Res* **2006**, *45*, 3248-3255.



CHAPTER 6

OXIDATIVE DEGRADATION OF SUPPORTED AMINE ADSORBENTS

Parts of this chapter are reproduced from 'Bollini, P.; Choi, S.; Drese, J. H.; Jones, C. W. Oxidative Degradation of Aminosilica Adsorbents Relevant to Postcombustion CO₂ Capture. *Energy Fuels* **2011**, *25*, 2416.'

6.1. Background

Flue gas from a coal plant typically contains 10-15% CO₂, 5-10% O₂, 4-5% water vapor, 2000 ppm SO₂ (before flue gas desulfurization), 1500 ppm NO (before selective catalytic reduction) and the balance N₂.^{1,2} Any adsorbent used for CO₂ capture from flue gas must be capable of adsorbing CO₂ reversibly for at least thousands of cycles. Testing under realistic flue gas conditions is thus extremely important in determining the economic viability of using an adsorbent material in an adsorption process.

Despite the emergence of supported amine adsorbents as an important class of adsorbents due to their high equilibrium CO₂ adsorption capacities,³⁻⁷ their performance under realistic flue gas conditions (in the presence of SO_x, NO_x and O₂) remains relatively unexplored. Khatri et al. studied the adsorption of SO₂ on amine impregnated SBA-15 and found that SO₂ adsorbed irreversibly onto the materials, thus blocking active

sites for CO₂ adsorption.² Beckman and co-authors studied the adsorption of all three acid gases, CO₂, SO_x and NO_x, onto amine-containing polymeric sorbents and found that the thermal reversibility of the capture process decreased in the order CO₂>SO_x>NO_x.^{8,9} Sayari's group studied adsorption of CO₂ on triamine functionalized pore expanded MCM-41 in the presence of oxygen at temperatures ranging from room temperature to 50°C and reported high selectivities of CO₂ over O₂ and no influence of oxygen on the recyclability of the materials.^{3,10} However, this particular study was focused on the potential co-adsorption of oxygen, rather than on the evaluation of oxidative degradation reactions on the supported amines over many cycles. Unlike aqueous amine solutions such as aqueous MEA, whose oxidative degradation has been studied in detail by several authors,^{1,11-19} the oxidative degradation of supported amine adsorbents is not very well understood. The goal of this study is to evaluate the oxidative degradation of an array of class 2, silane-based amine functionalized silica materials, representing a variety of types of amine groups (primary, secondary, tertiary monoamines, and a primary-secondary diamine) under accelerated oxidation conditions, spanning a range of temperatures. The results demonstrate that the different types of amine sites have different reactivities with oxygen, and the observed behavior allows an initial assessment of the stability of these adsorbents over many repeated adsorption and desorption cycles.

6.2. Experiments

6.2.1. Mesocellular foam synthesis

Silica mesocellular foam (MCF) was chosen as the support for this study due to its large pore size and 3-D interconnected pore structure, thus providing minimal

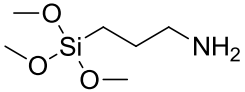
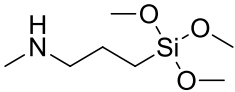
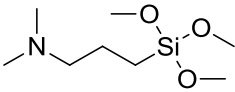
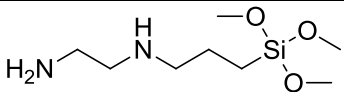
resistance to diffusing gas molecules. MCF was synthesized based on a procedure reported in the literature.²⁰ Pluronic P-123 (poly(ethylene glycol)-block-poly(propylene glycol)-block-poly(ethylene glycol)) with an average molecular weight of 5800, purchased from Sigma Aldrich, was the surfactant used, 16.0 g of which was dissolved in 260 g water with 47.4 g concentrated HCl in a capped 500 ml Erlenmeyer flask at room temperature. After complete copolymer dissolution, 16.0 g 1,3,5-trimethylbenzene (TMB) was added and the solution was stirred vigorously at 39 °C for 2 hours, after which 34.6 g tetraethylorthosilicate (TEOS) was added. The solution was stirred for an additional 5 minutes and then left quiescent for 20 hours in an oven at 40 °C. NH₄F (184 g dissolved in 20 ml water) was added as the mineralization agent, and the mixture was swirled for a minute before aging at 100 °C for an additional 24 hours. The resulting precipitate was filtered, washed with copious amounts of water, dried, and calcined in air at 550 °C for 6 hours (1°C min⁻¹ ramp).

6.2.2. *Synthesis of amine functionalized silica*

First, 2.0 g of calcined mesocellular foam silica was dried on a Schlenk line for 8 hours at 105°C under a pressure of 15 mtorr. The silica support was then added to a toluene solution and stirred for 2 hours, after which 4.0 g of silane coupling agent was added into the reaction flask. The mixture was allowed to stir at room temperature for 24 hours. The resulting solid was filtered, washed with toluene and then dried overnight at 75°C in a vacuum oven. Four different silane coupling agents were used for surface functionalization, representing primary, secondary and tertiary amines with propyl linkers connecting the amines to the surface, as well as the commonly used diamine silane

containing a primary and a secondary amine group. Table 6.1 shows the silane coupling agents used in this study and the nomenclature used to refer to the materials.

Table 6.1: Silane coupling agents used to prepare aminosilica materials for oxidative stability studies.

Coupling Agent	Structure of the Coupling Agent	Sample Name	Amine Type
3-aminopropyltrimethoxysilane		MCF_APS (APS)	Primary
(N-methylaminopropyl)-trimethoxysilane		MCF_MAPS (MAPS)	Secondary
(N,N-dimethylaminopropyl)-trimethoxysilane		MCF_DMAP S (DMAPS)	Tertiary
N-(3-(trimethoxysilyl)propyl)ethylenediamine		MCF_DA (Diamine)	Primary & Secondary

Materials treated at various temperatures are referred to by specifying the treatment temperature as a suffix. As an example, MCF_MAPS that has been oxidized at 75°C is referred to as MCF_MAPS_75.

6.2.3. *Oxidation of adsorbents*

To evaluate the oxidative stability of the materials described above, 400 mg of the adsorbent was packed into a Pyrex tube, 1 cm in diameter, with a frit at the center to allow flow of gas through the sample without loss of the adsorbent. To remove residual water from the system, the bed was first heated to 110 °C and argon was passed through the bed at 20ml/min for an hour. The temperature was then set to the desired oxidation temperature and the flow was switched to pure oxygen at 20ml/min. The oxygen flow was stopped after 24 hours and the material was recovered for post-oxidation chemical analysis. The adsorbents were exposed to O₂ at 5 different temperatures: 25, 45, 75, 105 and 135°C, representative of potential adsorption and desorption temperatures used in cyclic TSA processes.⁶

6.2.4. *Characterization of the adsorbent materials*

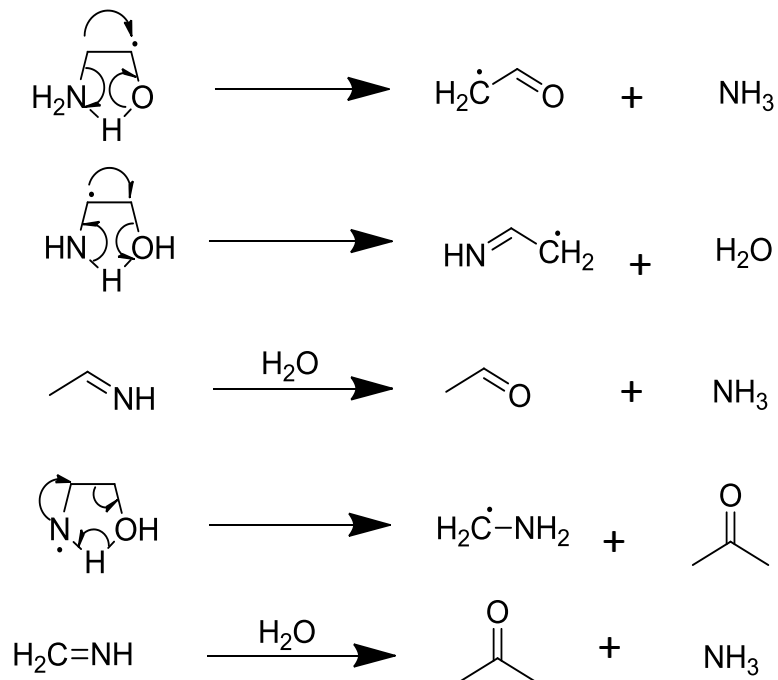
¹³C CP-MAS solid state NMR measurements were carried out on a Bruker DSX-300 spectrometer. The samples were spun at a frequency of 5KHz and 18000 scans were taken. X-ray photoelectron spectroscopy (XPS) measurements were carried out on a Thermo Scientific K-Alpha XPS. The X-ray source was aluminum K alpha and 284.8 eV, the binding energy for C 1s, was used as a reference. Nitrogen physisorption measurements were carried out on a Micromeritics Tristar II at 77K. Surface areas, pore

diameters and pore volumes were calculated from the collected isotherm data. Surface areas were calculated using the Brunauer-Emmett-Teller method²¹ and pore diameters and pore volumes were calculated using the Broekhoff-de Boer - Frenkel Halsey Hill (BdB-FHH) method.²² Pore diameters of the spherical cells are calculated from the adsorption branch of the isotherm whereas the window diameters are calculated from the desorption branch. A TA Instruments TGA Q500 thermogravimetric analyzer was used to measure the adsorption capacities of the materials under dry conditions. Two adsorption-desorption cycles were measured for each sample. All measurements were performed in this manner under dry conditions except for the MCF_DMAPS materials, whose adsorption capacities were measured under humidified conditions using a fixed bed adsorption system coupled with a mass spectrometer, using a procedure described in our previous work,^{6,23,24} since tertiary amines do not appreciably adsorb CO₂ under dry conditions. To verify this fact, the CO₂ adsorption capacity of MCF_DMAPS was evaluated under dry conditions at 45° C using the TGA, as noted above for the other samples, and a meager CO₂ capacity of 0.04 mmol/g was measured.

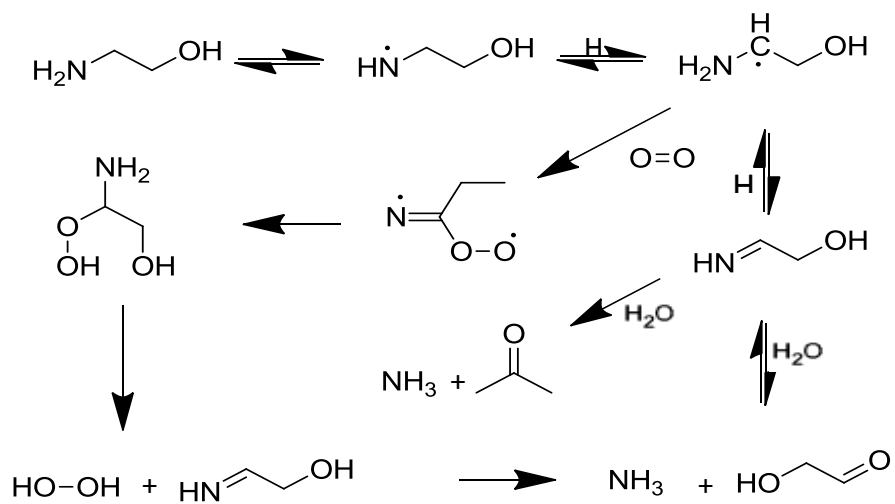
6.3. Results & Discussion

Monoethanolamine (MEA) is a solvent of choice for commercial CO₂ separation applications. It has been estimated that makeup of lost or degraded MEA is responsible for about 10% of the overall CO₂ capture cost using aqueous MEA absorption technology.²⁵ Three distinct types of degradation account for these high amine makeup rates (2.2 kg MEA per tonne of CO₂ captured)-carbamate polymerization, thermal degradation, and oxidation. Of the degradation mechanisms mentioned above, oxidation reactions account for about half the total amine degradation.^{1,11,14,16,26} They are also

responsible for the formation of organic acids that severely corrode the absorption tower equipment, generally carbon steel. The major products of MEA oxidative degradation are organic acids (mostly formic acid) and ammonia. There are two distinct oxidation mechanisms that have been proposed for MEA, the hydrogen abstraction mechanism and the electron abstraction mechanism. Primary and secondary amines are oxidized primarily by the hydrogen abstraction mechanism. Molecular simulation studies have shown that in aqueous solutions, MEA stabilizes in the cyclic hydrogen bonded conformation shown in Figure 3.1a.^{27,28} In the first step of the reported reaction mechanism, abstraction of a hydrogen radical takes place. This hydrogen may be a hydrogen attached to the nitrogen atom, one attached to the α -carbon or to the β -carbon in the cyclic conformation. Electron transfer then takes place in the resulting cyclic amine radical as shown in Figure 6.1a, resulting in the cleavage of the C-N bond to yield formaldehyde and ammonia. For tertiary amines, however, the electron abstraction mechanism shown in Figure 6.1b dominates. The ferric ion promotes removal of an electron from MEA forming an aminium radical, which loses a proton to form an imine radical. This radical then gets oxidized to either an amino peroxide in the presence of oxygen or an imine in the presence of a ferric ion. As is evident from Figure 6.1b, in the case of aqueous amine oxidation, metal ions like the ferric ion, which are present in solution as a direct consequence of equipment corrosion, play an important role in the oxidation mechanisms. Several authors have investigated the role of ferric ions in monoethanolamine oxidation.^{1,29}



(a)



(b)

Figure 6.1: Hydrogen abstraction mechanism for MEA oxidation (a) and electron abstraction mechanism for MEA oxidation (b).¹³

Apart from MEA, oxidative degradation studies have also been carried out on other amines.²⁹ The major oxidation products detected were still the same (aldehydes and ammonia), but there were differences observed in the rates of oxidation. There are two conflicting reports on the issue of oxidation rates. Rosenblatt et al.³⁰ found that primary amines were the most stable under oxidizing conditions followed by secondary amines and later by tertiary amines. In contrast, Lepaumier et al.²⁹ reported that tertiary amines were more stable than either primary or secondary amines. In the first case, most of the amines studied were aromatic amines and the oxidant was chlorine dioxide, whereas in the latter case the amines were aliphatic and the experiments were carried out in the presence of oxygen. It may be anticipated that the observed differences in these two studies are closely related to the differences in the amine structures and the nature of the oxidants. These reports highlight the need to study the specific amine materials proposed to be used as adsorbents, rather than to extrapolate the stability of the supported adsorbents from studies of oxidative stability of related liquid amines.

It is worth noting that apart from aldehydes, acids and ammonia, there are a number of side products that have also been identified.¹⁵ Acid gases like nitric oxide (NO), nitrogen dioxide (NO₂), nitrous acid, and heat stable salts have been detected in small quantities. Figure 6.2 lists some of the other side products that result from oxidation of MEA. Most of the mechanistic studies on MEA oxidative degradation have focused exclusively on the major oxidation products and not on the side products (as expected for initial studies), although production of some of the side products merits further study, as they pose serious environmental hazards (e.g. oxides of nitrogen, ammonium formate, amino peroxides).³¹

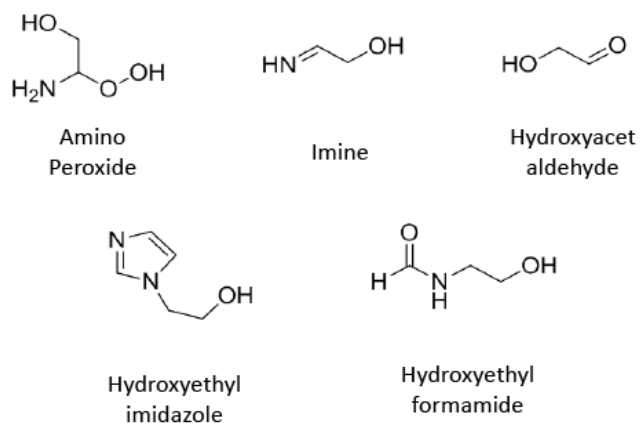


Figure 6.2: Minor products resulting from the oxidation of aqueous MEA solutions³¹

There are two key differences between oxidation of solid amine adsorbents and aqueous amines. First, with amine functionalized silica adsorbents, it is possible to generate oxidation sites that are isolated from each other, in contrast to the case where amines are mobile in aqueous solutions. Second, almost all of the amines in an aqueous solution are surrounded by water whereas in aminosilicas there may be limited access of water to some of the amine sites.

6.3.1. TEM & nitrogen physisorption

Figure 6.3 shows a TEM image of the support MCF3 clearly showing the spherical cells characteristic of the material. Nitrogen physisorption was performed on the two batches of mesocellular foam support used in this study (MCF3 and MCF5), the four amine functionalized silica materials whose oxidative stability was investigated (MCF_APS, MCF_MAPS, MCF_DMAPS, MCF_DA) and the four batches of materials treated at 135°C (MCF_APS_135, MCF_MAPS_135, MCF_DMAPS_135,

MCF_DA_135). MCF3 was the batch used to synthesize the MCF_APS and MCF_MAPS materials whereas MCF5 was used to synthesize the MCF_DMAPS and MCF_DA materials. The isotherms of each of these samples were type IV isotherms with loop hysteresis, typical of mesoporous materials. The adsorption data were used to infer surface area, pore volume, and porosity characteristics of the solids. As an example, Figure 6.4 shows the isotherm of the sample MCF3, which is one of the bare MCF supports. BdB-FHH(Brockhoff de Boer-Frenkel Halsey Hill) analysis of the adsorption isotherm was performed to calculate the pore size distribution and pore volume of the material.

The two mesocellular foam silica supports had a surface area of 540-590 m²/g, pore volumes of ca. 1.9 cc/g and cell and window diameters of 35 and 17 nm respectively. The surface areas as well as the pore volumes of the materials dropped drastically once amine groups were incorporated into the pores of the mesocellular foam silica, as shown in Table 6.2. More specifically, the surface areas dropped by almost 50%, while pore volumes dropped by about one third. There are however, no significant differences in the pore characteristics of the materials before and after oxidative treatment. It is thus clear that the oxidative treatment does not significantly alter the mesocellular foam support itself or the porosity of the various solids, under the experimental conditions used in this study. Amine oxidation does not occur to an extent where there is significant loss of organic amine species from the supports via production of volatile products.

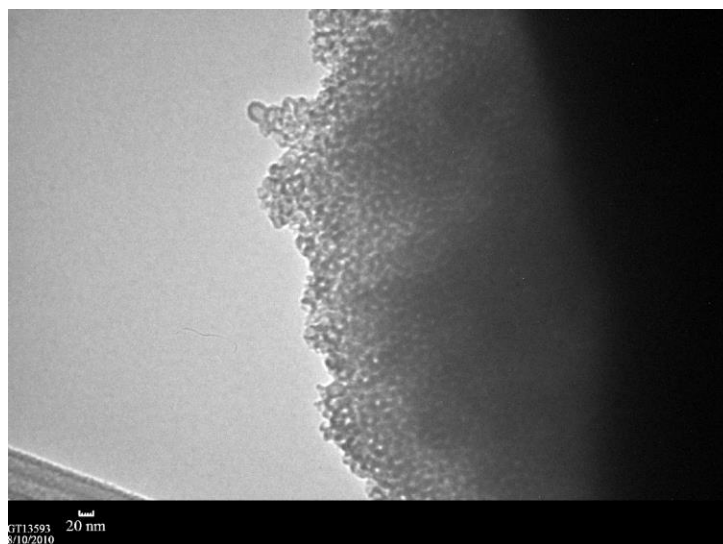


Figure 6.3: TEM image of the mesocellular foam support MCF3

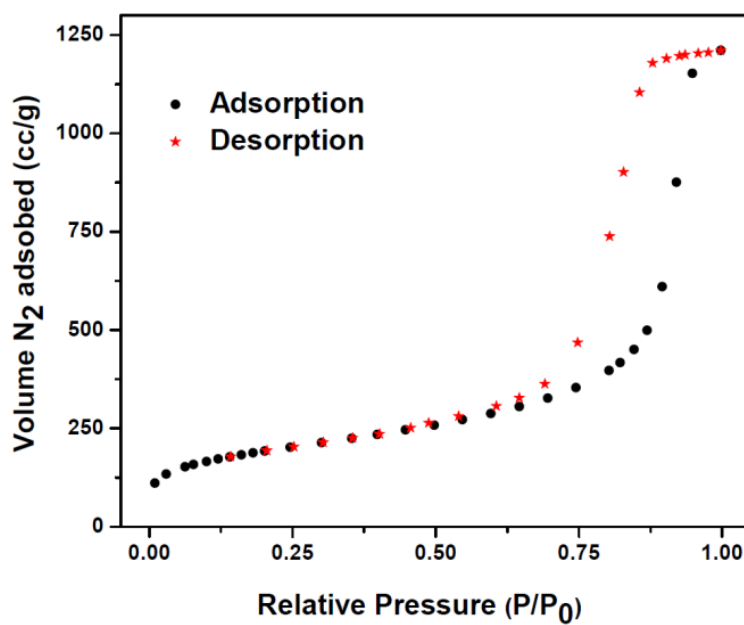


Figure 6.4: Nitrogen physisorption isotherm of the mesocellular foam support, MCF3.

Table 6.2: Physical characteristics of the various amine functionalized silica adsorbents.

Sample	Amine Loading (mmol N/g silica)	BET surface area (m ² /g)	Pore Volume (cc/g)	Cell diameter (nm)	Window diameter (nm)
MCF3	-	540	1.90	35	17
MCF5	-	590	1.92	35	17
MCF_APS	2.39	288	1.42	35	17
MCF_APS_135	-	332	1.64	35	17
MCF_MAPS	2.28	261	1.39	30	17
MCF_MAPS_135	-	329	1.6	35	17
MCF_DMAPS	2.49	229	1.2	30	17
MCF_DMAPS_135	-	229	1.18	30	17
MCF_DA	3.52	173	1.07	35	17
MCF_DA_135	-	193	1.04	35	17

6.3.2. Thermogravimetric analysis

After treatment under oxidative conditions as described above, the weight ratio of organic to silica of all the adsorbents was assessed on a thermogravimetric analyzer as described in the experimental section. Figure 6.5 shows the organic to silica weight ratios of the materials treated at various temperatures normalized by the corresponding weight ratios for the untreated samples. The organic to silica weight ratio varies between plus 10% and minus 20% of the value of the untreated adsorbent. Two samples show an

increasing trend in combustible mass with treatment temperature, MCF_DA and MCF_DMAPS. The other two samples, MCF_MAPS and MCF_APS showed decreasing trends. As noted below in the section on CO₂ adsorption capacity, MCF_DMAPS and MCF_APS were relatively unaffected by the oxidative treatments, whereas MCF_DA and MCF_MAPS were substantially affected by the treatments. Thus, in one sample that appeared to have an increasing combustible fraction after treatment and one sample that had a decreased combustible fraction after treatment appeared to be relatively stable to oxidation. Similarly, one sample from each category appeared to be relatively unstable. Thus, the change in organic fraction (combustible or volatile mass fraction) did not appear to track with the stability of the adsorbents for carbon capture applications. Thus, additional studies were needed, as shown below.

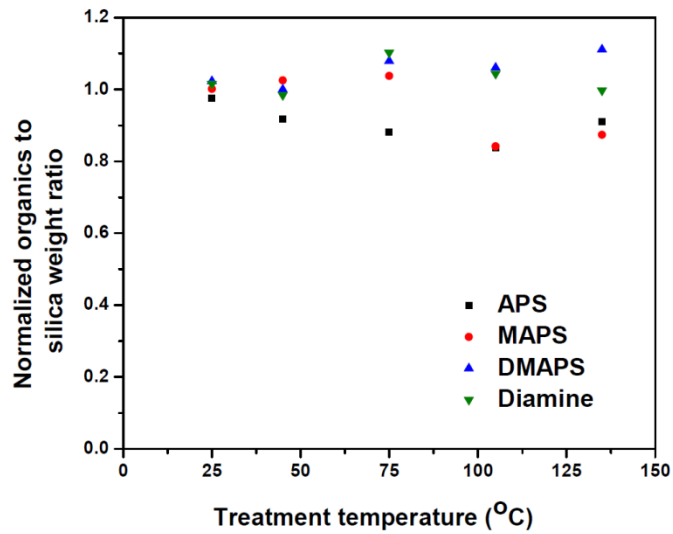


Figure 6.5: Organic to silica weight ratio of samples treated under oxidizing conditions at various temperatures normalized by the organic to silica weight ratio of the corresponding untreated adsorbents.

6.3.3. Adsorption capacity measurements

To assess the stability of the various types of amines to oxidizing conditions, the adsorption capacities of the materials were measured using a TGA. Figure 6.6 shows the CO₂ adsorption capacities of the adsorbents treated under oxidative conditions normalized by their adsorption capacities before treatment, plotted as a function of treatment temperature. For this study, treatment temperatures were chosen such that they covered the entire range of adsorption (25-75°C) and desorption conditions (75-135°C) typically reported for supported amine materials in post-combustion CO₂ capture applications. A flow rate of 20 ml/min of the analysis gas was used in 1 cm diameter adsorbent bed.

On the time scale of the experiments, it is evident that all four of the adsorbents tested were not affected by the oxidative treatment in temperature ranges corresponding to low temperature adsorption conditions (Figure 6.6, 25-55°C). However, in the range of elevated temperature desorption conditions (Figure 6.6, 105-135°C), the MCF_MAPS and the MCF_DA materials showed significant decreases in adsorption capacities. This implies that for these two adsorbents, the presence of a gas containing oxygen in the regeneration step may reduce the life of the adsorbent, perhaps significantly. Also, even though the lifetimes of the MCF_MAPS and MCF_DA materials are not accurately known at lower temperatures, it is possible they will also degrade after a very large number of cycles of exposure to oxygen in the adsorption step, where it is expected that larger oxygen partial pressures will be present than in the desorption stage. Of course, the behavior of the adsorbents under real cyclic adsorption/desorption conditions found in post-combustion CO₂ capture processes is not directly being simulated with the experiments described here, which used gas flows of 100% O₂ to accelerate any oxidative changes that might occur in the temperature range of interest. Thus, these

results simply show the propensity for the various amine species to oxidize under strongly oxidizing conditions, and the extent of oxidation in a real process cannot yet be accurately estimated from this initial study.

From the data, it can be concluded that under the experimental conditions used in this study, primary and tertiary amines attached to identical propyl linkers are more stable to accelerated oxidative degradation than secondary amines. Another interesting observation is that while the (relatively) isolated primary amines in the MCF_APS did not degrade, primary amines separated from secondary amines by an ethyl group did deactivate (MCF_DA), indicating a potentially co-operative, intramolecular degradation mechanism. Note that this type of functional group ($\text{RNHCH}_2\text{CH}_2\text{NH}_2$) is ubiquitous in reported supported amine CO_2 adsorbents, including those based on poly(ethyleneimine)^{32–35}, and supported diamine (described here)^{6,24,36} and triamines^{3,4,37–39}. Thus, the oxidative stability of this particular functional group merits additional attention.

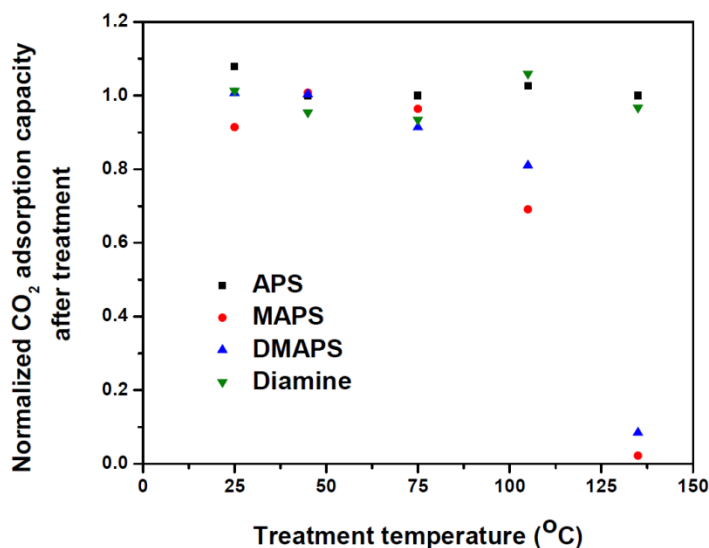
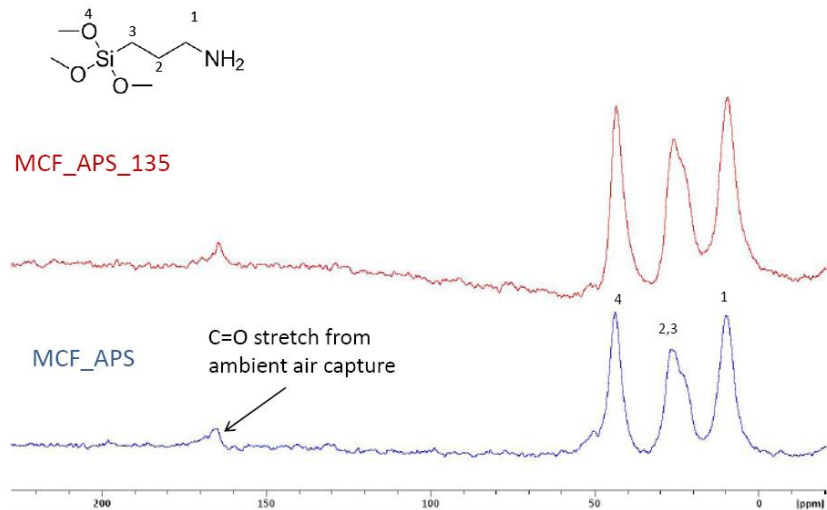


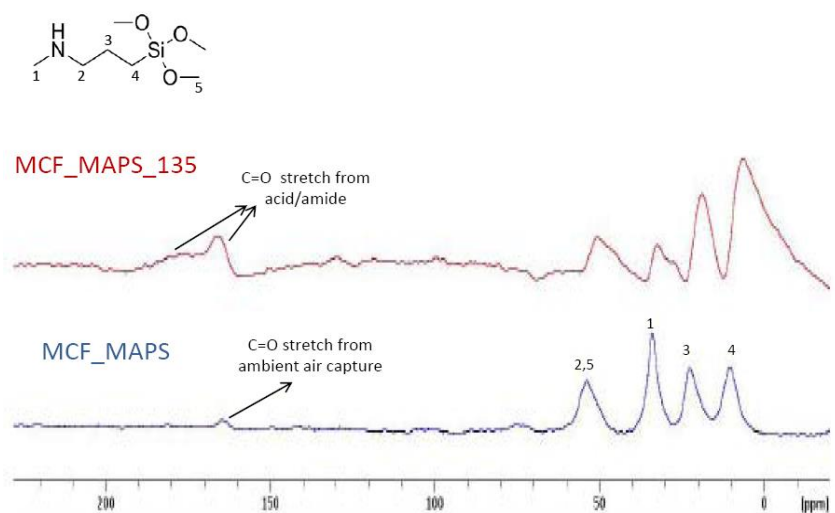
Figure 6.6: CO_2 adsorption capacities of oxygen-treated adsorbents normalized by the original CO_2 adsorption capacities as a function of the temperature of oxidation.

6.3.4. *Solid state NMR*

Figure 6.7 shows the ^{13}C CPMAS NMR spectra of the adsorbent samples before and after treatment under oxidizing conditions at 135°C . The MCF_APS and the MCF_DMAPS materials do not show a significant change in chemical structure even after treatment at 135°C . However, the MCF_MAPS material treated at 135°C clearly shows the appearance of a broad C=O peak between 160 and 180 ppm, corresponding to an acid/amide group, consistent with oxidative degradation reactions. In addition to the C=O peak, the spectrum for the oxidized MCF_DA material also shows peaks between 115 and 140 ppm that correspond to aliphatic C=C, and/or heterocyclic C-N, and/or aromatic C=C groups. The presence of these functional groups (which are also typically found in the aqueous amine oxidative degradation products discussed above (Figure 6.2)), show that the MCF_DA material is highly reactive under these oxidizing conditions. These results support the earlier hypothesis that a secondary amine separated from a primary one by an ethyl group (as found in MCF_DA) undergoes one or more degradation reactions that an isolated secondary amine does not (Figures 6.7b and 6.7d).

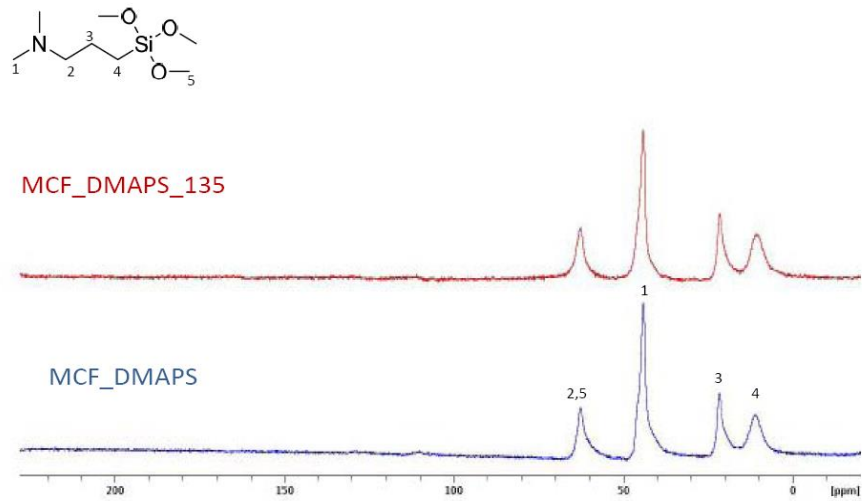


(a)

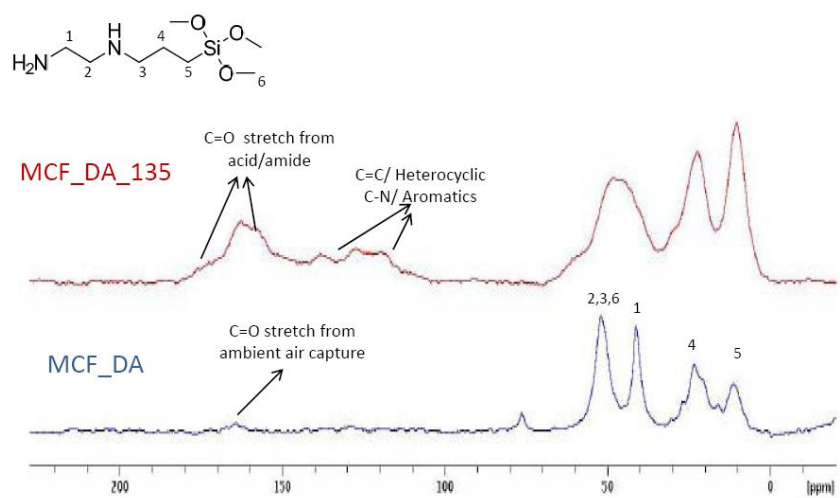


(b)

Figure 6.7: ¹³C CP MAS NMR spectra of the untreated samples (blue, bottom) and samples treated at 135°C (red, top). a: MCF_APS, b: MCF_MAPS



(c)



(d)

Figure 6.7: ^{13}C CP MAS NMR spectra of the untreated samples (blue, bottom) and samples treated at 135°C (red, top). c: MCF_DMAPP, d: MCF_DA.

6.3.5. X-ray photoelectron spectroscopy

To gain further insight into the chemical structure of the oxidized materials and to verify the interpretations of previously discussed characterization results, XPS measurements were carried out on the adsorbents before and after oxidative treatment. Table 6.3 shows the various peak assignments for the untreated and treated MCF_MAPS and MCF_DA materials. As expected, no changes were observed in the XPS spectra of the APS and DMAPS samples after oxidative treatment. As shown in Table 6.3, the MAPS material before oxidation has C peaks corresponding to the propyl and methyl groups and N peaks corresponding to the secondary propyl amine group only. After oxidative treatment at 135°C, in addition to the aforementioned peaks, the MCF_MAPS adsorbent shows a peak at 288.8 eV corresponding to a C atom in an acid, and/or amide, and/or urea linkage. A peak at 400.1 eV corresponding to N is also observed, corresponding to an amide, and/or urea linkage, providing further evidence of the presence of one or more of these functional groups derived from oxidation reactions. The oxidized MCF_DA material showed the same peaks as the oxidized MCF_MAPS material, except it lacked the two additional peaks in the MCF_MAPS_135 XPS spectra that could not be assigned. Based on the solid state NMR data, one would expect that the MCF_DA material treated at 135°C would show some additional peaks that are not present in the oxidized MAPS adsorbent, thus shedding some light on the hypothesized cooperative degradation mechanism discussed above for this sample. However, no significant changes were observed between the MCF_MAPS_135 and MCF_DA_135 samples via XPS. One possible reason for this may be that the concentration of MCF_DA degradation products formed via this cooperative degradation mechanism is too small for detection by XPS, or that these oxidized species could be predominantly located on the interior of the adsorbent particles and were thus missed by the surface

sensitive XPS technique. Apart from this one difference between the XPS and NMR data, the XPS data match well with the adsorption capacity and NMR results discussed above. The data do not, however, help verify or disprove the hypothesis that the diamine degrades via a cooperative mechanism.

Table 6.3: Carbon and nitrogen XPS binding energies of the aminosilica adsorbents before and after oxidative treatments, along with possible functional group assignments.

Sample	Binding Energy (eV)	Element	Group
MCF_MAPS	285.5	C	$\begin{array}{c} \text{H}_2 \quad \text{H} \\ \quad \\ \text{R}-\text{C}^*-\text{C}^*-\text{C}^*-\text{N}^*-\text{CH}_3 \\ \quad \\ \text{H}_2 \quad \text{H}_2 \end{array}$
	399.07	N	$\begin{array}{c} \text{H}_2 \quad \text{H} \\ \quad \\ \text{R}-\text{C}-\text{C}-\text{C}-\text{N}-\text{CH}_3 \\ \quad \\ \text{H}_2 \quad \text{H}_2 \end{array}$
MCF_MAPS_135	285.5	C	$\begin{array}{c} \text{H}_2 \quad \text{H} \\ \quad \\ \text{R}-\text{C}^*-\text{C}^*-\text{C}^*-\text{N}^*-\text{CH}_3 \\ \quad \\ \text{H}_2 \quad \text{H}_2 \end{array}$
	288.8	C	$\begin{array}{ccc} \begin{array}{c} \text{O} \\ \\ \text{R}-\text{C}^*-\text{OH} \end{array} & \begin{array}{c} \text{O} \\ \\ \text{R}-\text{C}^*-\text{N}^*-\text{H} \end{array} & \begin{array}{c} \text{O} \quad \text{O} \\ \quad \\ \text{R}-\text{N}^*-\text{C}^*-\text{N}^*-\text{C}^*-\text{R} \\ \quad \\ \text{H} \quad \text{H} \end{array} \end{array}$

	290.7	C	Not assigned
	292.8	C	Not assigned
	399.07	N	$ \begin{array}{c} \text{H}_2 \quad \text{H} \\ \quad \\ \text{R}-\text{C}-\text{C}-\text{C}-\text{N}-\text{CH}_3 \\ \quad \quad \\ \text{H}_2 \quad \text{H}_2 \quad * \end{array} $
	400.1	N	$ \begin{array}{cc} \begin{array}{c} \text{O} \\ \\ \text{R}-\text{C}-\text{N}-\text{R} \\ \\ \text{H} \end{array} & \begin{array}{c} \text{O} \quad \text{O} \\ \quad \\ \text{R}-\text{N}-\text{C}-\text{N}-\text{C}-\text{R} \\ \quad \\ \text{H} \quad \text{H} \end{array} \end{array} $
MCF_DA	285.5	C	$ \begin{array}{cc} \begin{array}{c} \text{H}_2 \\ \\ \text{R}-\text{C}^*-\text{C}^*-\text{C}^*-\text{NH}-\text{R} \\ \quad \\ \text{H}_2 \quad \text{H}_2 \end{array} & \begin{array}{c} \text{H}_2 \\ \\ \text{R}-\text{C}^*-\text{C}^*-\text{NH}_2 \\ \\ \text{H}_2 \end{array} \end{array} $
	399.07	N	$ \begin{array}{cc} \begin{array}{c} \text{H}_2 \\ \\ \text{R}-\text{C}-\text{C}-\text{C}-\text{NH}-\text{R} \\ \quad \quad \\ \text{H}_2 \quad \text{H}_2 \quad * \end{array} & \begin{array}{c} \text{H}_2 \\ \\ \text{R}-\text{C}-\text{C}-\text{NH}_2 \\ \quad \\ \text{H}_2 \quad * \end{array} \end{array} $

MCF_DA_135	285.5	C	$\begin{array}{c} \text{H}_2 \\ \\ \text{R}-\text{C}^*-\text{C}^*-\text{NH}-\text{R} \\ \quad \\ \text{H}_2 \quad \text{H}_2 \end{array}$ $\begin{array}{c} \text{H}_2 \\ \\ \text{R}-\text{C}^*-\text{C}^*-\text{NH}_2 \\ \\ \text{H}_2 \end{array}$
	288.8	C	$\begin{array}{c} \text{O} \\ \\ \text{R}-\text{C}^*-\text{OH} \end{array}$ $\begin{array}{c} \text{O} \\ \\ \text{R}-\text{C}^*-\text{N}-\text{R} \\ \\ \text{H} \end{array}$ $\begin{array}{c} \text{O} \quad \text{O} \\ \quad \\ \text{R}-\text{N}-\text{C}^*-\text{N}-\text{C}^*-\text{R} \\ \quad \\ \text{H} \quad \text{H} \end{array}$
	399.07	N	$\begin{array}{c} \text{H}_2 \\ \\ \text{R}-\text{C}-\text{C}^*-\text{NH}-\text{R} \\ \quad \\ \text{H}_2 \quad \text{H}_2 \end{array}$ $\begin{array}{c} \text{H}_2 \\ \\ \text{R}-\text{C}-\text{C}^*-\text{NH}_2 \\ \\ \text{H}_2 \end{array}$
	400.1	N	$\begin{array}{c} \text{O} \\ \\ \text{R}-\text{C}^*-\text{N}-\text{R} \\ \\ \text{H} \end{array}$ $\begin{array}{c} \text{O} \quad \text{O} \\ \quad \\ \text{R}-\text{N}-\text{C}^*-\text{N}-\text{C}^*-\text{R} \\ \quad \\ \text{H} \quad \text{H} \end{array}$

6.3.6. Comparison to practical CO₂ capture conditions

It should be noted that especially harsh oxidation conditions were used in this initial study, compared to conditions found in a real process, to accelerate any oxidative changes that might occur in post-combustion CO₂ capture processes. In particular, 100% O₂ streams were used for the treatments, whereas the oxygen partial pressure in typical adsorption or desorption cycles will likely be much lower. Thus, one might expect that samples that are stable under the conditions used here will also be stable to the oxygen levels present in a real process, whereas those that degrade here might (but might not) degrade under the conditions found in a cyclic post-combustion CO₂ capture process.

To compare and contrast the conditions used here with those from a hypothetical process, one can consider the recent work of Lively et al.⁴⁰. If the bed void fraction is assumed to be 0.5, the O₂ interstitial velocity in the experiments used here can be calculated to be about 10 mm/s. Based on Lively et al.'s proposed adsorber design, flue gas velocities in the adsorption column will be on the order of about 1 m/s. This implies that the interstitial velocity of oxygen through the bed will be about 100 mm/s (assuming that the flue gas has 10% O₂ and flows at a velocity of 1m/s). Assuming a hypothetical cycle time of 1 minute (30 seconds for adsorption and 30 seconds for desorption), the adsorbents were exposed to an equivalent of 2880 adsorption cycles during the oxidative treatments used here. Since in these experiments, oxygen flowed through the bed with an interstitial velocity of 1 mm/s and not 100 mm/s as would be the case in a full scale operation, 2880 cycles in these experiments might correspond to only 288 cycles in a practical temperature swing adsorption process. This is much less than the number of cycles an adsorbent would have to withstand in any practical packed bed adsorption process.

It should be noted the above analysis results in gross extrapolations that, while useful in this first of its kind study, should not be over-interpreted. In particular, extrapolating the reactivity of oxygen at a partial pressure of 0.05 bar from data taken at 1 bar partial pressure is problematic. In addition, the presence of water and other species in real flue gas can also significantly influence the oxidative reaction pathways. Thus, the most important findings of this study are the highly differentiated reactivities of the various types of amines used in CO₂ adsorption studies in the literature. In particular, the observation that secondary amines preferentially oxidize relative to primary and tertiary amines is unique compared to amine reactivity in aqueous solution. Furthermore, the cooperative oxidation of primary-secondary amine pairs in the

RNHCH₂CH₂NH₂ groups that are found in many supported amine adsorbents based on poly(ethyleneimine), diamine, and triamine silanes suggests that oxidative stability of adsorbents containing these groups may be an important area for further study.

6.4. Conclusions

This study describes for the first time differences in oxidative stability of aminosilica adsorbents with different types of amine groups, providing insights into potential stability in post-combustion CO₂ capture applications. Primary and tertiary amines on propyl linkers were found to be more stable to oxidative degradation compared to secondary amines. Also, intramolecular cooperativity in the degradation mechanism of diamine functionalized mesocellular foam silica materials was inferred, where oxidation of the secondary amine leads to simultaneous degradation of the terminal primary amines. The propensity for secondary amine groups to oxidize upon exposure to oxygen at elevated temperatures is an important issue that warrants further investigation, owing to the ubiquity of secondary amines in many supported amine adsorbents. Oxidation studies on a wider range of aminosilica materials could further help elucidate oxidation mechanisms of these materials.

6.5. References

- (1) Chi, S.; Rochelle, G. T. Oxidative degradation of monoethanolamine. *Ind. Eng. Chem. Res.* **2002**, *41*, 4178-4186.
- (2) Khatri, R. A.; Chuang, S. S. C.; Soong, Y.; Gray, M. Thermal and Chemical Stability of Regenerable Solid Amine Sorbent for CO₂ Capture. *Energy Fuels* **2006**, *196*, 1514.
- (3) Belmabkhout, Y.; Serna-Guerrero, R.; Sayari, A. Amine-bearing Mesoporous Silica for CO₂ Removal from Dry and Humid Air. *Chem. Eng. Sci.* **2010**, *65*, 3695.
- (4) Serna-Guerrero, R.; Belmabkhout, Y.; Sayari, A. Further investigations of CO₂ capture using triamine-grafted pore-expanded mesoporous silica. *Chem. Eng. J.* **2010**, *158*, 513-519.
- (5) Qi, G.; Wang, Y.; Estevez, L.; Duan, X.; Anako, N.; Park, A. H. A.; Li, W.; Jones, C. W.; Giannelis, E. P. High Efficiency Nanocomposite Sorbents for CO₂ Capture Based on Amine-functionalized Mesoporous Capsules. *Energy Environ. Sci.* **2011**, *4*, 444.
- (6) Choi, S.; Drese, J. H.; Jones, C. W. Adsorbent Materials for Carbon Dioxide Capture from Large Anthropogenic Point Sources. *ChemSusChem* **2009**, *2*, 796.
- (7) Bollini, P.; Didas, S. A.; Jones, C. W. Amine-oxide Hybrid Materials for Acid Gas Separations. *J. Mater. Chem.* **2011**, *21*, 15100.
- (8) Diaf, A.; Garcia, J. L.; Beckman, E. J. Thermally Reversible Polymeric Sorbents for Acid Gases: *J. Appl. Polym. Sci.* **1994**, *53*, 857.

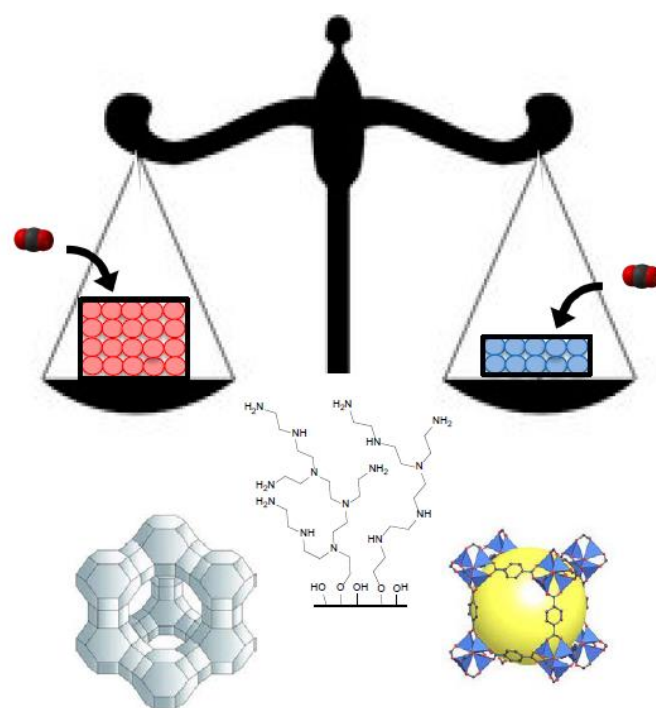
- (9) Diaf, A.; Beckman, E. J. Thermally Reversible Polymeric Sorbents for Acid Gases, IV. Affinity Tuning for the Selective Dry Sorption of NO_x. *React. Polym.* **1995**, *25*, 89.
- (10) Belmabkhout, Y.; Serna-guerrero, R.; Sayari, A. MCM-41 silica : Application for gas purification. *Ind. Eng. Chem. Res.* **2010**, *49*, 359-365.
- (11) Goff, G. S.; Rochelle, G. T. Oxidation inhibitors for copper and iron catalyzed degradation of monoethanolamine in CO₂ capture processes. *Ind. Eng. Chem. Res.* **2006**, *45*, 2513-2521.
- (12) Rochelle, G.; Chen, E.; Freeman, S.; Van Wagener, D.; Xu, Q.; Voice, A. Aqueous Piperazine as the New Standard for CO₂ Capture Technology. *Chem. Eng. J.* **2011**, *171*, 725.
- (13) Goff, G. S.; Rochelle, G. T. Monoethanolamine degradation : O₂ mass transfer effects under CO₂ capture conditions. *Ind. Eng. Chem. Res.* **2004**, *43*, 6400-6408.
- (14) Sexton, A. J.; Rochelle, G. T. Catalysts and inhibitors for MEA oxidation. *Energy Procedia* **2009**, *1*, 1179-1185.
- (15) Lawal, O.; Bello, A.; Idem, R. The Role of methyl diethanolamine (MDEA) in preventing the oxidative degradation of CO₂ loaded and concentrated aqueous monoethanolamine (MEA) -MDEA blends during CO₂ absorption from flue gases. *Ind. Eng. Chem. Res.* **2005**, *44*, 1874-1896.
- (16) Strazisar, B. R.; Anderson, R. R.; White, C. M. Degradation pathways for monoethanolamine in a CO₂ capture facility. *Energy Fuels* **2003**, *17*, 1034-1039.

- (17) Supap, T.; Idem, R.; Tontiwachwuthikul, P.; Saiwan, C. Kinetics of sulfur dioxide- and oxygen-induced degradation of aqueous monoethanolamine solution during CO₂ absorption from power plant flue gas streams. *Int. J. Greenhouse Gas Control* **2009**, *3*, 133-142.
- (18) Supap, T.; Idem, R.; Veawab, A.; Aroonwilas, A.; Tontiwachwuthikul, P.; Chakma, A.; Kybett, B. D. Kinetics of the oxidative degradation of aqueous monoethanolamine in a flue gas treating unit. *Ind. Eng. Chem. Res.* **2001**, *40*, 3445-3450.
- (19) Uyanga, I. J.; Idem, R. O. Studies of SO₂- and O₂-induced degradation of aqueous MEA during CO₂ capture from power plant flue gas streams. *Ind. Eng. Chem. Res.* **2007**, *46*, 2558-2566.
- (20) Ping, E. W.; Wallace, R.; Pierson, J.; Fuller, T. F.; Jones, C. W. Highly dispersed palladium nanoparticles on ultra-porous silica mesocellular foam for the catalytic decarboxylation of stearic acid. *Microporous Mesoporous Mater.* **2010**, *132*, 174-180.
- (21) Sing, K. S. W.; Everett, D. H.; Haul, R. A. W.; Moscou, L.; Pierotti, R. A.; Rouquerol, J.; Siemieniowska, T. Reporting physisorption data for gas/solid systems with special reference to the determination of surface area and porosity. *Pure & Appl. Chem.* **1985**, *57*, 603-619.
- (22) Lukens, W. W.; Schmidt-winkel, P.; Zhao, D.; Feng, J.; Stucky, G. D. Evaluating Pore Sizes in Mesoporous Materials : A Simplified Standard Adsorption Method and a Simplified Broekhoff-de Boer Method. *Langmuir* **1999**, *50*, 5403-5409.

- (23) Drese, J. H.; Choi, S.; Lively, R. P.; Koros, W. J.; Fauth, D. J.; Gray, M. L.; Jones, C. W. Synthesis-Structure-Property Relationships for Hyperbranched Aminosilica CO₂ Adsorbents. *Adv. Funct. Mater.* **2009**, *19*, 3821.
- (24) Hicks, J. C.; Drese, J. H.; Fauth, D. J.; Gray, M. L.; Qi, G.; Jones, C. W. Designing Adsorbents for CO₂ Capture from Flue Gas-Hyperbranched Aminosilicas Capable of Capturing CO₂ Reversibly. *J. Am. Chem. Soc.* **2008**, *130*, 2902.
- (25) Rubin, E. S.; Rao, A. B. A technical , economic and environmental assessment of amine-based CO₂ capture technology for power plant greenhouse gas control. *DOE/DE-FC26-00NT40935* **2002**.
- (26) Arcadi, A.; Alfonsi, M.; Marinelli, F. Facile reaction of thiols and amines with alkyl 4-hydroxy-2-alkynoates in water under neutral conditions and ultrasound irradiation. *Tetrahedron Letters* **2009**, *50*, 2060-2064.
- (27) Vorobyov, I.; Yappert, M. C.; Dupre, D. B. Hydrogen bonding in monomers and dimers of 2-aminoethanol. *J. Phys. Chem. A* **2002**, *106*, 668-679.
- (28) Field, F.; Rivera, L.; Mora, M. A.; Garza, de la V. Force field of monoethanolamine. *J. Phys. Chem. B* **2000**, *104*, 1332-1337.
- (29) Lepaumier, H.; Picq, D.; Carrette, P.-louis New amines for CO₂ capture . II . Oxidative degradation mechanisms. *Ind. Eng. Chem. Res.* **2009**, *48*, 9068-9075.
- (30) Rosenblatt, D. H.; Williams, H. K. R.; Hull, L. A.; De Luca, D. C.; Davis, G. T.; Weglein, R. C. Oxidations of amines. Substituent effects in chlorine dioxide oxidations. *J. Am. Chem. Soc.* **1967**, *191*, 1158-1163.

- (31) Sexton, A. J. *Amine oxidation in CO₂ capture processes. Dissertation, University of Texas at Austin*; 2008.
- (32) Ma, X.; Wang, X.; Song, C. "Molecular basket" sorbents for separation of CO₂ and H₂S from various gas streams. *J. Am. Chem. Soc.* **2009**, *131*, 5777-83.
- (33) Wang, X.; Schwartz, V.; Clark, J. C.; Ma, X.; Overbury, S. H.; Xu, X.; Song, C. Infrared study of CO₂ sorption over "Molecular Basket" sorbent consisting of polyethylenimine-modified mesoporous molecular sieve. *J. Phys. chem. C.* **2009**, *113*, 7260-7268.
- (34) Wang, X.; Ma, X.; Schwartz, V.; Clark, J. C.; Overbury, S. H.; Zhao, S.; Xu, X.; Song, C. A Solid Molecular Basket Sorbent for CO₂ Capture From Gas Streams With Low CO₂ Concentration Under Ambient Conditions. *Phys. Chem. Chem. Phys.* **2012**, *14*, 1485.
- (35) Xu, X.; Song, C.; Miller, B. G.; Scaroni, A. W. Adsorption Separation of Carbon Dioxide from Flue Gas of Natural Gas-fired Boiler by a Novel Nanoporous "Molecular Basket" Adsorbent. *Fuel Process. Technol.* **2005**, *86*, 1457.
- (36) Khatri, R. A.; Chuang, S. S. C.; Soong, Y.; Gray, M. Carbon Dioxide Capture by Diamine-Grafted SBA-15: A Combined Fourier Transform Infrared and Mass Spectrometry Study. *Ind. Eng. Chem. Res.* **2005**, *44*, 3702.
- (37) Serna-Guerrero, R.; Belmabkhout, Y.; Sayari, A. Modeling CO₂ Adsorption on Amine-functionalized Mesoporous Silica: 1. A Semi-empirical Equilibrium Model. *Chem. Eng. J.* **2010**, *161*, 173.

- (38) Belmabkhout, Y.; Sayari, A. Isothermal versus Non-isothermal Adsorption–Desorption Cycling of Triamine-Grafted Pore-Expanded MCM-41 Mesoporous Silica for CO₂ Capture from Flue Gas. *Energy Fuels* **2010**, *24*, 5273.
- (39) Harlick, P. J. E.; Sayari, A. Applications of Pore-Expanded Mesoporous Silica . 5 . Triamine Grafted Material with Exceptional CO₂ Dynamic and Equilibrium Adsorption Performance. *Ind. Eng. Chem. Res.* **2007**, *46*, 446.
- (40) Lively, R. P.; Chance, R. R.; Koros, W. J. Enabling Low-Cost CO₂ Capture via Heat Integration. *Ind. Eng. Chem. Res.* **2010**, *49*, 7550.



CHAPTER 7

OTHER CONSIDERATIONS IN ADSORBENT EVALUATION: SORBENT DENSITY & WATER TOLERANCE

7.1. Background

A wide variety of adsorbent materials have been evaluated as candidates for post-combustion CO₂ capture, a topic that has been the subject of several reviews.¹⁻³ The most common metric used to assess adsorbents for post-combustion CO₂ capture in the academic community is adsorption capacity (working/equilibrium) per unit mass of adsorbent, typically mmol/g (mol/kg). Other metrics such as adsorption/desorption kinetics, CO₂/N₂ selectivity and stability, which are additional important considerations in evaluating adsorbents for post-combustion CO₂ capture, are often evaluated only for materials that firstly have a significant CO₂ capture capacity under relevant capture conditions. From a material selection standpoint, a sufficiently high working capacity is the most fundamental requirement for any adsorption based separation process. As emphasized in chapter 1, arguably, the most attractive feature of supported amine adsorbents compared to other adsorbent candidates is the exceptionally high CO₂ adsorption capacities achieved at low CO₂ partial pressures (~0.1 bar) and temperatures (25-75°C) under humid conditions. Hence, the supported amine adsorbent community has focused a significant amount of effort on synthesizing amine adsorbents with increasingly large CO₂ adsorption capacities (see section 1.3).

The capacities used to assess adsorbents, however, have mostly been based on the amount of CO₂ adsorbed per unit mass of adsorbent. This, despite the fact that for a

given bed size (bed diameter, height) and feed flow rate, it is the adsorbent breakthrough capacity per unit volume and not the breakthrough capacity per unit mass that determines adsorbate breakthrough time, a critical process variable. More specifically, given the extremely high flow rates of flue gas (1 MMSCFM), one of the challenges in the field is to design adsorbents/processes that would reduce the overall process footprint. To this end, evaluation of capacities per unit volume merit investigation as well. Even though capacities per unit volume allow for more meaningful comparison between sorbents without the confounding effect of sorbent density, they have mostly been ignored in the evaluation of adsorbents for post-combustion CO₂ capture. Of the various types of adsorbents evaluated for post-combustion CO₂ capture, three stand out as having significantly high adsorption capacities at low CO₂ partial pressures (~0.1 bar) and low temperatures (25 - 75°C): zeolites, supported amine adsorbents, and metal organic frameworks (MOFs). Zeolites and MOFs are microporous materials with pore diameters less than 2 nanometers, whereas supported amine adsorbents are typically synthesized by incorporating amine groups into mesoporous oxide supports having larger pores (2-50 nm), resulting in significantly higher pore volumes per unit mass of adsorbent. One can hypothesize that the larger pore volumes of these mesoporous supports result in lower bulk densities that may potentially offset the exceptionally high adsorption capacities (measured on a per unit mass basis) achievable using this class of materials. From this perspective, it is critically important that one evaluate the effect of adsorbent densities on adsorption capacities per unit volume for supported amine adsorbents as well as MOFs and zeolites. To the best of our knowledge, a direct comparison of zeolites, supported amine materials, and MOFs on a volumetric basis does not currently exist in the literature. In this chapter, we report a systematic assessment of the relative adsorption performance of an array of well-known adsorbent candidates, both on a per unit mass basis and a per unit volume basis. In

addition, the most promising materials from each of the three categories are further evaluated, using CO₂ adsorption capacity per unit volume under humid conditions as the metric for comparison.

Eight promising candidate materials from three different categories (zeolites, supported amine adsorbents, and MOFs) were chosen for this study. Zeolite 13X, which has a high affinity for CO₂, is the most widely studied zeolite adsorbent for post-combustion CO₂ capture.⁴⁻¹⁰ Silicalite-1, a hydrophobic zeolite, has the potential to capture CO₂ from humid streams, a key requirement for flue gas capture applications. Three metal organic framework materials: Mg-DOBDC, CuBTC, and ZIF-90 were also tested in this study. The metal organic framework Mg-DOBDC has been shown to have extremely high CO₂ adsorption capacities at 0.1 bar.^{11,12} CuBTC is one of the most widely studied MOFs for gas separation and storage,¹³⁻¹⁷ and has been shown to have very high CO₂/N₂ selectivities at low pressures.¹⁴⁻¹⁶ Zeolite Imidazolate frameworks (ZIFs) represent an emerging sub-class of metal organic frameworks that have interesting CO₂ adsorption properties.¹⁸⁻²² In particular, ZIF-90 has been shown to possess favorable CO₂ adsorption capacities and high CO₂/N₂ selectivities.^{18,20} PEI impregnated adsorbents on three different mesoporous supports: mesocellular foam silica (MCF), SBA-15, and alumina were tested as well. This set of 8 adsorbent materials was chosen with the goal of evaluating the effect of sorbent density on material performance while encompassing a wide range of adsorbent physical and chemical properties.

7.2. Experiments

7.2.1. Materials Synthesis

The mesocellular foam silica synthesis has been described in chapter 6. The SBA-15 was synthesized using the procedure reported in chapter 2.

γ -Alumina was synthesized using the procedure described by Bali et al.²³ First, pseudoboehmite (74.3% Al₂O₃, 13.75 grams) was peptized in a solution of 0.9 ml nitric acid (70%) in 200 ml distilled water. The suspension thus obtained was sonicated for 90 minutes at room temperature, followed by stirring at 60°C for 17 hours. The suspension was then cooled to room temperature and added to a solution of Pluronic (P123) in 200 ml ethanol (200 proof). Following this step, the solution was stirred for 24 hours at room temperature, the solvent evaporated at 60°C, and the resulting alumina dried overnight in an oven at 75°C. The alumina thus synthesized was calcined in flowing air at 700°C for 4 hours with an intermediate step lasting 1 hour at 150°C. A ramp rate of 1°C/min was used during the heating step.

Before PEI impregnation, the mesoporous oxide supports were dried on a high vacuum line at 120°C for 8 hours. After being cooled down to room temperature, 1.5 grams of the support was stirred with 30 ml methanol for 2 hours. Separately, the corresponding amount of PEI was dispersed in 5 ml methanol and stirred for 30 minutes. The PEI containing methanol solution was then added to the solution containing the support and stirred for an additional 24 hours. The sample was then moved to a rotary evaporator to remove the methanol under vacuum.

ZIF-90 was synthesized using the procedure reported by Thompson et. al.¹⁹ A solution of 20 mmol carboxaldehyde-2-imidazole in 50 ml methanol was heated to 50°C

until clear. A separate solution of 5 mmol zinc nitrate hexahydrate in 50 ml distilled water was prepared. Once the linker solution became clear, it was cooled down to room temperature and the zinc salt solution added to it. On stirring this solution for an hour, a white precipitate was formed, which was centrifuged at 8000 rpm and washed with 300 ml methanol. The powder was then dried overnight at 75°C.

Mg-DOBDC was synthesized using the procedure reported by Choi et. al.²⁴ A solution containing 44.11 ml DMF, 2.94 ml ethanol, and 2.94 ml distilled water was added to an erlenmeyer flask containing 0.111 grams H4DOBDC and 0.475 grams Mg(NO₃)₂·6H₂O. This solution was stirred at 350 rpm for 1 hour. The reaction solution was then transferred to five 20 ml vials in a secondary container, and placed in an oven at 125°C for 20 hours. The vials were removed from the oven and allowed to cool for 6 hours. The mother liquor was gradually removed from the yellow material and replaced with methanol. The methanol was decanted from the vials four times with an interval of 12 hours between each decanting step and finally dried at room temperature to obtain a dark yellow powder.

Zeolite 13X, Silicalite-1, and Cu-BTC were purchased from Sigma Aldrich.

7.2.2. Material Characterization

Powder X-ray diffraction, N₂ physisorption, and thermogravimetric analysis measurements were carried out as described in the experimental section in chapter 2.

7.2.3. Density measurements

Bulk density measurements were performed using two different techniques. In the first case, the appropriate amount of sample was loaded into a measuring cylinder

such that the sample would occupy 3 cc of volume in the measuring cylinder. The powder was packed by tapping the measuring cylinder on the counter 20 times, thus allowing the powder to pack as a result of gravity. These measurements are referred to as normal packing in figure 7.1. In the second set of bulk density measurements, referred to as 'packing under pressure', the samples were loaded into a cylindrical steel container, 1.12 cc in volume. A fixed weight of 74.76 g was placed on the packed powder and more sample was added until a packed bed that filled the cylinder was obtained. The cylinder was subsequently emptied out and the sample mass weighed on a balance to obtain the bulk density.

7.2.4. Equilibrium CO₂ adsorption capacity measurements

CO₂ adsorption capacities for the mesoporous oxide supported amine materials were measured on a thermogravimetric analyzer using the procedure described in chapter 3. CO₂ adsorption capacities for the microporous materials were measured in a pressure decay apparatus. Humid CO₂ adsorption capacities were measured in a packed bed adsorption setup coupled with a mass spectrometer. The details of the experimental procedure can be found in chapter 2. The simulated flue gas was humidified to a relative humidity of 70% at 25°C (2.3% water vapor) and both water vapor and CO₂ concentrations were monitored at the packed bed outlet.

7.3. Results & Discussion

7.3.1. Sorbent Densities

Figure 7.1 shows the bulk densities of the materials measured using the two techniques described in the experimental section: normal packing and packing under pressure. The packing technique used was found to affect the absolute value of the bulk density, implying that interparticle voids contribute significantly to total void volume in the bed (intraparticle + interparticle). Nevertheless, the bulk density trend for this set of materials is independent of the density measurement technique used (normal packing vs packing under pressure). The PEI impregnated alumina material was found to have the highest bulk density amongst the materials tested and the PEI impregnated MCF material, the lowest. Interestingly, both, the choice of mesoporous support as well as amine loading had a significant effect on bulk densities of supported amine adsorbents. As shown in figure 7.2, bulk density increased roughly linearly as a function of PEI loading. The PEI impregnated material with 49% PEI loading was found to have a bulk density roughly 2.3 times that of the bare support, thus suggesting that in addition to increasing the CO₂ adsorption capacity, increasing amine loading also has a significant favorable impact on sorbent densities. On the other hand, the bulk densities of the zeolites and MOFs fell within a narrow range of values (approximately 500-700 kg/m³ under pressure), despite the fact that a diverse set of materials was tested. This has important implications for assessing adsorbents for post-combustion CO₂ capture. In the case of microporous adsorbents like zeolites and MOFs, evaluating adsorbents based on adsorption capacities per unit mass may be an acceptable first-order estimate of the relative adsorption performance. On the other hand, for mesoporous-oxide supported amine adsorbents, a comparison of adsorbents based on adsorption capacities per unit

mass is less likely to yield an appropriate relative comparison due to the significant impact of support type (figure 7.1) and amine loading (figure 7.2) on bulk densities.

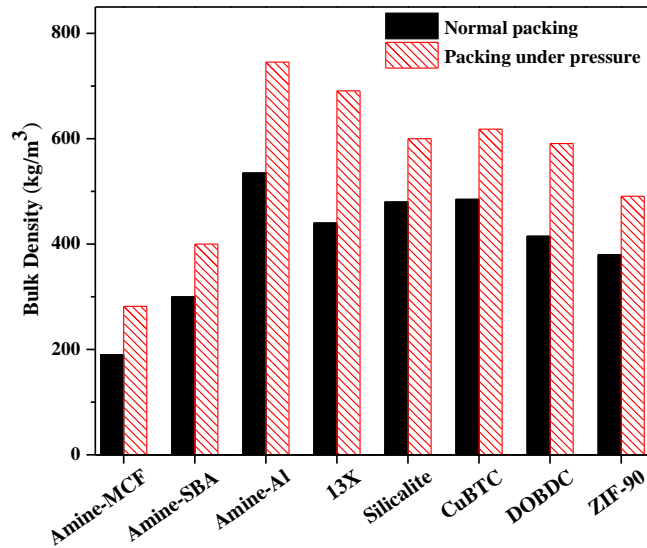


Figure 7.1: Bulk densities of tested materials using different packing techniques: Normal packing (black, solid) and under pressure (red, dashed)

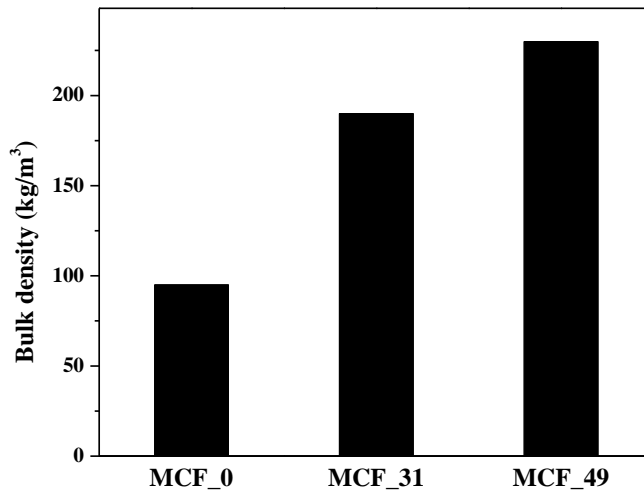


Figure 7.2: Bulk density as a function of amine loading (numbers following MCF indicate percentage weight loading of PEI on a dry basis)

Figure 7.3 shows a plot of bulk density as a function of adsorbent pore volume. As expected, the bulk density decreases as the pore volume of the material increases, due to the increasing void fraction in the packed bed. Interestingly, pore volumes of materials reported in this study vary by a factor of 20, whereas bulk densities vary only by a factor of 2.7, suggesting that widely differing porosities do not necessarily imply widely different sorbent bulk densities.

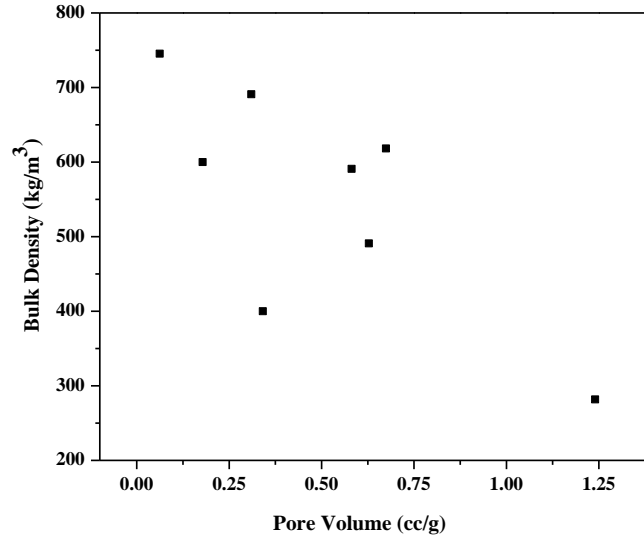


Figure 7.3: Bulk densities (under pressure) as a function of adsorbent pore volume

The increase in bulk density with packing pressure (figure 7.1) implies that interparticle voids contribute significantly to the overall bed void fraction. A further increase in packing pressure would likely decrease the interparticle void volume further, thereby increasing bulk density. The theoretical maximum bulk density reached in the limit of zero interparticle void volume is the framework density. To see how the sorbent

densities would compare after elimination of interparticle voids, framework density values from the literature are plotted in figure 7.4 along with the measured bulk densities of the zeolites and MOFs tested in this study. Unlike bulk densities, which varied by a factor of 1.4, framework densities for this subset of materials varied by a factor of 2.2, again suggesting that the interparticle void volume serves to temper the large differences in framework densities. Also, unlike in the case of bulk densities, zeolites have significantly higher framework densities compared to the MOF materials tested in this study. Since bulk densities are more relevant to evaluation of adsorbents for practical applications, they were used to calculate CO₂ adsorption capacities on a per unit volume basis, which are discussed further below.

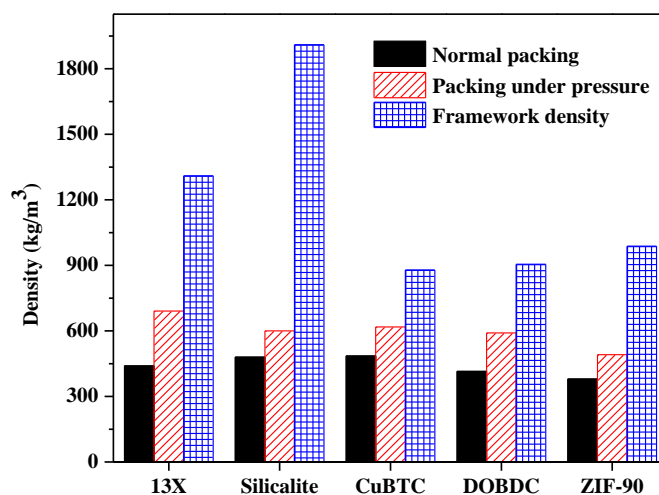


Figure 7.4: Comparison of bulk and framework densities for the crystalline materials used in this study. References: 13X,²⁵ Silicalite-1,^{26,27} CuBTC,²⁸ Mg DOBDC,²⁸ ZIF-90²⁹

7.3.2. *CO₂ adsorption capacities*

Figure 7.5 shows the mass and volume-based CO₂ adsorption capacities (calculated using bulk densities measured under pressure) measured at 0.1 bar CO₂ pressure and 45°C. In terms of mass-based adsorption capacities, Mg-DOBDC outperforms all other materials tested in this study, followed by the PEI impregnated alumina material and zeolite 13X. PEI impregnated MCF and PEI impregnated SBA-15 perform reasonably well, but not as well as the PEI impregnated alumina adsorbent, despite similar amine loadings on all three materials. The MFI, CuBTC, and ZIF-90 materials do not exhibit significant adsorption capacities compared to Mg-DOBDC MOF, zeolite 13X, and the amine-oxide materials under the experimental conditions used in this study. The adsorption capacities reported in this study are in reasonably good agreement with reported data in the literature. Figure 7.5 also shows the adsorption capacities per unit volume. The order of relative adsorption performance of the adsorbents remains approximately the same as when compared on the basis of adsorption capacities per unit mass. This is a direct consequence of the fact that bulk density variations in the materials tested in this study are not as significant as corresponding variations in pore volume (*vide supra*).

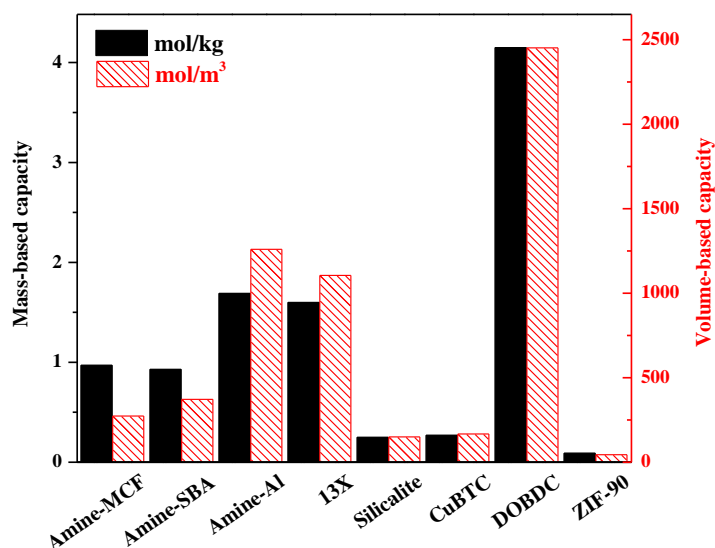


Figure 7.5: Mass-based (black, solid) and volume-based capacities (red, dashed) for materials tested.

Any viable adsorbent candidate for post-combustion CO₂ capture must be capable of adsorbing CO₂ in the presence of humidity. Hence, the most relevant metric for comparing adsorption characteristics of various materials is the adsorption capacity per unit volume in the presence of humidity. The top 3 candidates from each category (Amine-alumina, Zeolite 13X, and Mg-DOBDC) were further tested to calculate adsorption capacities in the presence of humidity.

Figure 7.6 shows the adsorption capacities measured on a fixed bed adsorption system using a feed stream having 70% relative humidity at 25°C (2.3% water vapor). The amine-alumina adsorption capacity is slightly enhanced by the presence of water vapor in the feed. On the other hand, the CO₂ adsorption capacities for the zeolite 13X and Mg-DOBDC materials fall drastically under the same conditions, in agreement with literature reports.^{30,31} Thus, using CO₂ adsorption capacities per unit volume in the

presence of humidity as the metric for comparing candidate adsorbent materials, PEI impregnated alumina, with a capacity of 1357 mol/m³, exhibits the best performance within the set of materials used in this study.

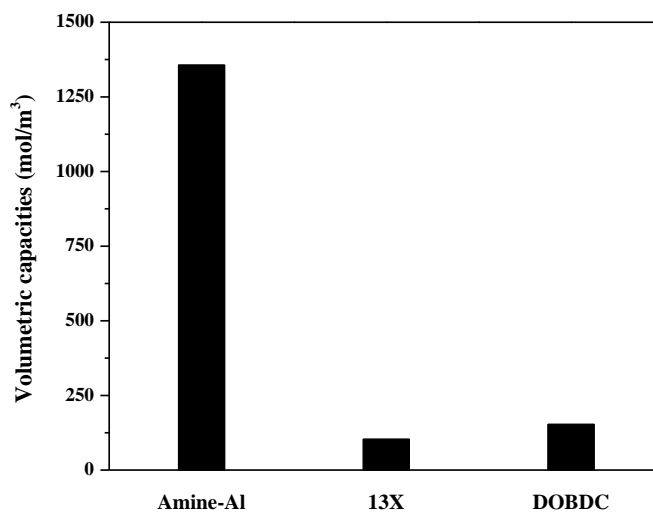


Figure 7.6: CO₂ adsorption capacities for materials measured in the presence of humidity

7.4. Conclusions

An array of porous materials from three different categories: zeolites, supported amine adsorbents, and MOFs have been compared on the basis of adsorption capacities per unit volume. Despite the presence of mesopores, supported amine adsorbents exhibited bulk densities not significantly different from the microporous ones tested in this study. Overall, as a consequence of the narrow distribution in bulk densities, sorbent densities did not have a significant impact on adsorbent evaluation under conditions relevant to post-combustion CO₂ capture. For supported amine materials though, the choice of oxide support and amine loading were found to have a significant impact on bulk density values, implying that bulk density may be an important consideration when comparing supported amine adsorbents amongst each other. In the absence of humidity, Mg-DOBDC outperformed the rest of the other adsorbents tested in this study. On the other hand, under humid conditions, PEI functionalized alumina showed exceptionally high adsorption capacities on a per unit volume basis. These results, combined with the fact that alumina supported amine adsorbents have been shown to be relatively stable to steam compared to mesoporous-silica supported adsorbents and MOFs,³² suggest that alumina-amine sorbents remain promising candidate materials for post-combustion CO₂ capture applications.

7.5. References

- (1) Choi, S.; Drese, J. H.; Jones, C. W. Adsorbent Materials for Carbon Dioxide Capture from Large Anthropogenic Point Sources. *ChemSusChem* **2009**, *2*, 796.
- (2) Hedin, N.; Chen, L.; Laaksonen, A. Sorbents for CO₂ capture from flue gas- aspects from materials and theoretical chemistry. *Nanoscale* **2010**, *2*, 1819-41.
- (3) Bollini, P.; Didas, S. A.; Jones, C. W. Amine-oxide Hybrid Materials for Acid Gas Separations. *J. Mater. Chem.* **2011**, *21*, 15100.
- (4) Lively, R. P.; Chance, R. R.; Kelley, B. T.; Deckman, H. W.; Drese, J. H.; Jones, C. W.; Koros, W. J. Hollow fiber adsorbents for CO₂ removal from flue gas. *Ind. Eng. Chem. Res.* **2009**, *48*, 7314.
- (5) Konduru, N.; Lindner, P.; Assaf-Anid, N. M. Curbing the Greenhouse Effect by Carbon Dioxide Adsorption with Zeolite 13X. *AIChE J.* **2007**, *53*, 3137-3143.
- (6) Zhao, Z.; Cui, X.; Ma, J.; Li, R. Adsorption of carbon dioxide on alkali-modified zeolite 13X adsorbents. *International Journal of Greenhouse Gas Control* **2007**, *1*, 355-359.
- (7) Li, G.; Xiao, P.; Webley, P.; Zhang, J.; Singh, R.; Marshall, M. Capture of CO₂ from high humidity flue gas by vacuum swing adsorption with zeolite 13X. *Adsorption* **2008**, *14*, 415-422.
- (8) Zhang, Z.; Zhang, W.; Chen, X.; Xia, Q.; Li, Z. Adsorption of CO₂ on Zeolite 13X and Activated Carbon with Higher Surface Area. *Sep. Sci. Technol.* **2010**, *45*, 710-719.

- (9) Mérel, J.; Clause, M.; Meunier, F. Carbon dioxide capture by indirect thermal swing adsorption using 13X zeolite. *Environ. Prog.* **2006**, *25*, 327-333.
- (10) Ho, M. T.; Allinson, G. W.; Wiley, D. E. Reducing the Cost of CO₂ Capture from Flue Gases Using Pressure Swing Adsorption. *Ind. Eng. Chem. Res.* **2008**, *47*, 4883-4890.
- (11) Liu, J.; Benin, A. I.; Furtado, A. M. B.; Jakubczak, P.; Willis, R. R.; LeVan, M. D. Stability effects on CO₂ adsorption for the DOBDC series of metal-organic frameworks. *Langmuir* **2011**, *27*, 11451-11456.
- (12) Mason, J. a.; Sumida, K.; Herm, Z. R.; Krishna, R.; Long, J. R. Evaluating metal-organic frameworks for post-combustion carbon dioxide capture via temperature swing adsorption. *Energy Environ. Sci.* **2011**, *4*, 3030-3040.
- (13) Min Wang, Q.; Shen, D.; Bülow, M.; Ling Lau, M.; Deng, S.; Fitch, F. R.; Lemcoff, N. O.; Semanscin, J. Metallo-organic molecular sieve for gas separation and purification. *Microporous Mesoporous Mater.* **2002**, *55*, 217-230.
- (14) Liang, Z.; Marshall, M.; Chaffee, A. L. CO₂ Adsorption-Based Separation by Metal Organic Framework (Cu-BTC) versus Zeolite (13X). *Energy Fuels* **2009**, *23*, 2785-2789.
- (15) Yang, Q.; Xue, C.; Zhong, C.; Chen, J.-F. Molecular Simulation of Separation of CO₂ from Flue Gases in Cu-BTC Metal-Organic Framework. *AIChE J.* **2007**, *53*, 2832-2840.
- (16) Aprea, P.; Caputo, D.; Gargiulo, N.; Iucolano, F.; Pepe, F. Modeling Carbon Dioxide Adsorption on Microporous Substrates : Comparison between Cu-BTC

Metal-Organic Framework and 13X Zeolitic Molecular Sieve. *J. Chem. Eng. Data* **2010**, *55*, 3655-3661.

- (17) Hamon, L.; Jolimaitre, E.; Pirngruber, G. D. CO₂ and CH₄ Separation by Adsorption Using Cu-BTC Metal-Organic Framework. *Ind. Eng. Chem. Res.* **2010**, *49*, 7497-7503.
- (18) Amrouche, H.; Aguado, S.; Perez-Pellitero, J.; Siperstein, F.; Farrusseng, D.; Bats, N.; Nieto-Draghi, C. Experimental and Computational Study of Functionality Impact on Sodalite-Zeolitic Imidazolate Frameworks for CO₂ Separation. *J. Phys. Chem. C* **2011**, *115*, 16425-16432.
- (19) Thompson, J. A.; Blad, C. R.; Brunelli, N. A.; Lydon, M. E.; Lively, R. P.; Jones, C. W.; Nair, S. Hybrid Zeolitic Imidazolate Frameworks: Controlling Framework Porosity and Functionality by Mixed-Linker Synthesis. *Chem. Mater.* **2012**, *24*, 1930-1936.
- (20) Venkatasubramanian, A.; Navaei, M.; Bagnall, K. R.; McCarley, K. C.; Nair, S.; Hesketh, P. J. Gas Adsorption Characteristics of Metal–Organic Frameworks via Quartz Crystal Microbalance Techniques. *J. Phys. Chem. C* **2012**, *116*, 15313-15321.
- (21) Millward, A. R.; Yaghi, O. M. Metal-organic frameworks with exceptionally high capacity for storage of carbon dioxide at room temperature. *J. Am. Chem. Soc.* **2005**, *127*, 17998-17999.

- (22) Phan, A.; Doonan, C. J.; Uribe-romo, F. J.; Knobler, C. B.; Keeffe, M. O.; Yaghi, O. M. Synthesis, Structure, and Carbon Dioxide Capture Properties of Zeolitic Imidazolate Frameworks. *Acc. Chem. Res.* **2010**, *43*, 58-67.
- (23) Bali, S.; Chen, T. T.; Chaikittisilp, W.; Jones, C. W. Oxidative Stability of Amino Polymer – Alumina Hybrid Adsorbents for Carbon Dioxide Capture. *Energy Fuels* **2013**, *27*, 1547-1554.
- (24) Choi, S.; Watanabe, T.; Bae, T.-hyun; Sholl, D. S.; Jones, C. W. Modification of the Mg/DOBDC MOF with Amines to Enhance CO₂ Adsorption from Ultradilute Gases. *J. Phys. Chem. Lett.* **2012**, *3*, 1136-1141.
- (25) Pechaf, T. W.; Tsapatsis, M.; Marand, E.; Davis, R. Preparation and characterization of a glassy fluorinated polyimide zeolite-mixed matrix membrane. *Desalination* **2002**, *146*, 3-9.
- (26) Ravishankar, R.; Kirschhock, C.; Schoeman, B. J.; Vanoppen, P.; Grobet, P. J.; Storck, S.; Maier, W. F.; Martens, J. A.; Schryver, F. C. D.; Jacobs, P. A.; Interfasechemie, D.; Voor, C.; Leuven, K. U.; Mercierlaan, K. Physicochemical characterization of Silicalite-1 nanophase material. *J. Phys. Chem. B* **1998**, *5647*, 2633-2639.
- (27) Janchen, J.; Stach, H.; Uytterhoeven, L.; Mortier, W. J. Influence of the framework density and the effective electronegativity of silica and aluminophosphate molecular sieves on the heat of adsorption of nonpolar molecules. *J. Phys. Chem. B* **1996**, *3654*, 12489-12493.

- (28) Xiang, S.; He, Y.; Zhang, Z.; Wu, H.; Zhou, W.; Krishna, R.; Chen, B. Microporous metal-organic framework with potential for carbon dioxide capture at ambient conditions. *Nature Communications* **2012**, *3*, 954.
- (29) Morris, W.; Doonan, C. J.; Furukawa, H.; Banerjee, R.; Yaghi, O. M. Crystals as molecules: postsynthesis covalent functionalization of zeolitic imidazolate frameworks. *J. Am. Chem. Soc.* **2008**, *130*, 12626-7.
- (30) Wang, Y.; LeVan, M. D. Adsorption Equilibrium of Binary Mixtures of Carbon Dioxide and Water Vapor on Zeolites 5A and 13X. *J. Chem. Eng. Data* **2010**, *55*, 3189-3195.
- (31) Kizzie, A. C.; Wong-Foy, A. G.; Matzger, A. J. Effect of humidity on the performance of microporous coordination polymers as adsorbents for CO₂ capture. *Langmuir* **2011**, *27*, 6368-73.
- (32) Chaikittisilp, W.; Kim, H. J.; Jones, C. W. Mesoporous Alumina-Supported Amines as Potential Steam-Stable Adsorbents for Capturing CO₂ from Simulated Flue Gas and Ambient Air. *Energy Fuels* **2011**, *25*, 5528.

CHAPTER 8

SUMMARY & FUTURE DIRECTIONS

8.1. Summary

The following is a summary of this dissertation along with the main conclusions:

Chapter 1

An overview was given of those aspects of supported amine adsorbents that are of relevance to post-combustion CO₂ capture applications. Key areas for research were identified. Better fundamental understanding of these areas can enable better evaluation of amine adsorbents for CO₂ capture and design of novel materials with improved adsorption properties.

Chapter 2

- Investigation of the impact of heat effects on CO₂ adsorption kinetics resulted in the finding that under certain experimental conditions, simple isothermal models can be used to derive kinetic parameters for CO₂ adsorption, despite large heats of CO₂ adsorption onto amine adsorbents.
- It was discovered that in the case of highly hydrophilic materials, water vapor breaks through much later compared to CO₂, resulting in a negligible effect of humidity on CO₂ adsorption kinetics.

Chapter 3

- In the case of adsorbents that had amine-polymer incorporated into the pores of the support, diffusion limitations were found to result in long tails in breakthrough curves, resulting in reduced CO₂ breakthrough times.
- A new model that takes into account diffusion heterogeneity was proposed, which fit the experimental breakthrough data extremely well.

Chapter 4

- The motivation underlying and the actual design, setup of an adsorption calorimeter capable of measuring isosteric heats of adsorption at unprecedentedly low pressures was described.
- The instrument has high sensitivity, reproducibility, and accuracy for measuring isosteric heats at ultra-low pressures/coverages.

Chapter 5

- Unlike previous reports in the literature, physisorption was found to have a significant impact on amine efficiencies for amine adsorbents with low amine loadings.
- The correlation between amine structure and efficiency was found to be heavily influenced by entropic factors.

Chapter 6

- Primary monoamines were shown to be relatively more stable to oxidative degradation compared to secondary monoamines on exposure to oxygen under accelerated degradation conditions.
- In the case of amine adsorbent structures where amines are connected by an alkyl chain, strong evidence for the presence of a cooperative degradation mechanism was presented.

Chapter 7

- The impact of sorbent bulk density on adsorbent evaluation was found to be insignificant for microporous materials, but extremely important when comparing amongst supported amine adsorbents. Both the nature of the mesoporous oxide support and amine loading were found to be important factors affecting sorbent densities of this class of materials.
- Using volumetric CO₂ adsorption capacities under humid conditions as the basis for comparison, the PEI impregnated alumina material appeared to be the most promising for CO₂ capture applications in the set of materials tested.

8.2. Future Directions

There are several research directions that could branch out of the work presented in this dissertation. Two of these potential research directions are briefly discussed here.

8.2.1. Effect of heteroatom incorporation: Elucidation of the mechanism underlying the enhancement effect

In section 4.1, the enhancement effect of incorporating heteroatoms like zirconium in the silica framework was discussed briefly. To date, there hasn't been a clear explanation of the reason underlying this enhancement effect. The tools for analyzing CO₂ adsorption kinetics discussed in chapters 2 and 3 can be used to understand the impact of zirconium incorporation on CO₂ adsorption kinetics. The adsorption calorimetry apparatus can be used to quantitatively assess any changes in the strength of interaction between CO₂ and the amine functional group. This deconvolution of kinetic and thermodynamic enhancements could prove extremely useful in the rational design of amine adsorbents with even better adsorption characteristics.

8.2.2. *Better description of CO₂-supported amine adsorption thermodynamics*

Arguably, the single most critical piece of information for accurately simulating an adsorption process is an appropriate equilibrium isotherm model. The poor performance of the Toth model in predicting heat-coverage relationships points to a lack of fundamental understanding of CO₂ adsorption thermodynamics onto supported amine adsorbents. Identification of models that do in fact lead to an accurate description of surface energetic heterogeneity can potentially lead to new insights into CO₂-amine adsorption. Since the number of isotherm models available in the literature is relatively large, one possible approach may be to first fit the heat-coverage curve and then fit the experimental data to the isotherm model derived from the heat-coverage curve. Do (Chemical Engineering Science, Vol. 52, No. 2, pp. 297-310, 1997) has shown that using this approach, an isotherm model can be obtained, which under different conditions reduces to specific adsorption isotherm types already known in the literature. The insights gained from these studies could not only transform our understanding of CO₂-amine adsorption but also enable more accurate simulation of adsorption processes involving supported amine adsorbents.